INVESTIGATIONS OF TRANSITION METAL CATALYSTS FOR THE HYDRATION OF CYANOHYDRINS AND LIGAND EFFECTS IN AQUEOUS MOLYBDOCENE CHEMISTRY

by

TAKIYA JANICE AHMED

A DISSERTATION

Presented to the Department of Chemistry
and the Graduate School of the University of Oregon
in partial fulfillment of the requirements
for the degree of
Doctor of Philosophy

September 2008

University of Oregon Graduate School

Confirmation of Approval and Acceptance of Dissertation prepared by:

Takiya Ahmed

Title:

"Investigations of Transition Metal Catalysts for the Hydration of Cyanohydrins and Ligand Effects in Aqueous Molybdocene Chemistry"

This dissertation has been accepted and approved in partial fulfillment of the requirements for the Doctor of Philosophy degree in the Department of Chemistry by:

Darren Johnson, Chairperson, Chemistry
David Tyler, Advisor, Chemistry
Catherine Page, Member, Chemistry
Mark Lonergan, Member, Chemistry
Robert Zimmerman, Outside Member, Physics

and Richard Linton, Vice President for Research and Graduate Studies/Dean of the Graduate School for the University of Oregon.

September 6, 2008

Original approval signatures are on file with the Graduate School and the University of Oregon Libraries.

An Abstract of the Dissertation of

Takiya Janice Ahmed for the degree of Doctor of Philosophy

in the Department of Chemistry to be taken September 2008

Title: INVESTIGATIONS OF TRANSITION METAL CATALYSTS FOR THE HYDRATION OF CYANOHYDRINS AND LIGAND EFFECTS IN AQUEOUS MOLYBDOCENE CHEMISTRY

Approved: _____
David R. Tyler

Efforts toward developing improved methods of synthesizing acrylamides are ongoing. Several homogeneous organometallic and coordination complexes have proven useful in catalytic acrylonitrile hydration; however, none of these complexes have been tested in the hydration of cyanohydrins used to synthesize substituted acrylamides.

This dissertation describes the reactivity of molybdocene and Pt phosphinito nitrile hydration catalysts toward cyanohydrin substrates and the effect of Cp ring substituents on aqueous molybdocene chemistry. Chapter I identifies the motivation for developing a transition metal-catalyzed process for cyanohydrin hydration and the strategy used to improve on the reactivity of molybdocene catalysts. Chapter II reports the effect of cyclopentadienyl ring substituents on the electronic and geometric structure, solution behavior, and hydrolytic activity of molybdocenes.

To examine the effect of Cp ring substituents, *ansa*-molybdocenes containing the fragment $\{C_2Me_4(C_5H_4)_2\}Mo^{2+}$ were compared to non-bridged molybdocenes containing $(C_5H_5)_2Mo^{2+}$ and $(C_5H_4Me)_2Mo^{2+}$. Addition of a tetramethylethylene-bridge decreases the electron density on the Mo center and exerts a small effect on the structure of the metallocene. However, the catalytic activity of the molybdocene catalysts is unchanged or slowed because of counteractive effects on the bound nucleophile and electrophile.

Although adding substituents to the Cp rings did not change the catalytic activity of the molybdocene, the substituents led to significant changes in the equilibrium behavior. The equilibria have practical consequences that warrant investigation. Chapters III and IV chronicle the effect of Cp ring substituents on the monomer-dimer equilibria and the acidity of the molybdocene complexes, respectively. Interestingly, the monomer-dimer equilibrium established by *ansa*-$\{C_2Me_4(C_5H_4)_2\}Mo(OH)(OH_2)^+$ exhibits a strong solvent dependence. New equilibrium schemes are reported for the *ansa* and non-*ansa* complexes.

Chapter V describes the reactivity of the molybdocene and Pt phosphinito catalysts toward cyanohydrins. Both catalysts gave unsatisfactory results; however, the α-hydroxy substituent of cyanohydrins facilitates nitrile hydration. The low reactivity exhibited by these systems was due to liberation of hydrogen cyanide from the cyanohydrin leading to acute poisoning of either catalyst. As discussed in Chapter VI, this study will expedite

the innovation of new catalysts that are better suited to overcome the challenges associated with cyanohydrin hydration.

This dissertation includes previously published and unpublished co-authored material.

CURRICULUM VITAE

NAME OF AUTHOR: Takiya J. Ahmed

PLACE OF BIRTH: New York, NY

DATE OF BIRTH: June 2, 1980

GRADUATE AND UNDERGRADUATE SCHOOLS ATTENDED:

University of Oregon, Eugene
Virginia Commonwealth University, Richmond

DEGREES AWARDED:

Doctor of Philosophy in Chemistry, 2008, University of Oregon
Bachelor of Science in Chemistry, 2003, Virginia Commonwealth University

AREAS OF SPECIAL INTEREST:

Aqueous Organometallic Chemistry
Homogeneous Catalysis
Catalytic Hydration and Hydrolysis Reactions

PROFESSIONAL EXPERIENCE:

Graduate Research Assistant, Department of Chemistry, University of Oregon, Eugene, 2004–2008

Graduate Teaching Assistant, Department of Chemistry, University of Oregon, Eugene, 2003–2004

Intern, Printed Wiring Boards Division, Shipley International, Marlborough, MA, 2003

Undergraduate Research Assistant, Department of Chemistry, Virginia Commonwealth Unversity, Richmond, 2002–2003

Teaching Assistant, Department of Chemistry, Virginia Commonwealth Unversity, Richmond, 2002–2003

Cooperative Education Student, Quality Assurance Laboratory, Honeywell International, Hopewell, VA, 2001–2002

GRANTS, AWARDS AND HONORS:

University Club Foundation Graduate Fellowship Award, University Club of Portland, 2007

University of Oregon Doctoral Research Fellowship, 2007

Mildred Braaten Archibald Scholarship in Science and Mathematics, University of Oregon, 2007

Best Poster- MSI-IGERT Retreat, University of Oregon, 2005

Rosaria Haugland Fellowship, University of Oregon, 2004–2007

National Organization for the Professional Advancement of Black Chemists and Chemical Engineers (NOBCChE) Undergraduate Research Award, 2003

Cooperative Education Achievement Award, Virginia Commonwealth University, 2003

American Chemical Society Outstanding Student Award, 2003

Ingraham Scholarship, Richmond Chromatography Discussion Group, 2002

PUBLICATIONS:

Ahmed, T. J.; Balzarek, C. Y.; Tyler, D. R. "Aqueous Speciation of *ansa*- and non-*ansa* Substituted $[Cp_2Mo(\mu\text{-}OH)]_2[OTs]_2$," *Inorganica Chimica Acta* **2008**, Submitted.

Ahmed, T. J.; Tyler, D. R. "Effect of Solvent on the Dimerization of the *ansa*-Molybdocene Catalyst $[C_2Me_4Cp_2Mo(OH)(OH_2)][OTs]$," *Organometallics* **2008**, *27*, 2608–2613.

Ahmed, T. J.; Zakharov, L. N.; Tyler, D. R. "Organometallic Catalysis in Aqueous Solution. The Hydrolytic Activity of a Water-Soluble *ansa*-Molybdocene Catalyst," *Organometallics* **2007**, *26,* 5179–5187.

Breno, K. L.; Ahmed, T. J.; Pluth, M. D.; Balzarek, C.; Tyler, D. R. "Organometallic Chemistry in Aqueous Solution: Reactions Catalyzed by Water-Soluble Molybdocenes," *Coord. Chem. Rev.* **2006**, 250, 1141–1151.

ACKNOWLEDGMENTS

I wish to express sincere appreciation to my advisor, Professor David R. Tyler, for challenging me to be my best.

Thanks also goes to Shannon R. Finnell, Brandy R. Fox, and Spring Medoly M. Knapp for their research assistance. I am grateful to Lev Zakharov for his crystallographic work and to Michael Strain for his NMR spectroscopy support throughout the years.

The friendship and support of my fellow angels, Bevin C. Daglen and Ginger Shultz, has been invaluable to my success in this program. I will forever be indebted to Nathaniel K. Szymczak for his scientific mentorship throughout my graduate career. The guidance of Professor Cathy Page, Professor Mark Lonergan, Dr. Jerrick Juliette, and Dr. Rosaria Haugland has been significant to my intellectual and professional development. Dr. Carla Gary has been an inspiration to me, and I thank her for her mentorship and the opportunities that she has awarded me.

My fiancé, Dajosha Lokur Foskey, my immediate family members, and my extended family members helped me to find the courage to pursue this work. I am blessed to have such caring and thoughtful people in my life. Know that I am because we are.

This work was supported by the Haugland Graduate Research Fellowship, Rohm and Haas Company, Texas, and the National Science Foundation Goali.

I dedicate my work to my grandmother, Susie Pleasantine Scott Townes, and my mother, Naila Iris Octavia Townes Ahmed. Your sacrifices, hard work, and dedication to excellence have enabled me to dream. I will never settle. I promise.

TABLE OF CONTENTS

LIST OF FIGURES

Figure Page

LIST OF TABLES

Table Page

CHAPTER V

LIST OF SCHEMES

CHAPTER I

INTRODUCTION: INDUSTRIAL NITRILE HYDRATION PROCESSES AND HOMOGENEOUS NITRILE HYDRATION CATALYSTS

1.1 Commercial Importance of Acrylic Amides

The catalytic hydration of nitriles (eq 1) provides an atom economical route to

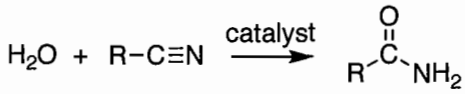

(1)

amides and is, therefore, an important transformation in the laboratory as well as in many chemical and pharmaceutical industries.[1] Amides are used in a host of industrial applications, such as detergent additives, lubricants, drug stabilizers, and monomers. By far, the most important class of amides is the acrylic amide (Figure 1**a**), used as monomers in the preparation of a variety of polymeric materials.[1] One such polymer, polyacrylamide, is prepared from the polymerization of acrylamide (Figure 1a, where R = H) and forms an absorbent gel that is used primarily in water treatment to remove organic waste through flocculation.[1-4] Polyacrylamide gels also find use in gel electrophoresis,

paper strengthening, and adhesives. The economic importance of acrylamide is attested to by the large amount manufactured. In 2001, two-hundred thousand metric tons of acrylamide were produced, and the market for acrylamide is projected to continue increasing at a rate of 4 % per year.[2] Some of the acrylamide generated is converted to acrylic acid and acrylic esters (Figure 1b and 1c, respectively, where R = H).[1] Polyacrylic acids are super absorbent polymers used in diapers and other hygiene products. Acrylic acids and esters are also copolymerized with other alkyl acrylates for the production of acrylic coatings and paints. Methacrylic acid and ester monomers (Figure 1b and 1c, where R = CH_3) are generated from the α-hydroxynitrile acetone cyanohydrin (vide infra), and represent an even larger global market with a demand for methylacrylic monomers exceeding several million metric tons.[1,5] Unlike the soft polyacrylates, polymethacrylates are typically inflexible due to the rigidity imparted by the methyl groups on alternating chains.[5] Polymethyl methacrylate, in particular, is a shatterproof, transparent plastic better known as Plexiglas™. These and other remarkable properties of methacrylic monomers are useful for a plethora of commercial products including windshields, signs, safety glasses, and bathtubs.

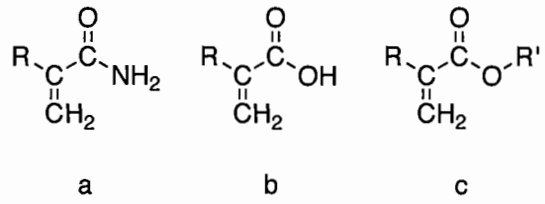

Figure 1. General structure of (a) an acrylic amide, (b.) an acrylic acid, and (c) an acrylic ester

1.2 Synthetic Strategies Used to Prepare Acrylic Amides, Acids, and Esters: Past, Present, and Pending

Clearly, acrylic amides are important to the global economy. However, classical methods of converting nitriles to amides present several disadvantages (i.e. high energy demands, harsh conditions, and the generation of wasteful byproducts). For example, under dilute acidic or basic conditions, the hydration of nitriles is less energetically favorable than the hydrolysis of the resulting amide (Scheme 1a), and a mixture of the amide and carboxylic acid is produced.[6] Generation of unwanted organic acid compromises the amide yield and also requires energy intensive purification steps. As a result, the classical industrial production of acrylic amides employs concentrated sulfuric acid.[1,4] Hydrolysis of the amide does not occur when concentrated sulfuric acid is used; however, the strongly acidic conditions lead to formation of the amide sulfate salt (Scheme 1b). Subsequent neutralization of the amide sulfate with ammonia affords the amide and ammonium sulfate, which is typically sold as fertilizer. The discovery of efficient Cu transition metal nitrile hydration catalysts (such as Raney Cu, various mixed

metal Cu oxides, and Cu(I) and Cu(II) salts) eliminated the need for acidic conditions and the additional processing steps required for conversion of the amide sulfate.[4,7] However, the use of Cu salts in the industrial production of acrylamide typically requires separation of unreacted acrylonitrile and of the Cu salt catalyst from the product stream.[2] Furthermore, Cu systems require complex preparation and regeneration procedures, which represent unnecessary costs.

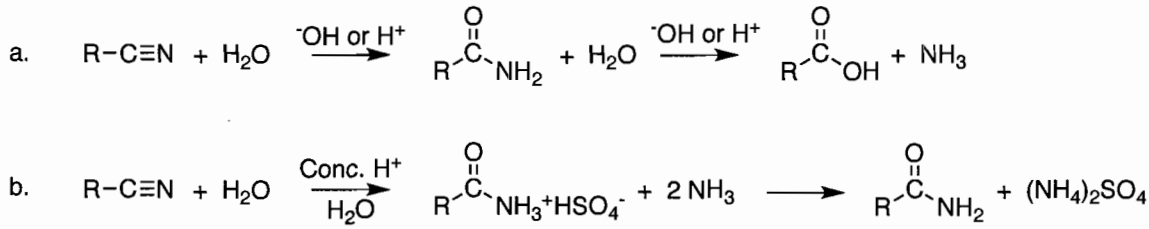

Scheme 1. (a.) Hydration of a nitrile and subsequent hydrolysis of the amide product catalyzed by dilute acid or base and (b.) the preparation of amides using concentrated acid.

Small improvements in the manufacture of such high demand commercial products can have a huge effect on production costs, retail costs, and the environmental and health risks associated with the process. As such, efforts toward developing greener and more cost effective methods of synthesizing vinyl amides are ongoing in industry and in academia. Recently, impressive advances have been made in the production of acrylamide using immobilized nitrile hydratases (or NHases).[2,3] NHases contain Fe(III) or Co(III) centers[8-10] and are used by microorganisms to hydrate nitriles exuded from

plant biomass for the generation of essential carboxylic metabolites.[10] The benefits of using biocatalysis for commercial production are the high selectivity of the enzymes and low energy input required. However, enzymes are expensive to isolate and extremely susceptible to product inhibition, making them impractical for batch reactions.[2,11] Nitto Chemical Industry Ltd in Japan was able to circumvent these problems in the production of acrylamide by immobilizing bacterial cells containing NHase in a cationic acyrlamide-based polymer.[2,3] Using this method, almost quantitative conversion of acrylonitrile is achieved below 10 °C even in the presence of 17.5 % acrylamide. The biocatalytic hydration of acrylonitrile is relatively simple and economical compared to Cu catalyzed processes. The usefulness of this technology was demonstrated in the late 1980s, and by 2002, at least six plants had replaced their technology with a similar immobilized enzyme approach.

Unfortunately, such advancements in the industrial production of methacrylates are still pending. One reason that the biocatalytic route has not been applied to the synthesis of methacrylates is the extreme sensitivity of many NHase enzymes toward α-hydroxynitrile substrates, such as the acetone cyanohydrin (ACH) starting material used in the synthesis of methyacrylates. It has been noted that many NHases are sensitive to cyanohydrin substrates and/or their dissociation products (aldehydes and prussic acid).[11] The dissociation of a cyanohydrin is illustrated in eq 2.

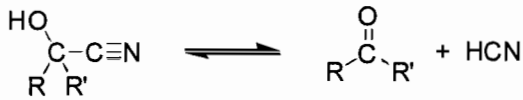

(2)

However, the use of NHases to promote the hydration of selected cyanohydrins, like lactonitrile and *p*-chloromandelonitrile, has received much attention in the chemical literature,[11-18] and these enzymes show promise for large-scale synthesis of α-hydroxyamides. A wide range of NHases (including those belonging to the genera *Rhodococcus*,[15,16] *Corynebacterium*,[11] *Pseudomonas*,[14] *Arthrobacter*,[11] *Alcaligenes*,[18] *Brevibacterium*,[11] and *Nocardia*)[11] have been used, often in combination with amidase, to prepare α-hydroxyamides and carboxylic acids. Efficient reactivity and optical resolution has been noted in several cases, and the use of NHases has been applied to the enantioselective syntheses of fine chemicals containing α-hydroxyamide and α-carboxylic acid moieties.

Interestingly, even the Cu salts that have proven useful in the industrial production of acrylamide give unsatisfactory results in the synthesis of methacrylic amides.[7] As a result, most industrial practices for the generation of methacrylate monomers still rely on concentrated sulfuric acid. The industrial process by which methacrylates are synthesized is shown in Scheme 2.[1] In this route, acetone is reacted with HCN to form acetone cyanohydrin (ACH), which is then reacted with sulfuric acid at moderate temperature to form the sulfuric ester of 2-hydroxy-2-methyl-propionamide. Heating leads to the elimination of sulfuric acid (or water) forming the methacrylamide sulfate. In this process, the amide sulfate salt is then either hydrolyzed with water to form methyacrylic acid (MAA), or it is esterified with a mixture of water and methanol to form methyl methyacrylate (MMA) in very high yield (> 92 %). However, the mass

balance includes undesired sulfonates, oligomers, polymers, and ammonium hydrogen sulfate (AHS) generated as a result of the strongly acidic reaction conditions.

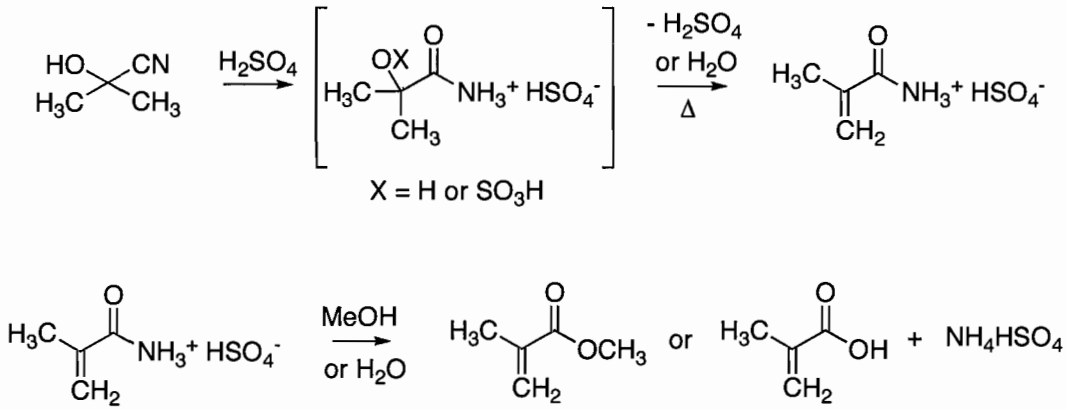

Scheme 2. Process for synthesizing methyl methacrylate (MMA) and methyl acrylic acid (MAA) using concentrated sulfuric acid.

The production of AHS is a major economic and environmental drawback of a large-scale sulfuric acid mediated process, because its disposal requires additional processing steps. The excess sulfuric acid used in the synthesis generates about 2.5 kg of AHS per kg of methacrylate product. The most common solution is to pyrolyze the AHS at around 1000 °C (Scheme 3). Pyrolysis releases SO_2, which upon oxidation to SO_3 is absorbed into water to form sulfuric acid. The sulfuric acid is then reused in the ACH process. This process is highly energy intensive and consumes copious amounts of natural gas as fuel for the pyrolysis. Ammonia is also formed but is not recovered because under these conditions it reacts with oxygen to form N_2. In an alternative

approach, the AHS is neutralized with ammonia to form ammonium sulfate, which has use as a fertilizer. As mentioned, there is considerable expense and effort associated with both of these methods, and so the elimination of AHS would allow for considerable savings and improvement in the industrial production of methacrylates. In view of the AHS by-product problem, there is a strong drive by methacrylate producers to find a replacement to the ACH process that does not involve sulfuric acid.

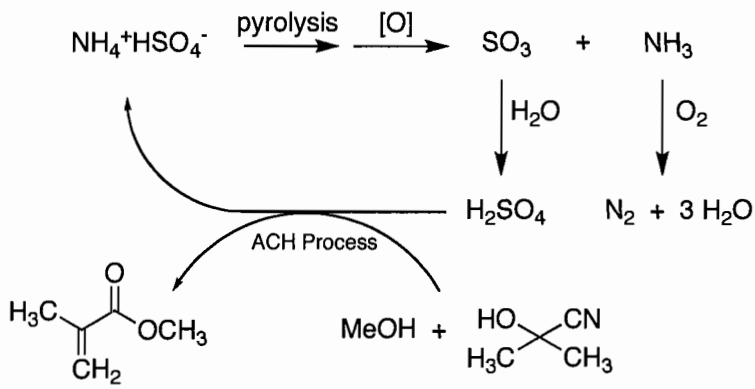

Scheme 3. Recycling scheme for ammonium hydrogen sulfate

Because Cu salts used in the production of acrylamides are ineffective in the conversion of ACH, several methacrylate manufacturers have opted to develop methods based on organic feedstocks other than nitriles. Among the new methods that have been proposed for the production of methacrylates are[1] i) a process using a direct catalytic oxidation of isobutylene or *t*-butanol, ii) the ammoxidation of *t*-butanol, iii) a method using ethylene, CO, and formaldehyde, originally developed by BASF for making

methacrolein and later refined by ICI, Ineos and Lucite for making MMA and MAA directly, iv) a route involving the direct oxidative esterification of methacrolein, developed by Asahi Chemical Co., and v) a process for the direct carbonylation of propyne (which is not viable due to a lack of sufficient feedstock). Despite considerable promise, each of these new processes has disadvantages that keep them from being widely adopted.

Mitsubishi Gas Chemical Company has developed a sulfuric acid-free ACH process using MnO_2,[7] and it is currently being used in the manufacture of methyl methacrylate.[1] In the Mitsubishi process (Scheme 4),[1] the hydration of ACH to α-hydroxyisobutyramide (HIBAM) is carried out catalytically using a slurry of MnO_2 in a water/acetone mixture. Methyl formate is used to esterify HIBAM to α-hydroxyisobutyrate, which generates formamide as a byproduct. Subsequent dehydration of α-hydroxyisobutyrate gives MMA, and heating of formamide releases HCN and water. The HCN produced in the thermal decomposition of formamide is recycled in the production of ACH. Thus, this process is advantageous for two reasons: 1.) The use of MnO_2 eliminates the generation of AHS. 2.) The use of methylformate allows the nitrogen in HIBAM to be captured as formamide and recycled into HCN. Interestingly, MnO_2 must be treated to modify its structure for optimal activity, which adds to overall manufacturing cost. Furthermore, even with treatment, the efficacy of the resulting catalyst is inconsistent from batch to batch, resulting in inconsistent product yields.[7] Because mechanistic investigations of heterogeneous catalytic systems are often ambiguous, the exact factors that affect the reactivity of these complexes toward

cyanohydrins have not been delineated. The reaction yields are improved by performing the reaction in acetone cosolvent; however, the use of excess acetone also increases production costs. Overall, the engineering costs associated with setting up this new ACH process make render it less cost effective than the current sulfuric acid chemistry employed.

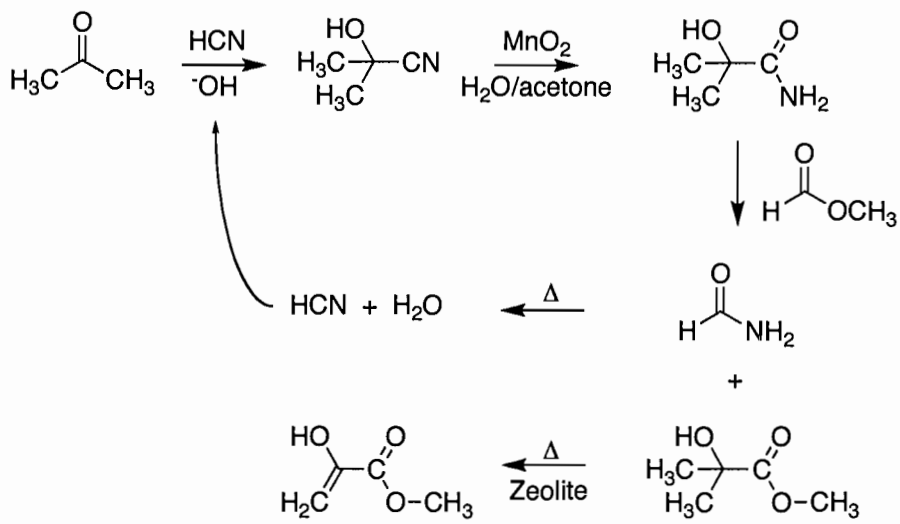

Scheme 4. The Mitsubishi ACH process for the manufacture of MMA and recycling of HCN.

Noteworthy examples of cyanohydrin hydration catalyzed by borate salts have also been disclosed in patents[19] and in the chemical literature,[20,21] but have not yet proven industrially viable. Borate salts are quite reactive toward cyanohydrins under alkaline conditions. Mechanistic investigations of the borates suggest that they activate the cyanohydrin by reacting with the cyanohydrin alcohol group to form a borate ester

(Scheme 5).[21] The activated cyanohydrin is then hydrated by transfer of a boron-bound hydroxide (Scheme 5a) or nucleophilic attack of a boron hydroxy group resulting in formation of either a five-membered intermediate (Scheme 5b). Discerning between these two mechanistic pathways has proven difficult, because both mechanisms involve negatively charged intermediates. Nonetheless, reaction of the hydroxy group with nitrile carbon is proposed to be rate determining, and the entropy of activation may distinguish between formation of the five-membered ring and hydroxide transfer. Activation parameters for the borate-catalyzed conversion have not been reported in the literature. The rates of hydration achieved using the borate salts are quite impressive (TOF = 0.25 hr^{-1} for ACH at 65 °C at pH = 8.9);[22] however, the low yields (70 – 80 %) and large amount of acetone cosolvent used in the conversion limit their practical utility.

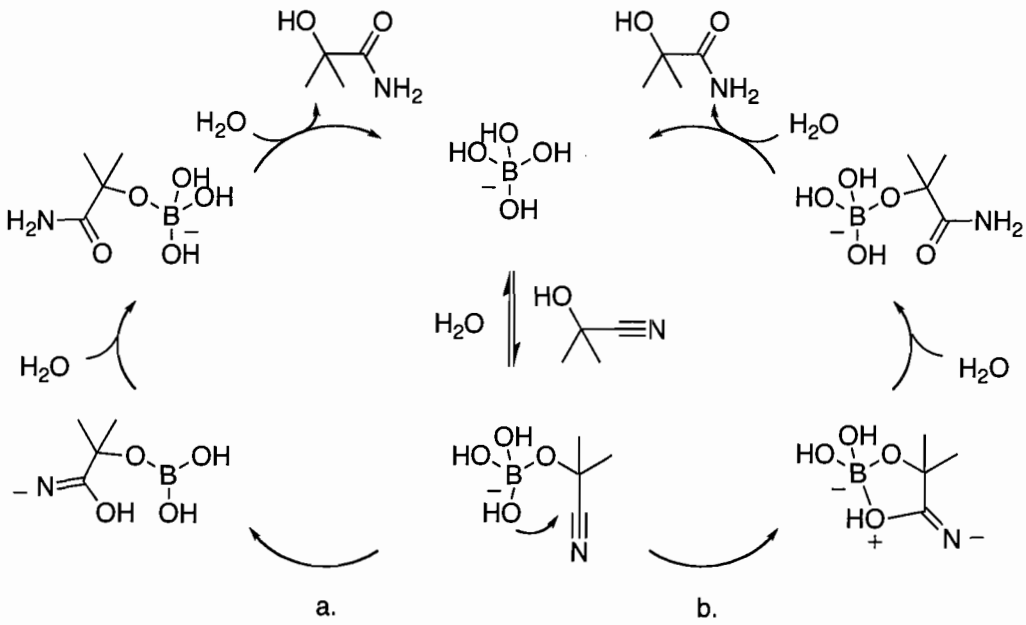

Scheme 5. Borate catalyzed hydration of ACH proceeding by (a) transfer of hydroxide from boron to the nitrile carbon and (b) attack of the boron hydroxy group to form a five membered ring.

Interestingly, several homogeneous transition metal nitrile hydration catalysts have proven useful in the regioselective conversion of acrylonitrile to acrylamide,[23,24] but these complexes have not been applied toward the hydration of cyanohydrins. This thesis describes the first thorough investigation of organometallic and coordination nitrile hydration catalysts (molybdocene and Pt phosphinito) in the hydration of ketone and aldehyde-derived cyanohydrins. Development of a low-cost, homogeneous, transition metal catalyst for the hydration of ACH in aqueous solution will provide a sulfuric acid-free route to the α-hydroxyamide product under mild conditions. Furthermore, the

electronic and structural environment of such a catalytic system can be tailored to afford a general synthetic route by which a range of chiral and achiral α-hydroxyamides, α-hydroxycarboxylic acids, and α-hydroxycarbocylic esters can be accessed. The homogeneous catalysts of interest are discussed in the following text.

1.3 Introduction to Molybdocene Nitrile Hydration Cataylsts

Investigations by our laboratory and others have demonstrated the impressive hydrolytic activity of water-soluble molybdocenes of the type $Cp^R_2Mo(OH)(OH_2)^+$ (where $Cp^R = \eta^5\text{-}C_5H_5$ or $\eta^5\text{-}C_5H_4Me$).[24-32] These molybdocene complexes promote the addition of water across C≡N,[24,31] C-O,[31] P-O,[25-27] and P-S[29,30] bonds in selected molecules containing these functional groups. The hydration and hydrolysis reactions were proposed to proceed via nucleophilic attack of the bound hydroxide on the activated organic substrate (e.g., see Scheme 6 for the case of nitrile hydration). As shown in Scheme 6, the inner-sphere coordination of solvent water to the molybdenum center is integral to the observed reactions. The aqua ligand of $Cp_2Mo(OH)(OH_2)^+$ is labile, and its dissociation provides a vacant site for the coordination of substrates. The metal-bound hydroxo ligand is quite nucleophilic and reacts with the coordinated substrate. Addition of the hydroxo ligand to the activated organic substrate provides a lower energy pathway to hydrolysis or hydration, yielding accelerations from $10^1 - 10^6 \times$ their normal rate.

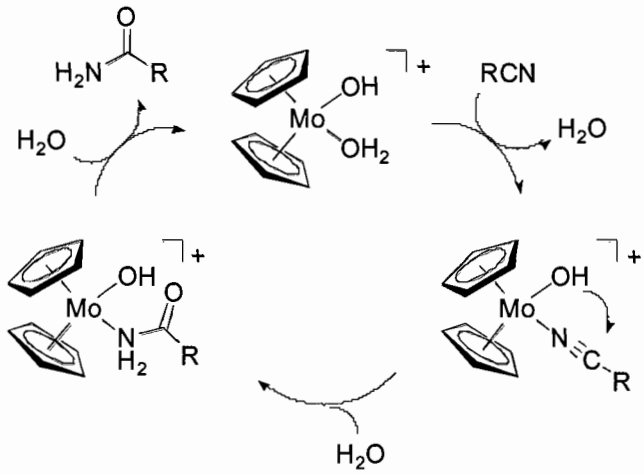

Scheme 6. Proposed mechanism for $Cp_2Mo(OH)(OH_2)^+$-catalyzed hydration of nitriles.

The hydration of C≡N bonds in nitrile substrates is selective affording amides without further hydration to the carboxylic acid, however, the complexes are not sufficiently active for commercial application.[24] (Only a ten-fold acceleration over base catalyzed hydration was observed for acetonitrile.) It is well known that the geometric and electronic environments of homogeneous catalysts can greatly affect their catalytic activity. Nevertheless, substituent effects had been unexplored in the aqueous catalysis of molybdocenes prior to the investigations reported herein. *ansa*-Ligands (bridged cyclopentadienyl rings; Figure 2b) offer a convenient method of altering the geometric structure and electronics of the cyclopentadienyl ligands without the use of substituents containing functional groups that may interfere with the catalyst active site. *ansa*-Bridged molybdocenes are also intriguing, because they have been shown to have a significant impact on the geometric structure, electronic structure, and reaction chemistry of molybdocenes.[33-45]

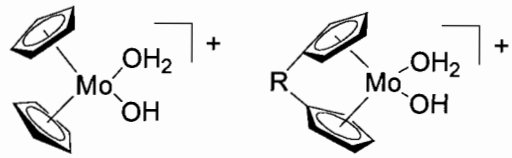

a. b.

Figure 2. Structures of (a) a water-soluble molybdocene catalyst and (b) a water-soluble *ansa*-molybdocene

1.3.1 Structure of ansa-Molybdocene Complexes

Changes in geometry of *ansa*-metallocene complexes are quantified by the geometric parameters shown in Figure 3. In an uncoordinated bidentate bis(cyclopentadienyl) ligand containing one bridging silicon or carbon atom, the interplanar-ring angle α is generally too large to accommodate a metal due to the tetrahedral geometry about the bridging atom. Consequently, binding to a metal can only be achieved by introducing some conformational strain about the metal center, the bridging atom(s), and the bridgehead (ipso) carbon leading to significant variations from the native metallocene structure. The most commonly used parameter is the bite angle, θ, which is the angle between the centroids of the ring and the metal center. The angle β represents the angle between the normals of the cyclopentadienyl rings. The degree of ring tilt in the system is represented by τ, which is $0.5(\theta-\beta)$. Lastly, geometric distortion about the bridging atom(s) as a result of binding to the metal center is reflected in the angle ε.

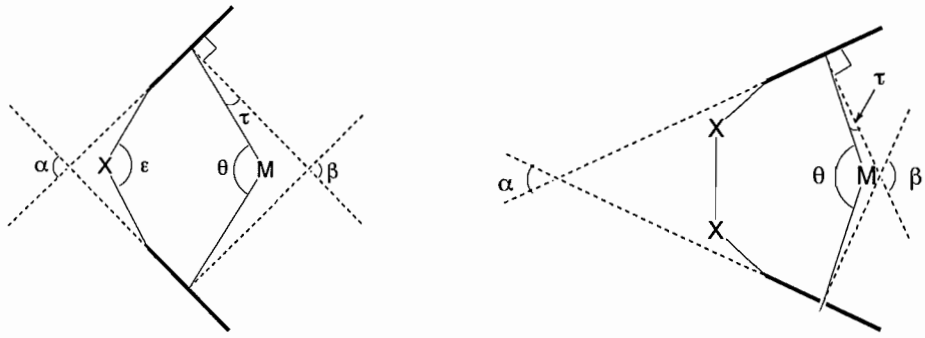

Figure 3. Angles commonly used to represent the effect of the interannular bridge

As shown in Table 1, the bite angles are the most distinctive parameter when comparing bridged and non-bridged molybdocene adducts; however, strain in the *ansa*-complexes is also evident in shortened molybdenum to ring normal distances, the distorted tetrahedral arrangement about the bridging atom ($\varepsilon < 109.5^{\circ}$), and ring tilt. The degree of distortion from the native metallocene structure is dependant on the identity of the bridging atom. The silicon-bridged molybdocenes made to date exhibit only a slight decrease in θ of 3° or less; while, the smaller carbon atom bridge results in a decrease in θ as great as 23° for $\{ CMe_2(C_5H_4)_2\}MoH_2$. The angle ε is reduced to 96° or less. Although it is not listed in Table 1, it is important to note that both the alkyl and silyl bridges are known to cause significant ring tilt; their crystals structures show decreased Mo-C bond lengths for the ipso carbon and adjacent carbons relative to the two distal carbons. Such variations are indicative of a shift toward η^3 coordination in the Cp rings. (A satisfactory comparison of ring tilt for the *ansa*-molybocenes listed was not possible

due discrepancies in the literature.) Surprisingly, the angles between the ancillary chloride ligands, X-Mo-X, appear unaffected by 'pulling back' the cyclopentadienyl rings. The M-X bond lengths are also comparable in all of the structures.

Table 1. Comparison of molybdocene dichlorides and dihydrides

Formula	Bite angle, θ	X-Mo-X, ϕ	M-X, Å	M-Cp, Å (⊥)	Cp-C_{br}-Cp	Refs
$(C_5H_5)_2MoCl_2$	130.9	82.0(2)	2.464(6), 2.470(5)	1.98, 1.97		46
$\{(C_5H_4)_2C(C_4H_8)\}MoCl_2$, **III**	114.6	82.66(2)	2.4621(4), 2.4694(4)	1.949, 1.950	93.6	41
$\{(C_5Me_4)_2SiMe_2\}MoCl_2$, **V**		82.56	2.4446, 2.4517		88.02	45
$(C_5H_5)_2MoH_2$	145.8	75.5(3)	1.685(3)	1.942, 1.946		47
$\{(C_5H_4)_2CMe_2\}MoH_2$, **II**	121	80.3	1.66(5), 1.72(7)	1.913, 1.912	96.0	40
$\{(C_5H_4)_2SiMe_2\}MoH_2$, **VI**	142.91		1.67(3), 1.70(3)		94.26	48

The geometric and electronic structural changes imparted by *ansa*-bridge ring substituents[13] can lead to radically different reactivity at the molybdenum center and possibly enhanced reaction rates. Various adducts of the bridged molybdocene complexes **I** – **VI** shown have been reported to date. Based on data from analogous *ansa*-tungestenocene and zirconocene systems,[33,37] *ansa*-molybdocenes containing an ethylene bridge are expected to have bite angles comparable to that of silyl-bridged complexes.

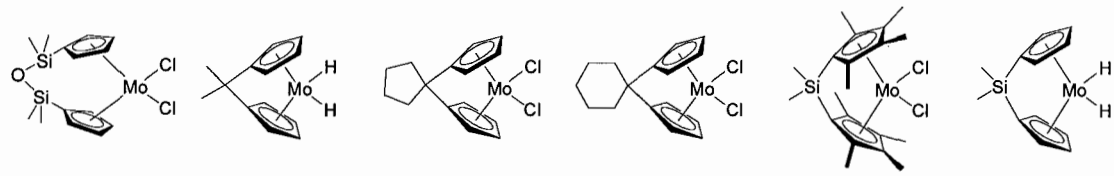

I II III IV V VI

1.3.2 Reactivity of ansa-Molybdocenes

Green and Parkin have spearheaded investigations into the *ansa*-effect (the effect of the interannular bridge on the geometry, electronics, and reactivity of a metallocene) in molybdocene chemistry by exploring the reactivity of *ansa*-molybdocene complexes **II** and **V** in organic solvents. They have reported accounts of fascinating reactivity unprecedented by non-bridged molybdocenes.[35,36,39,40,42,45] For example, molybdocene complexes react photochemically to form dimeric or tucked in $\eta^1\eta^5$- species in the presence of organic solvents such as benzene and acetonitrile as illustrated in Scheme 7.[49,50] The *ansa* complexes **II** and **V**, however, have been shown to activate the C-H bond in benzene and the C-C bond in acetonitrile, respectively, under the same conditions.[40,45] The dimethylsilyl bridged complex **V** has also been reported to activate the C-S bond in thiophene, which may be useful for the industrial hydrodesulfurization process.[36] Moreover, dihydrides of **II** and **V** are protonated to yield dihydrogen-hydrides as the thermodynamic product; whereas, non-bridged dihydrides oxidatively add H_2 to give Mo(VI) trihydrides.[39,42] (See Schemes 7, 8, and 9.) These *ansa*-molybdocene trihydrides are the only examples of complexes of the d^2 electronic configuration with a cis geometry observed to date. These reports demonstrate two fundamental effects of the

one atom interannular bridge on molybdocenes: the reactivity of *ansa*-complexes is significantly different in reactions that proceed through the 16e⁻ metallocene intermediate (i.e., reductive elimination), and that complexes with extremely poor π-acceptors ligands are stabilized by the *ansa*-bridge.

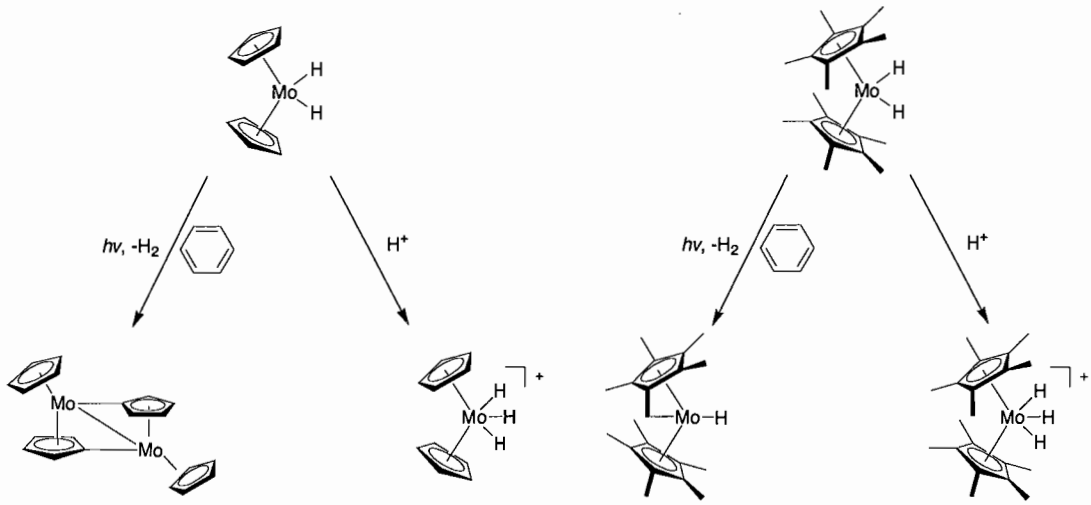

Scheme 7. Photolysis of $CpMoH_2$ and Cp^*MoH_2 in benzene solvent.

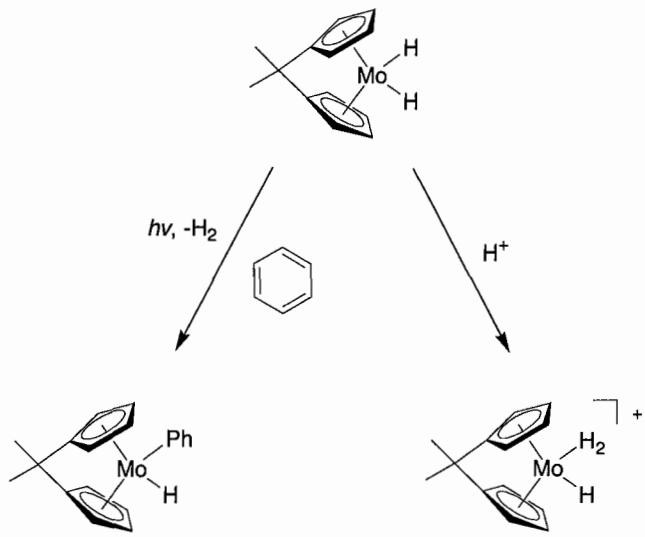

Scheme 8. Photolysis of *ansa*-{$CMe_2(C_5H_4)_2$}MoH_2 in benzene solvent affording oxidative addition of benzene as well as protonation of the *ansa*-{$CMe_2(C_5H_4)_2$}MoH_2 to give the nonclassical trihydride *ansa*-{$CMe_2(C_5H_4)_2$}$Mo(\eta^2\text{-}H_2)(H)$.

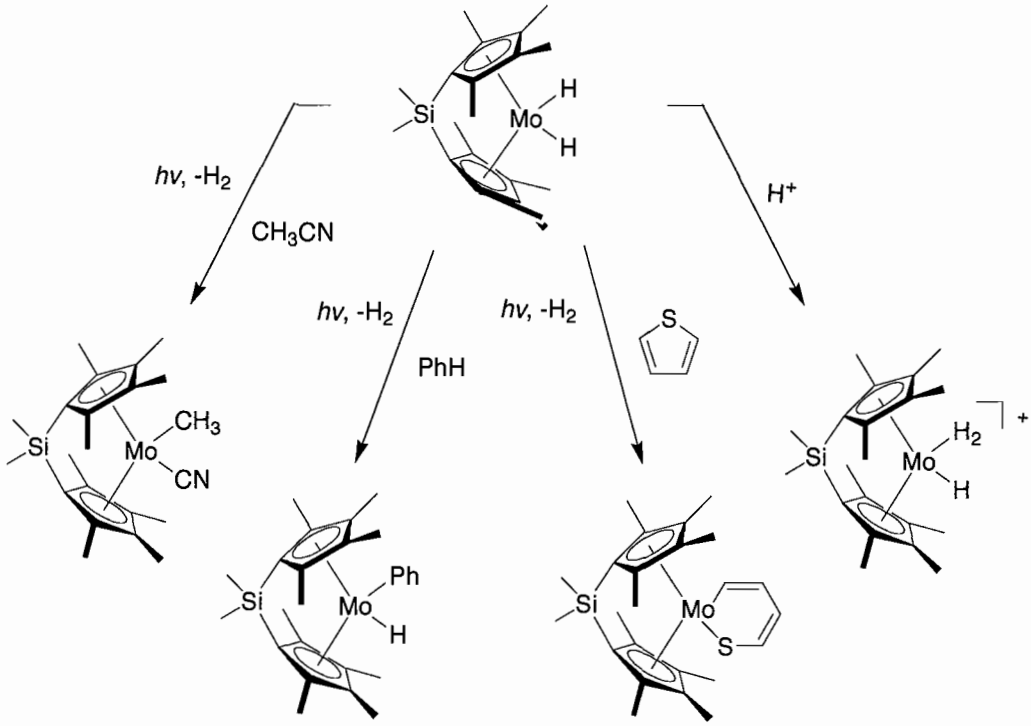

Scheme 9. Photolytic oxidative addition of acetonitrile, benzene and thiophene to *ansa*-$\{SiMe_2(C_5Me_4)_2\}MoH_2$ and protonation of $\{SiMe_2(C_5Me_4)_2\}MoH_2$ to give the nonclassical trihydride $\{SiMe_2(C_5Me_4)_2\}Mo(\eta^2\text{-}H_2)H$.

1.3.3 Electronic Consequences of the ansa-Bridge

Green has performed theoretical and computational studies to explain the electronic consequence of structural changes.[51] She reports that the distinct reactivity exhibited by the strained complexes can be explained by relatively high energy frontier molecular orbitals in the $16e^-$ *ansa*-metallocene fragment relative to the non-bridged metallocene fragment. The changes in the frontier molecular orbitals of the 16 e^- metallocene fragment for a linear (D_{5h}) and bent metallocene (C_{2v}) are illustrated in

Figure 4. As the metallocene symmetry is lowered from D_{5h} to C_{2v}, two of the three highest occupied molecular orbitals (a_1 and e_2) mix and become the same symmetry (a_1). One of the orbitals becomes the $3a_1$ and is slightly lowered in energy. The other orbital, $4a_1$, is significantly raised in energy. The third HOMO (the degenerate e_2 orbital) becomes the $2b_1$ orbital and is slightly destabilized to give the splitting shown in Figure 4. Due to the relative energies of the frontier molecular orbitals, a bent metallocene (containing one or two d electrons) must rearrange to the more stable parallel structure upon reductive elimination to avoid occupation of the high-energy $2b_1$ and $4a_1$. However, the restraints enforced by an *ansa*-bridge prevent such rearrangement; thus, the activation barrier to reductive elimination is much higher for an *ansa*-metallocene than for a non-bridged metallocene. When the 16 e^- *ansa*-metallocene intermediate is accessible (as in the case of the *ansa*-molybdocenes discussed above), it is extremely reactive.

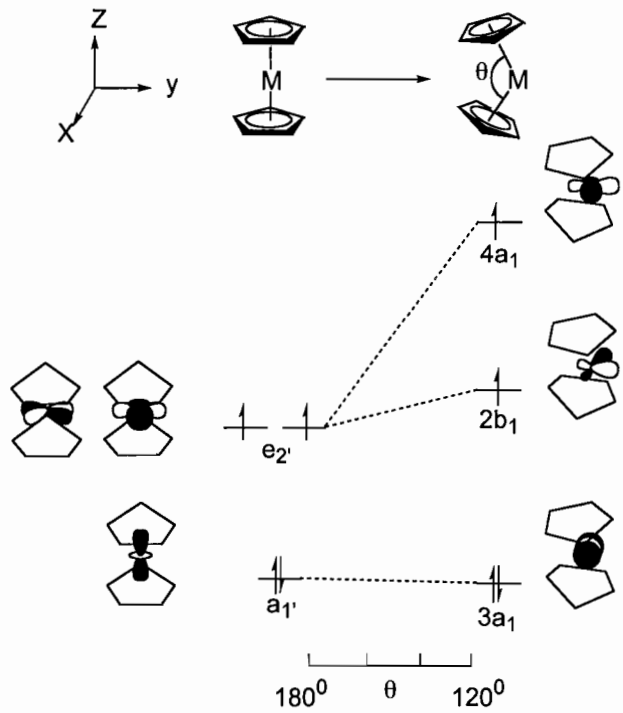

Figure 4. Change in frontier orbitals of the Cp_2M fragment in going from D_{5h} to C_{2v} symmetry.

Additional stabilization of the $3a_1$ orbital is achieved in *ansa*-compounds containing one-bridging atom due to overlap with the a_1 orbital of the bridged ligand (Figure 5A).[33] This bonding interaction creates a lower lying acceptor orbital in which the Cp rings are in an eclipsed conformation with the vertices pointed towards the back of the metallocene wedge. The energy and orientation of the a_1 ligand acceptor orbital enables optimal interaction with filled metal $3a_1$ orbital (Figure 5B) leading to enhanced back-donation and a more acidic metal center. Greater overlap between the Cp ligand acceptor and the metal orbital is achieved as the cyclopentadienyl ligands become closer

together (i.e., θ decreases and τ increases). This phenomenon is thought to contribute to the increased stability of the dihydrogen-hydride molybdocene complexes discussed above; stabilization of the lone pair reduces back-donation into the H_2 σ^* orbital and prevents oxidative addition to the trihydride.[42]

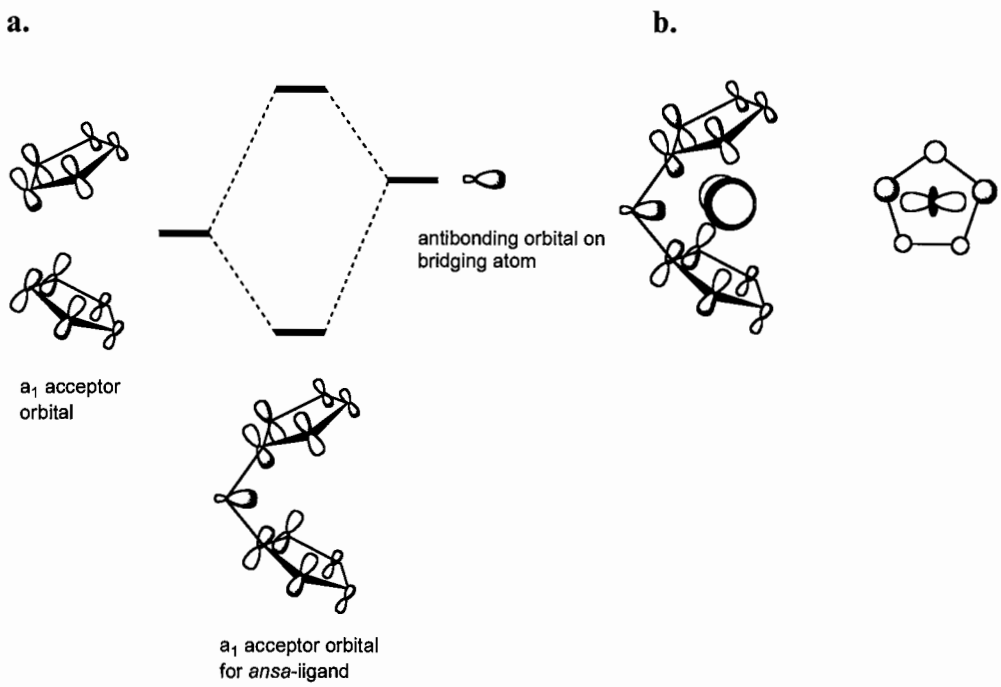

Figure 5. (a.) Interaction of antibonding orbitals of the cyclopentadienyl a_1 and the bridging atom to give a lower lying p-acceptor orbital and (b.) side and top views of the back bonding from the metal-based $3a_1$ into the ligand a_1 acceptor orbital[33]

The studies reported herein were conducted in order to investigate the reactivity of the more electrophilic metal center of *ansa*-molybdocenes in aqueous-phase hydration and hydrolysis reactions. As discussed above, the general mechanism of

$Cp^{(')}_2Mo(OH)(OH_2)^+$-mediated hydrolysis ($Cp^{(')}$ = η^5-C_5H_5 or η^5-C_5H_4Me) is Lewis acid activation of the substrate followed by intramolecular attack of the coordinated hydroxo ligand (Scheme 6).[31] In prior studies, improved catalytic performance was noted for transformations of nitriles containing electron-withdrawing groups due to a greater positive charge on the electrophilic carbon center (which bodes well for the catalytic hydration of cyanohydrins).[24] For similar reasons, it was postulated that a more electrophilic metal center might also lead to enhanced activation of the substrate and enhanced reactivity. Alternatively, a more electrophilic metal center will also influence the rate of attack by a coordinated nucleophile. To investigate the effect of the more electrophilic metal center of the *ansa*-molybdocenes, the previously unexplored ethylene-bridged *ansa*-molybdocene [{$C_2Me_4(\eta^5$-$C_5H_4)_2$}$Mo(OH)(OH_2)$][OTs] and its related binuclear analog [{$C_2Me_4(\eta^5$-$C_5H_4)_2$}$Mo(\mu$-$OH)]_2$[OTs]$_2$ were prepared (Figure 6). *ansa*-Molybdocenes containing two bridging atoms were absent from the literature prior to this investigation. Consequently, considerable effort was devoted to determining the structural and electronic effect of the ethylene bridge. In the following chapters, the synthesis, characterization, aqueous behavior, and catalytic activity of the complexes are explored and compared to that of the non-*ansa* molybdocenes [(η^5-$C_5H_5)_2Mo(OH)(OH_2)$][OTs] and [(η^5-$C_5H_4Me)_2$}$Mo(OH)(OH_2)$][OTs] (and the respective dimers).

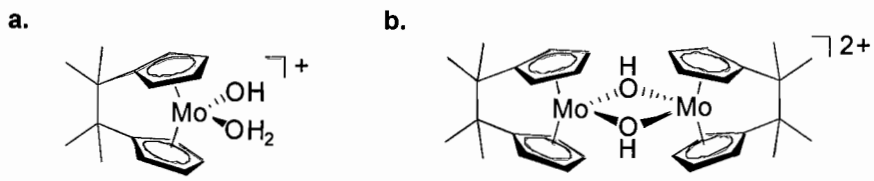

Figure 6 (a) The water-soluble ethylene-bridged molybdocene catalyst [{$C_2Me_4(\eta^5$-$C_5H_4)_2$}Mo(OH)(OH_2)][OTs] and (b) its binuclear analog [{$C_2Me_4(\eta^5$-$C_5H_4)_2$}Mo(μ-OH)]$_2$[OTs]$_2$.

1.3.4 Aqueous Behavior of Molybdocene

The aqueous behavior of the molybdocene is significantly affected by substituents on the Cp rings.[52] Changes in the aqueous-phase behavior of the molybdocene complexes are relevant to its hydrolytic behavior, because the inner-sphere coordination of solvent water to the molybdenum center is integral to the observed reactions (vide supra). As shown in Scheme 10, the active molybdocene catalyst is related to several other molybdocene species by a series of reversible hydrolysis and protonation reactions.[52,53] From an applications standpoint, each of the equilibrium processes in Scheme 10 (dimerization, protonation, or deprotonation) serves to complicate kinetic analysis and to reduce the rates of hydration or hydrolysis by altering the identity of the catalyst. For example, the rates of molybdocene-promoted ester hydrolysis and nitrile hydration were slower at low and high pH, and fastest at pH 6 and pH 7.[24,26] Based on the pK_a values measured for complex **2** (5.5 and 8.5 ± 0.3), it was speculated that lower rates are measured at acidic pH due to protonation of the hydroxo nucleophile to give the

less reactive aqua ligand. At high pH, the aqua ligand of the $Cp_2Mo(OH)(OH_2)^+$ is deprotonated to give a second M-OH bond. The hydroxo ligand is relatively inert to substitution by the aforementioned organic molecules, and therefore the rate rapidly falls off above pH 8. Because these equilibria can adversely affect reaction rates, a thorough investigation of the equilibrium behavior of the variously substituted molybdocene complexes was warranted. The equilibrium studies conducted herein helped to delineate rate changes due to changes in the equilibrium parameters in Scheme 10 (i.e. K_{eq} and pK_a) and those due to changes in electronic structure of the molybdocene catalysts.

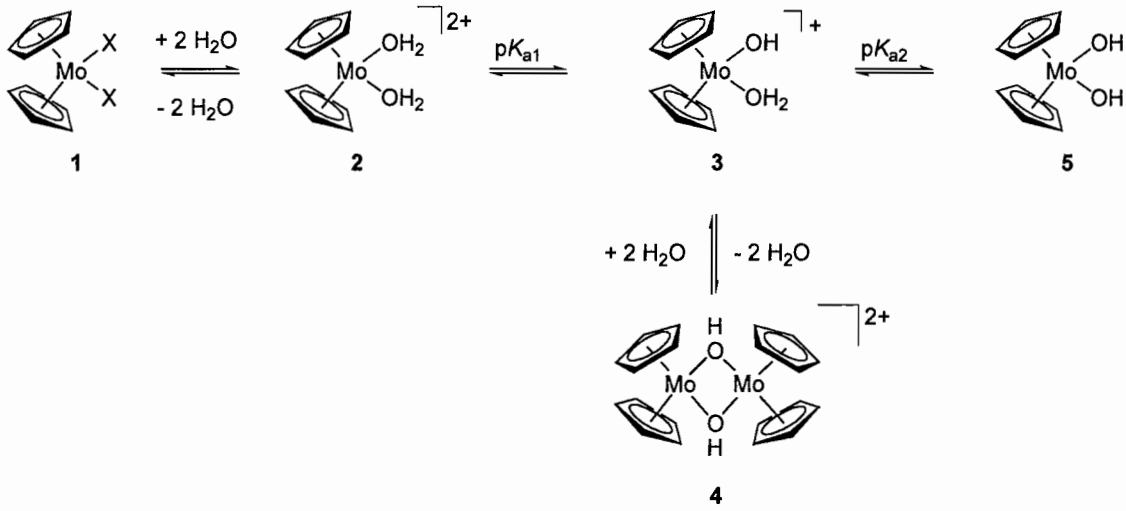

Scheme 10. Equilibria established by molybdocene complexes in water.

1.4 Pt Phosphinito Nitrile Hydration Catalysts

Of the transition metal complexes reported in the literature, the Pt phosphinito complexes, $[PtX(PR_2OH)\{(PR_2O)_2H\}]$ where x = Cl or H, first developed by Parkins and coworkers[22,23,54] are the most reactive and versatile in aqueous-phase nitrile hydrations.

For example, acrylonitrile is hydrated regioselectively to acrylamide in refluxing aqueous ethanol at a turnover frequency of 0.5 s^{-1} using only 0.015 mol % of [PtCl(PMe-$_2$OH){$(PMe_2O)_2H$}].[23] Moreover, the catalyst is long lived, and turnovers up to 7.7×10^4 were observed. These highly active Pt phosphinito complexes were proposed to activate nitrile substrates by intramolecular attack of the phosphine hydroxy group on the nitrile carbon (Scheme 11). If the [PtCl(PMe_2Ph){$(PMe_2O)_2H$}] complex is used, wherein PMe_2OH is replaced by PMe_2Ph, the turnover frequency is reduced by a third; however, the reaction still proceeds. Although the reduction in the reaction rate was attributed to the reduced availability of the phosphine hydroxy group in the PMe_2Ph substituted analog, it may also be due to the increase steric bulk of the catalyst. Because the sterics of the catalyst were so drastically altered in the [PtCl(PMe_2Ph){$(PMe_2O)_2H$}] complex, the published interpretation should be considered with caution.

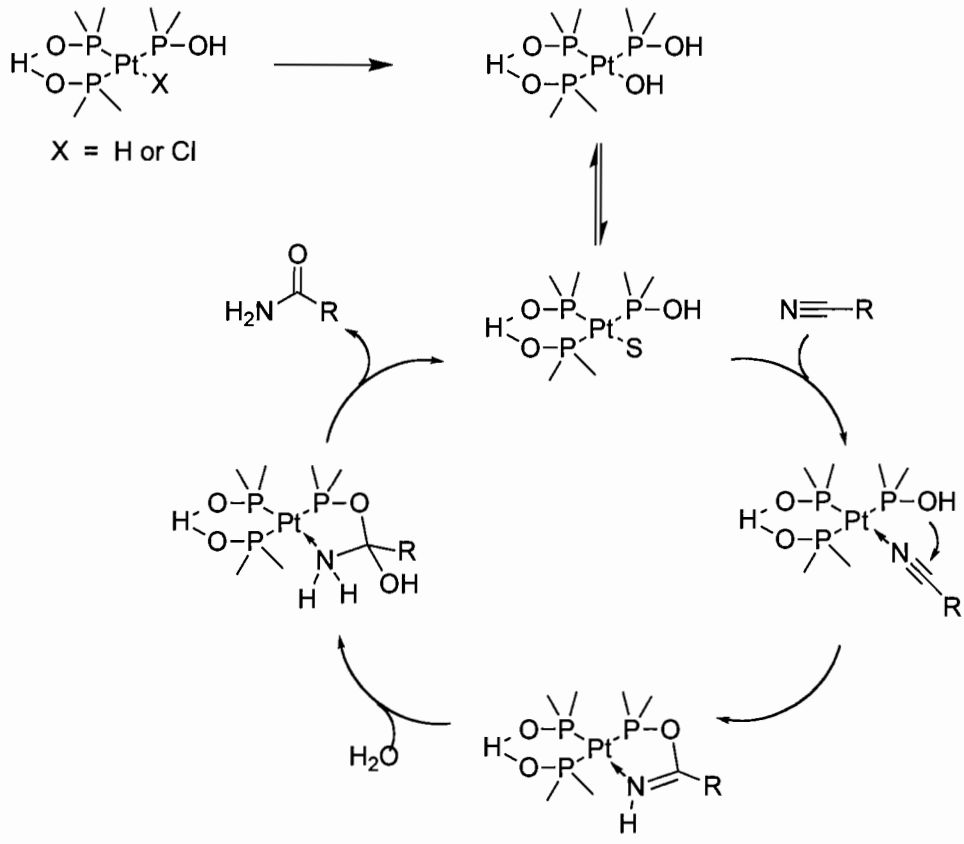

Scheme 11. Mechanism of [PtX(PMe$_2$OH){(PMe$_2$O)$_2$}]-catalyzed nitrile hydration proposed by Ghaffar et al.[23,54]

Cobley et al. extended the utility of this class of molecules to the hydrolytic amidation of nitriles to N-substituted amides using alkylamines.[55] Further work done by Jiang et al. demonstrated that the Pt phosphinito complexes are also efficient in the hydration of bulky nitriles and those containing acid- or base-sensitive functionalities (i.e. ether and carbohydrate functionality),[56] which typically show very low reactivity and selectivity with other nitrile hydration catalysts. The broad applicability and high activity

of the Pt phosphinito complexes toward nitrile substrates makes them excellent candidates for catalytic conversions of cyanohydrins.

1.5 Summary

The development of industrially viable transition metal catalyzed processes for the conversion of cyanohydrins to α-hydroxyamides would provide a greener synthetic route to methyacrylate monomers. Consequently, the reactivity of molybdocene and Pt phosphinito nitrile hydration catalysts toward cyanohydrins was explored.

These studies began with an effort to enhance the reactivity of the molybdocene catalyst by altering the electronics of the ancillary Cp ligands. This dissertation describes the synthesis and characterization of the tetramethyethylene-bridged *ansa*-molybdocene complexes $[\{C_2Me_4(\eta^5\text{-}C_5H_4)_2\}Mo(OH)(OH_2)][OTs]$ and its related binuclear analog $[\{C_2Me_4(\eta^5\text{-}C_5H_4)_2\}Mo(\mu\text{-}OH)]_2[OTs]_2$. Comparison of the *ansa*-molybdocene complex to several non-*ansa* moylbdocene analogs was made in order to access the effect of Cp ring substituents on the electronic structure, geometry, aqueous behavior, and the reactivity molybdocenes complexes.

In Chapter V, a thorough investigation of the reactivity of molybdocene and Pt phosphinito catalysts with cyanohydrin substrates was conducted. This investigation is the first of its kind, and the results reported herein provide useful information on the challenges involved with hydration of cyanohydrins catalyzed by transition metals. Elucidation of these challenges will expedite the innovation of an industrially viable process for production of methacrylate monomers using homogeneous organometallic or coordination catalysts.

1.6 Acknowledgments

This dissertation contains my co-authored material. Authorship of Chapter II is shared with David Tyler, my advisor, and Lev Zakharov, who obtained the crystallographic information contained therein. Authorship of Chapter III is shared with David Tyler, my advisor. Authorship of Chapter IV is shared with my advisor, David Tyler, and Gregory Baxley, who performed titration experiments reported for the Cp_2MoO complex. Authorship of Chapter V is shared with Brandy Fox, who obtained the ^{13}C NMR data summarized in Table 2, studied the degradation of the Pt phosphinito complex in the presence of Ag salts, and contributed significantly to the intellectual development of the work. Spring Knapp contributed to the experiments reported in Chapter V by testing the effect of Hg on the rate of Pt-catalyzed acetonitrile hydration. Authorship of Chapter V is also shared with Jerrick Juliette, an industrial partner from Rohm and Haas, who contributed to the intellectual development of the project and my advisor, David Tyler. Lev Zakharov collected all of the crystallographic data collected in Appendices A and C.

CHAPTER II

SYNTHESIS, CHARACTERIZATION, AND REACTIVITY OF TETRAMETHYLETHYLENE-BRIDGED MOLYBDOCENES: INVESTIGATION OF THE EFFECT OF AN *ANSA*-BRIDGE ON THE HYDROLYTIC ACTIVITY OF MOLYBDOCENE CATALYSTS

2.1 Introduction

Molybdocenes containing aqua and hydroxo ligands are water-soluble, and several such complexes have been extensively used as catalysts and mediators in aqueous-phase reactions.[1-12] The $Cp_2Mo(OH)(OH_2)^+$ complex was the first organometallic complex reported to hydrolyze phosphate esters[7,10,11] at rates comparable to the excellent Co(III) amine hydrolysis catalysts studied by Chin et al.[13] Later investigations of the $Cp'_2Mo(OH)(OH_2)^+$ ($Cp' = \eta^5$-C_5H_4Me) complex (Figure 1a) in our laboratory extended the utility of the molybdocenes to catalytic hydration[2,3] and H/D exchange reactions,[4-6] the latter being one of the few examples of C-H bond activation in water. Ongoing efforts to exploit molybdocenes for environmentally benign transformations of organic substrates have continued with an exploration of the electronic

and steric effects of substituted cyclopentadienyl ligands on the reactivity of the molybdocenes. *ansa*-Ligands (bridged cyclopentadienyl rings; Figure 1b) offer a convenient method of altering the geometric structure and electronics of the cyclopentadienyl ligands without the use of substituents containing functional groups that may interfere with the catalyst active site.

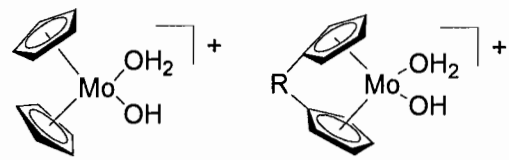

a. b.

Figure 1. Structures of (a) a water-soluble molybdocene catalyst and (b) a water-soluble *ansa*-molybdocene

ansa-Bridges were shown to have a significant impact on the geometric structure, electronic structure, and reaction chemistry of molybdocenes.[14-26] Molecules with one-atom bridges (the type most commonly studied) significantly reduce the bite angle of the metallocene moiety and enhance the bonding of the Cp rings to the metal center. The stronger Cp-M bonds in these molecules were recently shown to be the result of a more stable acceptor orbital on the Cp ligand with consequent increased back-donation from the metal center.[27] In a Mo(IV) metallocene, this results in an even more electrophilic metal center.[17]

The studies reported herein were conducted in order to investigate the reactivity of the more electrophilic metal center of *ansa* molybdocenes in aqueous-phase hydration

and hydrolysis reactions. As discussed in Section 1.3, the general mechanism of $Cp^{(')}_2Mo(OH)(OH_2)^+$-mediated hydrolysis ($Cp^{(')} = \eta^5$-C_5H_5 or η^5-C_5H_4Me) is Lewis acid activation of the substrate followed by intramolecular attack of the coordinated hydroxo ligand (Scheme 1).[2] In prior studies, improved catalytic performance was noted for transformations of nitriles containing electron-withdrawing groups due to a greater positive charge on the electrophilic carbon center.[3] For similar reasons, it was postulated that a more electrophilic metal center might also lead to enhanced activation of the substrate and enhanced reactivity. Alternatively, a more electrophilic metal center will also influence the rate of attack by a coordinated nucleophile.

Other molecular parameters may influence the rate, as well. Investigations of Co(III)-,[13,28,29] Ir(III)-,[30] Cu(II)-,[31-35] and Zn(II)-catalyzed[36-40] hydrolysis reactions that proceed by intramolecular nucleophilic attack demonstrated that the rate of hydrolysis can be affected by 1) the acidity of the protonated hydroxo nucleophile, 2) the tendency of the active catalyst to dimerize, and by 3) steric changes that lead to stabilization of the cyclic intermediate. As illustrated in Scheme 1, the acidity of the protonated nucleophile (pK_a) and the tendency of the catalyst to dimerize (K_{eq}) will effect the reaction rate by altering the concentration of active catalyst in solution; whereas, stabilization of the cyclic intermediate will actually facilitate intramolecular nucleophilic attack. With regard to the first of these factors in the molybdocene-catalyzed reactions, note that the protonated nucleophile in water-soluble molybdocene complexes is relatively acidic ($pK_{a1} \sim 5.5$). Therefore, the expected decrease in the pK_a of the relatively electrophilic *ansa* complex is not expected to influence the concentration of the active catalyst or the

reactivity of the molybdocene at neutral pH. As for the second factor, the tendency of the molybdocenes to dimerize may influence the rate of catalysis and must be taken into account. Lastly, because *ansa* linkages are known to alter the geometric structure of metallocenes, any structural changes in the *ansa* complex must be carefully analyzed to determine their significance.

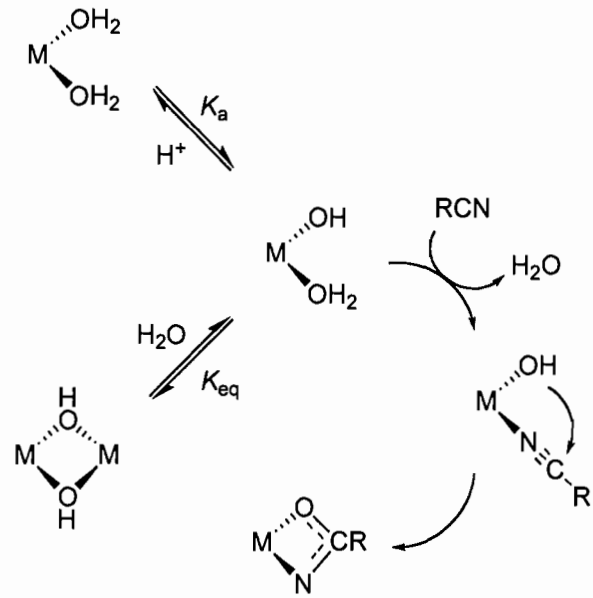

Scheme 1. Proposed mechanism of intramolecular nucleophilic attack on nitrile substrate.

In an initial study of how a more electrophilic molybdocene complex reacts toward intramolecular nucleophilic attack, the silyl-bridged *ansa*-molybdocene $[SiMe_2(C_5H_4)_2Mo(OH)(OH_2)][OTs]$ was studied.[1] Unfortunately, the Si-Cp bonds of $[SiMe_2(Cp_2Mo(OH)(OH_2)]^{2+}$ were unstable to hydrolysis, and an aqueous solution of the

complex readily degraded to give the $[Cp_2Mo(OH)(OH_2)]^+$ and $[Cp_2Mo(\mu\text{-}OH)]_2^{2+}$ complexes. To avoid problems associated with the hydrolysis of C-Si bonds, the previously unexplored ethylene-bridged *ansa*-molybdocene $[\{C_2Me_4(\eta^5\text{-}C_5H_4)_2\}Mo(OH)(OH_2)][OTs]$ and its related binuclear analog $[\{C_2Me_4(\eta^5\text{-}C_5H_4)_2\}Mo(\mu\text{-}OH)]_2[OTs]_2$ were prepared (Figure 2). In addition to being less susceptible to hydrolysis, the ethylene bridges were also chosen because they generally induce minimal structural changes in the bite-angles and ring-tilts of bent metallocenes,[27] thereby avoiding the large structural changes caused by one-atom *ansa* bridges. The changes in reactivity for an ethylene-bridged *ansa*-catalyst, therefore, can be solely attributed to electronic changes at the metal center and not to steric changes. The results reported below expand our understanding of the reactivity of substituted molybdocenes as well as the general *ansa*-effect in molybdocene systems. (In this paper, "substituted molybdocenes" refers to substitution on the cyclopentadienyl rings. Likewise, "unsubstituted" refers to a molecule with η^5-C_5H_5 rings.)

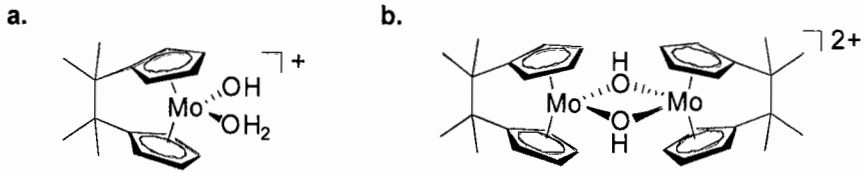

Figure 2. (a) The water-soluble ethylene-bridged molybdocene catalyst [{$C_2Me_4(\eta^5$-$C_5H_4)_2$}Mo(OH)(OH_2)][OTs] and (b) its binuclear analog [{$C_2Me_4(\eta^5$-$C_5H_4)_2$}Mo(μ-OH)]$_2$[OTs]$_2$.

2.2 Experimental

2.2.1 General Procedures

All experiments were performed under a nitrogen atmosphere using a glovebox or a Schlenk line. All solvents were dried and distilled from appropriate drying agents. Solvents and substrates were then purged with nitrogen or degassed using three freeze-pump-thaw cycles. Solutions buffered to pD 6.8 were prepared by dissolving N-morpholinopropylsulfonic acid (MOPS) hemisodium salt in D_2O. The compounds $C_2Me_4(C_5H_4MgCl)_2$,[41] $MoCl_4$·dme,[42] [$Cp_2Mo(\mu$-OH)]$_2$[OTs]$_2$,[43] and [$Cp'_2Mo(\mu$-OH)]$_2$[OTs]$_2$[44] were prepared as described in the literature.

All hydrolysis and hydration reaction samples were prepared in a glovebox under an atmosphere of N_2 in Wilmad 9 in. precision NMR tubes or Wilmad J-Young screw cap NMR tubes. Reactions carried out in the Wilmad 9 in. NMR tubes were flame sealed while frozen. Reaction tubes were heated in an oil bath. ^{1}H NMR spectra were obtained using a Varian Inova 500 MHz (500.104 MHz for ^{1}H and 125.764 MHz for ^{13}C) or 600

MHz NMR spectrometer (599.982 MHz for ^{1}H and 150.879 MHz for ^{13}C). ^{1}H NMR resonances were integrated relative to the 7.657 ppm tosylate peak from the catalyst counter ion or to the 2.10 ppm MOPS buffer resonance. Phosphate ester hydrolysis was monitored using a Hewlett Packard 8453 UV/Vis spectrophotometer. IR spectra were obtained using a Nicolet Magna IR 530 spectrometer.

2.2.2 Synthesis of [{$C_2Me_4(\eta^5$-$C_5H_4)_2$}$MoCl_2$] (1)

The following preparation was adapted from that reported by Green et al.[23] for the analogous tungsten complex. Approximately 300 mL Et_2O was added to a previously stirred mixture of $MoCl_4$·dme (7.8 g, 24 mmol) and $C_2Me_4(C_5H_4MgCl)_2$ (15 g, 24 mmol) to obtain a grayish brown suspension. After 3 days, the solvent was removed from the red-brown suspension in vacuo, leaving a pale, pink-brown solid that was extracted with toluene in a Soxhlet apparatus for 24 hours. The toluene was removed under reduced pressure, and the red-brown solid was washed with hexanes to yield 2.3 g (26 %) of {$C_2Me_4(\eta^5$-$C_5H_4)_2$}$MoCl_2$ as a fine brown powder. ^{1}H NMR ($CDCl_3$): δ 6.14 (m, 4, C_5H_4), 5.84 (m, 4, C_5H_4), 1.00 (s, 12, C_2Me_4). ^{13}C-{^{1}H} NMR ($CDCl_3$): δ 127.59 (s, C_5H_4, C_{ipso}), 122.41 (s, C_5H_4), 82.95 (s, C_5H_4), 45.89 (s,C_2Me_4) , 27.45(C_2Me_4). Anal. Found: C, 52.53; H, 5.87; Cl, 17.61. Calculated for $C_{16}H_{20}Cl_2Mo$.20 C_7H_8: C, 52.56; H 5.48; Cl, 17.83.

2.2.3 Synthesis of [{$C_2Me_4(\eta^5$-$C_5H_4)_2$}MoH_2] (2)

A suspension of $NaBH_4$ (0.80 g, 21 mmol) in THF was added to a solution of **1** (2.0 g, 5.3 mmol) in THF dropwise at -78 °C. The brown suspension was allowed to warm to room temperature and stirred overnight. After removing the THF under reduced

pressure, the orange solid was extracted into benzene and pumped to dryness leaving an oily orange solid. The [{$C_2Me_4(\eta^5\text{-}C_5H_4)_2$}$MoH_2$] thus obtained (0.850 g, 52 %) was not purified further but immediately used to generate complexes **3** and **5**, as described in the next section. However, compound **2** may be sublimed at 110 °C at 1 torr, but this decreases the yield considerably. The ^1H and ^{13}C NMR spectra for **2** are provided in the Supporting Information and show the material obtained by sublimation is spectroscopically pure. ^1H NMR (C_6D_6): δ 4.92 (m, 4, C_5H_4), 4.69 (m, 4, C_5H_4), 0.75 (s, 12, C_2Me_4), -6.88 (2, s, MoH_2). ^{13}C-{^1H} NMR (THF-d_8): δ 106.82 (s, C_5H_4, C_{ipso}), 82.99 (s, C_5H_4), 72.94 (s, C_5H_4), 46.32 (s,C_2Me_4) , 27.23(C_2Me_4). IR (Nujol mull): 1774 cm^{-1} (ν(Mo-H)).

2.2.4 Synthesis of [{$C_2Me_4(\eta^5\text{-}C_5H_4)_2$}$Mo(\mu\text{-}OH)]_2[OTs]_2$ (5)

This synthesis were adapted from the preparation of [$Cp'_2Mo(\mu\text{-}OH)]_2[OTs]_2$.[44] A solution of *p*-toluenesulfonic acid monohydrate (0.48 g, 2.5 mmol) in acetone:water (70 mL/0.70 mL) was added to the orange solid (0.850 g, 2.7 mmol) obtained by the preceding description . The orange-red solution was refluxed for 8 hours, during which time a gray-green suspension formed. The solvent was removed under reduced pressure to leave a light, brown-grey solid that was rinsed with benzene and hexanes. As discussed in the Results and Discussion section, this procedure, which with non-*ansa* Cp ligands gives dimer complexes of the type [$Cp_2Mo(\mu\text{-}OH)]_2[OTs]_2$, instead gives **3** as the major product when using the *ansa*-$C_2Me_4(\eta^5\text{-}C_5H_4)_2$ ligand (0.73 g, 57 % based on all monomer product). In this instance, the dimeric [{$C_2Me_4(\eta^5\text{-}C_5H_4)_2$}$Mo(\mu\text{-}OH)]_2[OTs]_2$ complex (**5**) formed only as a minor product. Attempts to purify **3** by crystallization

yielded pure [{$C_2Me_4(\eta^5$-$C_5H_4)_2$}Mo(μ-OH)]$_2$[OTs]$_2$ (**5**). Specifically, upon standing for 2-3 days, a saturated solution of **3** yielded green crystals of **5** as the dihydrate. (The water molecules could be readily removed by heating under reduced pressure.) Anal. for **5**. Found: C, 55.78; H, 5.79; S, 6.22. Calculated for $C_{23}H_{28}SO_4Mo$: C, 55.64; H 5,68; S, 6.46. Data for **3**: ^{1}H NMR (DMSO): δ 7.71 (d, 2, *p*-OTs), 7.32 (d, 2, *p*-OTs), 6.95(m, 4, C_5H_4), 6.00 (m, 4, C_5H_4), 2.29 (s, 3, *p*-OTs-Me), 0.726 (s, 12, C_2Me_4). ^{13}C-{^{1}H} NMR (D_2O): δ 142.70 (s, *p*-OTs), 139.60 (s, *p*-OTs), 132.99 (s, C_5H_4, C_{ipso}), 129.65 (s, *p*-OTs), 125.57 (*p*-OTs), 119.89 (s, C_5H_4), 84.73 (s, C_5H_4), 43.73 (s, C_2Me_4) , 26.17 (s, C_2Me_4), 20.67 (s, *p*-OTs-Me). Data for **5**: ^{1}H NMR (DMSO): δ 7.71 (d, 2, *p*-OTs), 7.32 (d, 2, *p*-OTs), 7.45(m, 4, C_5H_4), 7.07 (m, 4, C_5H_4), 6.13 (m, 4, C_5H_4), 5.99 (m, 4, C_5H_4), 2.29 (s, 3, *p*-OTs-Me), 0.689 (s, 24, C_2Me_4).

2.2.5 Generation of [{$C_2Me_4(C_5H_4)_2$}Mo(CO)H][OTs] (4)

A J-Young tube containing 0.5 mL of 0.5 mM **3** in D_2O was charged with 20 psi CO. After heating at 90 °C for 12 hours, the D_2O was removed under reduced pressure and $CDCl_3$ was immediately added and the ^{1}H NMR and IR spectra obtained. ^{1}H NMR ($CDCl_3$): δ 7.87 (d, 2, *p*-OTs), 7.17 (d, 2, *p*-OTs), 6.35(m, 2, C_5H_4), 6.23 (m, 2, C_5H_4), 5.75 (m, 2, C_5H_4), 5.12 (m, 2, C_5H_4), 2.35 (s, 3, *p*-OTs-Me), 1.29 (d, 12, C_2Me_4), -7.29 (s, 1, Mo-H). IR ($CDCl_3$): 2028 cm^{-1} (ν(C≡O)).

2.2.6 X-ray structure determinations of [{$C_2Me_4(\eta^5$-$C_5H_4)_2$}MoH_2] (2) and [{$C_2Me_4(\eta^5$-$C_5H_4)_2$}Mo(μ-OH)]$_2$[OTs]$_2$·2H_2O (5)

Crystals suitable for X-ray diffraction analysis were grown by slow evaporation of benzene solutions of **2** and saturated aqueous solutions of **3**. X-ray diffraction

experiments were carried out on a Bruker Smart Apex diffractometer at 173 K (**2**) or 150 K (**5**) using MoKα radiation (λ=0.71070 Å). Absorption corrections were done by SADABS. Crystallographic data for **2** and **5** and the details of data collection and refinement of the crystal structures are given in the Supporting Information. The structures were solved using direct methods and refined with full-matrix least-squares methods based on F^2. All non-H atoms were refined with anisotropic thermal parameters. The H atoms coordinated to the Mo atom in **2** and all H atoms in **5** were found on the F-map and refined with isotropic thermal parameters. Other H atoms in **2** were treated in calculated positions and refined in a rigid group model. It should be mentioned that on the residual density of **2** there are two relatively high peaks, 6.04 and 4.53 $e \cdot Å^{-3}$. The distances from the Mo(1) atoms and these peaks are about 1.6 Å and they form with the Mo atom a linear fragment with angle 177°. Attempts to remove these two peaks by changing absorption corrections failed. Data collection with two different crystals of **2** were done and in both cases such peaks were found. Crystals of **2** are extremely unstable in air and the existence of these peaks seems to be related to a small amount of decomposition during crystal mounting on the diffractometer. All calculations were performed using SHELXTL package.

Crystals of **5** have two polymorphic phases and the structures of both of them were determined (see Supporting Information). Both structures have the same dimeric Mo units and tosylate as counter ions, but the structural function of a solvent water molecule is different. In **5**, the μ–OH groups of the dimeric Mo hydrogen bond to the O atoms of the OTs counter ions (Fig. 5). In the second polymorph, the μ–OH groups form

hydrogen bonds with the solvent water molecules, which form a further hydrogen bonding network with the tosylate anions.

2.2.7 Preparation of Catalyst Stock Solutions

Stock solutions of **3**, $[Cp_2Mo(OH)(OH_2)][OTs]$, and $[Cp'_2Mo(OH)(OH_2)][OTs]$ were prepared by dissolving crystals of the respective dimeric complex **5,** $[Cp_2Mo(\mu\text{-}OH)_2]_2[OTs]_2$, or $[Cp'_2Mo(\mu\text{-}OH)_2]_2[OTs]_2$ in 0.13 M MOPS buffered D_2O to give solutions ranging from 2 to 15 mM total molybdenum concentration ($[Mo]_{total}$). The total molybdenum concentration in each solution was determined using a known amount of tetrabutylammonium tetrafluoroborate as an internal standard. The catalyst concentration for the non-*ansa* catalysts was calculated from the total molybdenum concentration using the relationships $[Mo]_{total} = [OTs^-] = 2[Dimer] + [Monomer]$ and $K_{eq} = [Monomer]^2/[Dimer]$. (As will be discussed below, the active monomeric catalyst is in equilibrium with an inactive dimeric species.) In the case of the *ansa*-catalyst, $[Mo]_{total} = [OTs^-] = [Monomer]$.

2.2.8 Hydration of 3-Hydroxypropionitrile

3-Hydroxypropionitrile (3 – 10 μL) was added to 0.50 mL of catalyst solution. The tube was then heated to 80 °C for 14 days. Addition of 3-HPN caused the stock solution of $[Cp'_2Mo(OH)(OH_2)][OTs]$ to turn pink, while the other two solutions remained yellow. ^1H NMR spectroscopy (D_2O) was used to monitor the disappearance of 3-hydroxypropionitrile at 3.78 ppm (t, J = 6.0 Hz, 2H, $HOCH_2CH_2CN$) and 2.67 ppm (t, J = 6.0 Hz, 2H, $HOCH_2CH_2CN$) and the appearance of 3-hydroxypropionamide at 3.76

ppm (t, J = 6.0 Hz), 2H, $HOCH_2CH_2CONH_2$) and 2.45 ppm (t, J = 6.0 Hz), 2H, $HOCH_2CH_2CONH_2$).

2.2.9 p-Nitrophenyl Phosphate Hydrolysis

The appropriate catalyst solution (2 mL) was added to a nitrogen filled cuvette and placed in a water bath heated to 30 °C. After 30 minutes, a 20 μL aliquot of 0.45 mM NPP was added to the catalyst solution. The production of *p*-nitrophenolate anion was monitored at 400 nm until no further change in absorbance was observed.

2.2.10 Ethyl Acetate Hydrolysis

Ethyl acetate (5 – 20 μL) was added to 0.50 mL of the catalyst stock solutions and heated to 80 °C for 7 - 9 days. The reaction was monitored by the disappearance of ester ^{1}H NMR resonances (500 MHz, D_2O) at 4.05 ppm (q, J = 7.0 Hz, 2H, $CH_3CO_2CH_2CH_3$), 1.96 ppm (s, 3H, $CH_3CO_2CH_2CH_3$), and 1.15 ppm (t, J = 7.0 Hz, 2H, $CH_3CO_2CH_2CH_3$) and the appearance of ethanol and acetic acid at 3.55 ppm (q, J = 7.0 Hz, 2H, $HOCH_2CH_3$), 1.08 ppm (t, J = 7.0 Hz, 3H, $HOCH_2CH_3$) and 1.95 (s, 3H, CH_3CO_2H).

2.2.11 Equilibrium Constant Determinations

Solutions containing various concentrations of $[Cp_2Mo(\mu\text{-}OH)]_2[OTs]_2$ and $[Cp'_2Mo(\mu\text{-}OH)]_2[OTs]_2$ were prepared using a 0.13 M MOPS D_2O solution. The concentrations of monomer and dimer were determined by integrating the respective Cp ^{1}H NMR resonances relative to the OTs resonance at 7.657 ppm. For Cp_2Mo^{2+}, the dimer resonance at 5.929 ppm decreased relative to the monomer resonance at 5.724 ppm with decreasing total molybdocene concentration. For Cp'_2Mo^{2+}, the dimer resonances at 5.904 and 5.623 ppm decreased relative to the monomer resonances at 5.389 and 5.352

ppm with decreasing total molybdocene concentration. Samples used for the determinations at 80 °C were preheated in an oil bath for one hour before insertion into a 600 MHz NMR spectrometer pre-heated to 80 °C. In all cases, the proton chemical shifts were referenced to residual HOD, and the chemical shifts at 80 °C are shifted slightly downfield. At 80 °C, the Cp resonance for $[Cp_2Mo(\mu\text{-}OH)]_2[OTs]_2$ appears at 6.384 ppm, and $[Cp_2Mo(OH)(OH_2)][OTs]$ shifts to 6.187 ppm. Likewise, at 80 °C, the $[Cp'_2Mo(\mu\text{-}OH)]_2[OTs]_2$ resonances appear at 6.345 and 6.038 ppm, and $[Cp'_2Mo(\mu\text{-}OH)(OH)_2][OTs]$ resonances appear at 5.926 and 5.775 ppm.

2.3 Results and Discussion

2.3.1 Aqueous Solubility and Behavior of Molybdocenes

The aqueous solubility of Cp_2MoX_2-type molecules is attributed to spontaneous and rapid hydrolysis of the Mo-X bonds to afford ionic complexes containing inner-sphere aqua and hydroxo ligands that are capable of hydrogen bonding. The aquated molybdocene $Cp_2Mo(OH_2)^{2+}$ was found to have pK_a values of 5.5 and 8.5.[45] Of the aquated species generated by hydrolysis of Cp_2MoX_2, the $Cp_2Mo(OH)(OH_2)^+$ cation present at neutral pH was shown to be catalytically most active.[6,10] However, in a previous study, the monomer species were shown to be in equilibrium with the inactive μ-hydroxo dimer, $[Cp_2Mo(\mu\text{-}OH)]_2^{2+}$ (eq 1).[44] The equilibrium constants for the reactions in eq 1 were determined to be $3.5 \times 10^{-2} \pm 0.1 \times 10^{-2}$ M and $7.9 \times 10^{-2} \pm 0.1 \times 10^{-2}$ M for R = H at pH 3.5 and R = Me at pH 7, respectively. Comparison of these values indicates that the addition of a methyl substituent to each Cp ring shifts the monomer-dimer equilibrium in favor of the monomer. However, the equilibria were measured at different

pH values. Because the equilibrium processes are sensitive to pH, for the accurate interpretation of the kinetic data it was necessary to measure K_{eq} for both systems under the conditions used for the catalysis reactions discussed below.

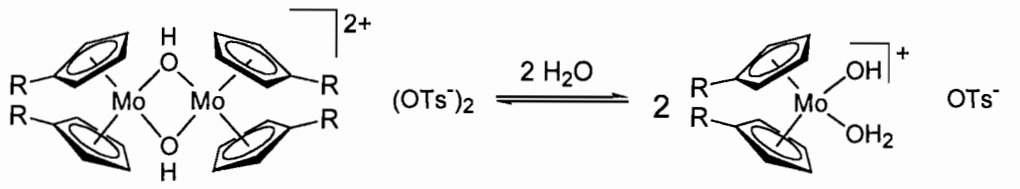

(1)

Table 1. Equilibrium constants and standard thermodynamic parameters for the equilibrium in eq 1 in 0.13 M MOPS Buffer (pH 6.8)

	R = H	**R = Me**
K_{eq} @ 25 °C **(M)**	$(2.7 \times 10^{-4}) \pm (0.1 \times 10^{-4})$	$(2.5 \times 10^{-2}) \pm (0.1 \times 10^{-2})$
K_{eq} @ 80 °C **(M)**	$(1.4 \times 10^{-3}) \pm (0.2 \times 10^{-3})$	$(3.7 \times 10^{-2}) \pm (0.3 \times 10^{-2})$
ΔH^{o} (kcal/mol)	6.2 ± 0.5	1.5 ± 0.1
ΔS^{o} (e.u.)	4.3 ± 0.3	-2.3 ± 0.2

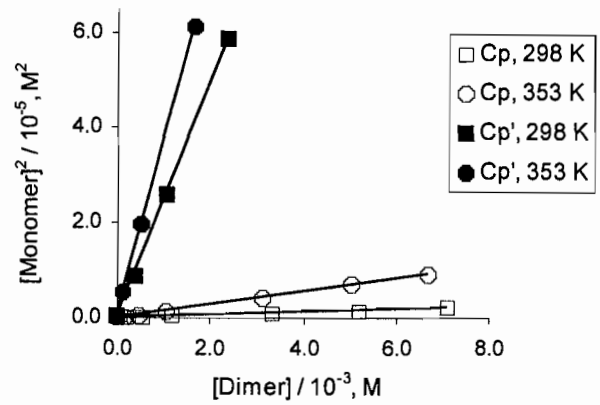

Figure 3. Plots of $([Cp^R_2Mo(OH)(OH_2)][OTs])^2$ versus $[Cp^R_2Mo(\mu\text{-}OH)]_2[OTs]_2$ in 0.13 M MOPS D_2O solution (pD 6.8): For R = H (□) $K_{eq} = (2.7 \times 10^{-4}) \pm (0.1 \times 10^{-4})$ M at 25 °C and (○) $K_{eq} = (1.4 \times 10^{-3}) \pm (0.2 \times 10^{-3})$ M at 80 °C. For R = Me, (■) $K_{eq} = (2.5 \times 10^{-2}) \pm (0.1 \times 10^{-2})$ M at 25 °C and (●) $(3.7 \times 10^{-2}) \pm (0.3 \times 10^{-2})$ M at 80 °C.

The equilibria in 0.13 M MOPS D_2O solutions (pD 6.8) at 25 °C and 80 °C were investigated by determining the change in the monomer and dimer concentrations in solutions containing various concentrations of total molybdocene. The respective monomer and dimer concentrations were plotted as $[monomer]^2$ versus [dimer] and are shown in Figure 3. From these data, the equilibrium constants, the changes in standard enthalpy, and the changes in standard entropy were calculated (Table 1). Consideration of the standard enthalpy and entropy changes gives some insight into the effect of adding a methyl substituent to each Cp ring. With both equilibria, formation of the monomer is enthalpically disfavored, roughly indicating that the Mo-OH bonds in the dimer are stronger than the Mo-OH_2 bonds in the monomer. Stronger solvation of the dicationic

dimer species compared to the monocationic monomer will also contribute to the positive $\Delta H°$. However, the $\Delta H°$ is 4.7 kcal/mol smaller for the equilibrium with the Cp′ ligand versus the unsubstituted Cp ligand.This result indicates that the stability gained through dimerization of $[Cp'_2Mo(OH)(OH_2)][OTs]$ is much less than that gained through dimerization of $[Cp_2Mo(OH)(OH_2)][OTs]$, consistent with a decrease in the Lewis acidity of the metal center in Cp'_2Mo^{2+}. The decreased stability of the Mo-OH bonds in $[Cp'_2Mo(\mu\text{-}OH)]_2^{2+}$ may also be due to unfavorable steric interactions between the Cp′ methyl substituents on dimerization.

The hydrolysis of $[Cp_2Mo(\mu\text{-}OH)]_2[OTs]_2$ is entropically favored but the hydrolysis of $[Cp'_2Mo(\mu\text{-}OH)]_2[OTs]_2$ is entropically disfavored (Table 1). Because hydrolysis of the dimer can superficially be described as three molecules reacting to give two, $\Delta S°$ was expected to be negative. On the other hand, conversion of the dication into two monocations should lead to a positive $\Delta S°$ because less solvent ordering is involved in solvating the less charged monomeric molecule. Accordingly, one may conclude that the latter factor is most important in determining the entropy in the hydrolysis of $[Cp_2Mo(\mu\text{-}OH)]_2[OTs]_2$, where $\Delta S°$ is positive. The addition of the methyl substituent decreases the solvation energy of the dimer, with a concomitant decrease in importance of the molecular charge and solvent order. In this case, the former factor apparently dominates, and the entropy of the system decreases because the dimer reacts with two water molecules to give two monomeric species.

In summary, the addition of a methyl substituent to the Cp rings shifts the monomer-dimer equilibrium in favor of the monomer because the Mo-OH bonds of

$[Cp'_2Mo(\mu\text{-}OH)]_2[OTs]_2$ are weaker due to the decreased electrophilicity of the metal center and because of unfavorable steric interactions between the methyl groups. Because of the negative $\Delta S°$, formation of the $Cp'Mo(OH)(OH_2)^+$ monomer becomes less favorable at elevated temperature.

2.3.2 Synthesis of [{$C_2Me_4(C_5H_4)_2$}Mo(OH)(OH_2)][OTs]; Effect of the Ethylene Bridge on Aqueous Solubility and Behavior

The *ansa* ligand had at least four effects on the behavior of molybdocenes in water. First, the $[\{C_2Me_4(C_5H_4)\}MoCl_2]$ complex exhibited different behavior in water from other Cp_2MoX_2-type complexes in that it did not undergo hydrolysis. The water-soluble *ansa*-complexes were, therefore, accessed from the dihydrido compounds $\{C_2Me_4(C_5H_4)_2\}MoH_2$ via hydrogenation of acetone in the presence of trace water in acetone solvent (eq 2).

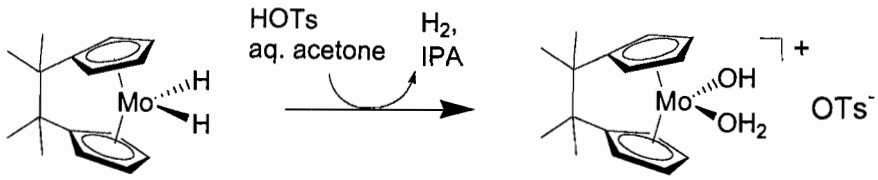

(2)

Second, although the route in eq 2 has been used previously for direct access to the dimeric structure $[Cp_2{}^{(\prime)}Mo(\mu\text{-}OH)]_2{}^{2+}$,[43,44] the reaction using the $\{C_2Me_4(C_5H_4)_2\}MoH_2$ complex produces the monomeric $[C_2Me_4Cp_2Mo(OH)(OH_2)]^+$ as the major product and the dimeric $[C_2Me_4Cp_2Mo(\mu\text{-}OH)]_2[OTs]_2$ only as a minor product. The dimeric $[C_2Me_4Cp_2Mo(\mu\text{-}OH)]_2[OTs]_2$ species was also generated in solution by dissolving

$[C_2Me_4Cp_2Mo(OH)(OH_2)]^+$ in aqueous methanol. This yielded a mixture of monomer and dimer. To obtain pure, solid $[C_2Me_4Cp_2Mo(\mu\text{-}OH)]_2[OTs]_2$, the dimer was crystallized from a super-saturated solution of $[C_2Me_4Cp_2Mo(OH)(OH_2)]^+$ in water or water was removed at reduced pressure from a solution of $[C_2Me_4Cp_2Mo(OH)(OH_2)]^+$. Once obtained by either of these methods, the dimer will readily undergo hydrolysis in water to afford the monomer. Third, no monomer-dimer equilibrium in D_2O was detectable by ^1H NMR spectroscopy. Last, the water-solubility of the molybdocene is greatly reduced upon addition of the tetramethylethylene linkage. The impact of this decreased solubility is shown by the fact that the hydrolysis and hydration reactions discussed below were performed using solutions of $C_2Me_4Cp_2Mo(OH)(OH_2)^+$ that were less than 3 mM, whereas solutions of $Cp_2Mo(OH)(OH_2)^+$ and $Cp'_2Mo(OH)(OH_2)^+$ were up to 15 mM in total molybdenum concentration. Further investigations of the aqueous behavior of the $C_2Me_4Cp_2Mo(OH)(OH_2)^+$ catalyst will be discussed in more detail in Chapter III.

2.3.3 Effect of the Ethylene Bridge on the Geometric Structure of Molybdocenes

Crystal structures of $C_2Me_4Cp_2MoH_2$ (**2**) and $[C_2Me_4Cp_2Mo(\mu\text{-}OH)]_2[OTs]_2$ (**5**) are shown in Figures 4 and 5, respectively. In both structures, the cyclopentadienyl rings adopt an eclipsed conformation enforced by the bridging atoms. In the structure of $C_2Me_4Cp_2MoH_2$, the bite angle and Mo-Cp bond distances are only slightly reduced from the unsubstituted dihydride molecule (Table 2). In contrast, the methylene-bridged molybdocene prepared by Labella et al. has a bite angle reduced by ≈20°.[18] The Mo-H

bond distances are essentially equal in all three molecules. More importantly, the *ansa*-molybdocene dimer **5**, shown in Figure 5, is essentially isostructural to that of the non-bridged analogs, $[(C_5H_5)_2Mo(\mu\text{-}OH)]_2[OTs]_2$ and $[(C_5H_4Me)_2Mo(\mu\text{-}OH)]_2[OTs]_2$. Each molybdocene center exhibits a distorted pseudo-tetrahedral environment (counting the Mo-$Cp_{centroid}$ as a single "coordination" site) with bridging hydroxo ligands hydrogen-bonded to the tosylate counter ions. A comparison of selected angles and bond lengths is shown in Table 3. Note that there are only marginal variations in the geometric parameters for the Mo-O-Mo-O core, the bite angles, and $Cp_{centroid}$-Mo distances.

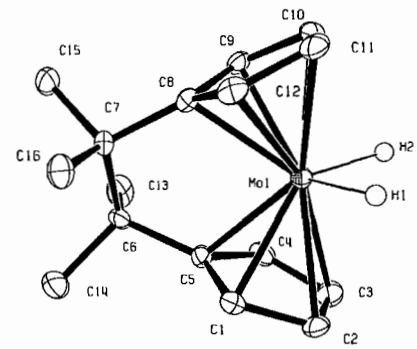

Figure 4. X-ray crystal structure of $(C_2Me_4Cp_2)MoH_2$. The Cp and bridge protons were omitted for clarity. Thermal ellipsoids are drawn at the 50% probability level.

Table 2. Comparison of selected bond distances and angles for the molybdocene dihydrides.

Ligand(s)	Cp-Mo-Cp (°)	H-Mo-H (°)	Cp-Mo (A)	H-Mo (A)	Ref.
$(C_5H_5)_2$	145.8	75.5(3)	1.942, 1.946	1.685(3)	46
$\{C_2Me_4Cp_2\}$	141.9	85(3)	1.936, 1.933	1.68(7), 1.70(6)	This work
$\{CMe_2Cp_2\}$	121	80.3	1.913, 1.912	1.66(5), 1.72(7)	18

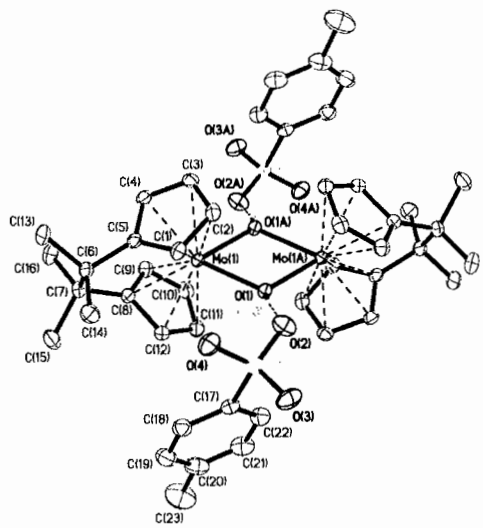

Figure 5. X-ray crystal structure of $[\{C_2Me_4(C_5H_4)_2\}Mo(\mu\text{-}OH)]_2[OTs]_2$ (**5**). The H atoms were omitted for clarity. Thermal ellipsoids are drawn at the 50% probability level.

Table 3. Comparison of selected bond distances and angles for the molybdocene dimers.

	$[\{C_2Me_4(C_5H_4)_2\}Mo(\mu\text{-}OH)]_2[OTs]_2$	$[\{(C_5H_4R)_2\}Mo(\mu\text{-}OH)]_2[OTs]_2$	
		R = H[a]	R = Me[b]
Mo-O	2.101(1)	2.092(2)	2.106(3)
Mo-O(1A)	2.112(1)	2.100(2)	2.095(3)
Mo-Cp(1)[c]	1.983	2.001(5)	2.001(3)
Mo-Cp(2)[c]	1.984	1.996(5)	1.997(3)
O(1)-Mo-(O1A)	66.90(5)	66.21(10)	67.0(1)
Mo1-O(1)-Mo1A	113.10(5)	113.79(10)	113.0(1)
Cp(1)-Mo-Cp(2)[c]	129.6	128.3	130.0

[a] Ref. 47. [b] Ref 44. [c] Distances and angles are to the centroid of the Cp rings.

2.3.4 Effect of the Ethylene Bridge on the Electronic Structure

In order to determine the effect of the ethylene-bridge on the electron density of the Mo center, the CO-containing $[\{C_2Me_4(C_5H_4)_2\}Mo(CO)H][OTs]$ complex was prepared with the idea of using the $\nu(C\equiv O)$ frequency as a probe. The complex was prepared using the method previously reported for the Cp' analog (eq 3). Note that other synthetic routes to the $Cp_2Mo(CO)H^+$ complex are reported in the literature. In those routes, the carbonyl complex was generated by the oxidation of Cp_2MoCO using $CpMoH(CO)_3$ (eq 4) or by reduction of Cp_2MoH_2 with $[CpMo(CO)_3]_2$ in the presence of CO (eq 5).[48] Selected spectroscopic data for the various CO-containing molybdocenes are shown in Table 4. Comparison of the carbonyl stretching frequencies reveals that the ethylene-bridged molybdocene is relatively electron-withdrawing, as indicated by the

C≡O stretch at highest frequency, followed by $Cp_2Mo(CO)(H)^+$ and $Cp'_2Mo(CO)H^+$. Note that this trend indicates that the electronic effect of the ethylene-bridge is not inductive (as is the case in the $Cp'_2Mo(CO)H^+$ complex containing nonbridging methyl substituents). Instead, it is logical to propose that the electron-withdrawing nature of the *ansa*-bridge is caused by enhanced back-donation into a relatively low-energy bis(cyclopentadienyl) ligand acceptor orbital, as explained by Parkin, Green, and coworkers in their comprehensive study of *ansa*-zirconocene complexes.[27]

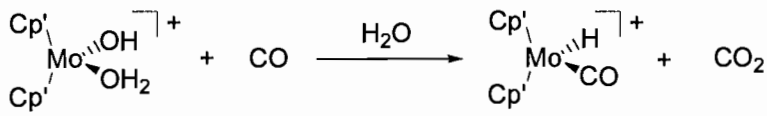

(3)

$$Cp_2MoCO + CpMoH(CO)_3 \longrightarrow [Cp_2Mo(CO)H][CpMoCO_3] \quad (4)$$

$$Cp_2MoH_2 + [CpMo(CO)_3]_2 \longrightarrow [Cp_2Mo(CO)H][CpMoCO_3] \quad (5)$$

Table 4. Comparison of selected spectral data for $Cp_2Mo(IV)$ carbonyl compounds.

Compound	C≡O (cm^{-1})	δ Mo-H	Reference
$(C_5H_4Me)_2Mo(CO)H$	2008[a]	-8.09[b]	2
$(C_5H_5)_2Mo(CO)H$	2020[c]	-	48
$\{C_2Me_4(C_5H_4)_2\}Mo(CO)H$	2028[d]	-7.29[d]	This work

[a] KBr pellet [b] $(CD_3)_2CO$ [c] $CHCl_3$ [d] $CDCl_3$

2.3.5 Effect of the Ethylene Bridge on Catalysis

To explore the effect of the more electrophilic molybdocene center in $C_2Me_4Cp_2Mo(OH)(OH_2)^+$ in reactions proceeding via intramolecular hydroxide attack, three reactions were investigated: 1) the hydration of 3-hydroxypropionitrile (HPN); 2) the hydrolysis of *p*-nitrophenyl phosphate (NPP); and 3) the hydrolysis of ethyl acetate (EtOAc). As explained in the introduction, the electron-withdrawing *ansa*-Cp ligand could lead to enhanced activation of a bound substrate; however, it could also reduce the reactivity of the coordinated hydroxo nucleophile. To investigate the relative importance of these two competing factors, the rate constants for the reactions above catalyzed by the relatively electron poor *ansa*-molybdocene complex **3** were compared to those of the nonsubstituted molybdocene complex $Cp_2Mo(OH)(OH_2)^+$ and to the relatively electron-rich $Cp'_2Mo(OH)(OH_2)^+$ catalyst. All reactions were performed in 0.13 M MOPS-buffered D_2O with less than 3 % catalyst. The rate constants (k_{app}) reported below are second-order rate constants for the hydrolysis and hydration reactions, obtained by dividing the observed rate constant obtained from first-order fits of substrate concentration versus time by the active catalyst concentration, or, in the case of HPN hydration, directly from the GIT iterative kinetics fitting program. The details of the GIT models and an example fit are shown below. The active catalyst concentration, [cat], was determined from the total molybdocene concentration using the appropriate equilibrium constants reported above. Because no monomer-dimer equilibrium was observed for the *ansa* catalyst, the total molybdocene concentration equals the active catalyst concentration.

Nitrile Hydration

Prior studies established the pathway in Scheme 1 for the hydration of nitriles catalyzed by molybdocenes.[3] It was also previously shown that the reactions are retarded by reversible coordination of the nitrile substrate (eq 6) and irreversible coordination of the amide product (eq 7), which leads to degradation of the catalyst.[3] Electron withdrawing nitriles, however, exhibited increased catalytic activity with no product inhibition. Of the molybdocene-catalyzed hydrations reported earlier, the hydration of 3-hydroxypropionitrile (HPN) was the most efficient and was, therefore, chosen for this study. Although no product inhibition was noted with HPN, H/D exchange of the α-hydrogen atoms was observed (eq 8).

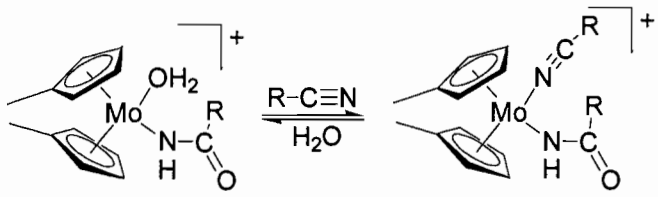

(6)

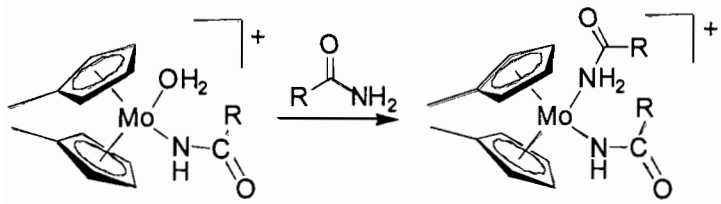

(7)

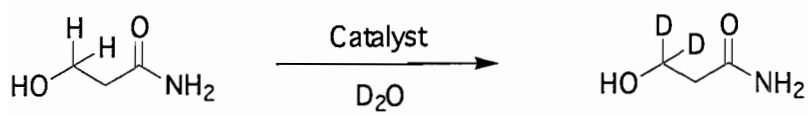

(8)

Table 5. Comparison of kinetic data for 3-hydroxypropionitrile hydration at 81 °C

Ligand	[Monomer] (mM)	[Substrate] (M)	k_{app} ($M^{-1}s^{-1}$ x 10^3)	k_2 ($M^{-1}s^{-1}$ x 10^4)
$C_2Me_4(C_5H_4)_2$	1.2	0.10	1.2 ± 0.1	3.9 ± 0.3
$(C_5H_5)_2$	1.3	0.26	5.3 ± 0.7	5.1 ± 0.7
$(C_5H_4Me)_2$	1.8	0.092	4.3 ± 0.5	1.6 ± 0.2

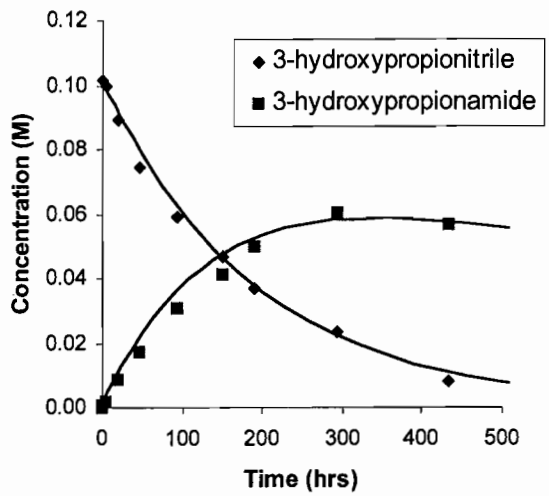

Figure 6. GIT fit of kinetics data for $C_2Me_4Cp_2Mo(OH)(OH_2)^+$-catalyzed hydration of 3-hydroxypropionitrile.

The reaction kinetics for nitrile hydration and product inhibition were modeled using an iterative kinetics fitting program (GIT) applied to eqs 9 and 10.

$$\text{catalyst} + \text{nitrile} \xrightarrow{k_{app}} \text{catalyst} + \text{amide} \quad (9)$$

$$\text{catalyst} + \text{amide} \xrightarrow{k_2} \text{catalyst} + \text{amide-}d_2 \quad (10)$$

An example of a fit is shown in Figure 6, and lists of the rate constants for 3-hydroxypropionitrile hydration (k_{app}) and H/D exchange (k_2) are shown in Table 5. The rate constants for HPN hydration decrease in the order $Cp_2Mo(OH)(OH_2)^+ \sim Cp'_2Mo(OH)(OH_2)^+ > C_2Me_4Cp_2Mo(OH)(OH_2)^+$. The rate constants for H/D exchange give a slightly different trend than those for nitrile hydration, decreasing in the order $Cp_2Mo(OH)(OH_2)^+ \sim C_2Me_4Cp_2Mo(OH)(OH_2)^+ > Cp'_2Mo(OH)(OH_2)^+$. Although the trends for nitrile hydration and H/D exchange are intriguing, it should be noted that the variations in the rate constants for the three catalysts are only marginal. Such small changes in the rate constants for these catalysts show that the rate of nitrile hydration and H/D exchange is effectively unchanged for molybdocenes within the range of electron densities studied herein.

The sensitivity of HPN hydration to changes in electron density of the molybdocene catalyst may be reduced due to preferential coordination of the alcohol functionality of HPN as opposed to the nitrile group. Several observations indicate that HPN does in fact bind to the active site of the *ansa*-catalyst through the alcohol functionality. Alcohol coordination was observed in the ^1H NMR spectrum of the reaction mixture by comparison of the aromatic Cp protons for the active catalyst to those of the catalyst in methanol:water mixtures (Figure 7). Note in the figure that the Cp resonances give two sets of pseudo-triplets at essentially the same shift value (about 6.2 and 6.5 ppm in both cases). This result implies a similar ligand environment for each Mo atom. The complex in aqueous methanol must bind through the oxygen, and the implication therefore is that the HPN is bonded through the oxygen atom. In addition,

H/D exchange of the α-hydrogens is observed over the course of the reaction, resulting in a decrease in intensity of the corresponding nitrile and amide resonances in the ^{1}H NMR spectrum. Molybdocene-catalyzed H/D exchange reactions in alcohols are known to proceed by initial coordination of the alcohol functionality.[6]

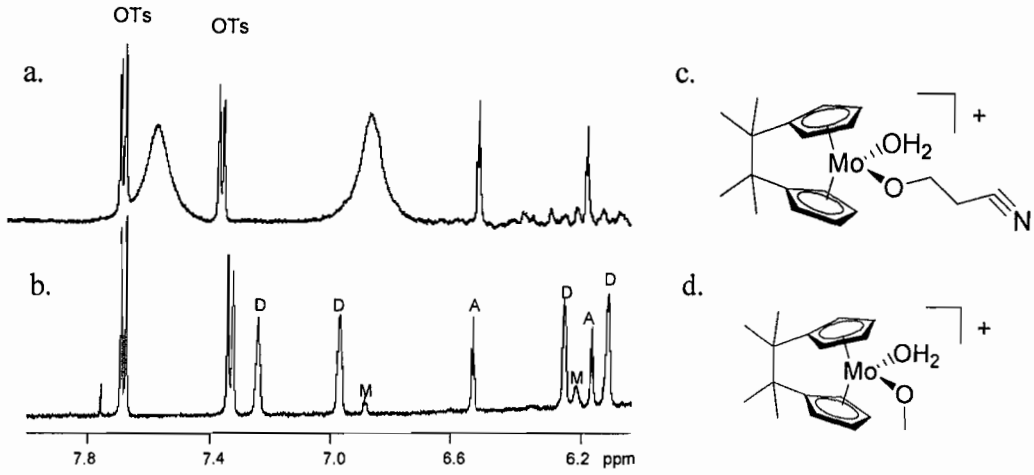

Figure 7. Aromatic regions of the ^{1}H NMR spectra of (a) a HPN hdyration reaction mixture at 8 hours and (b) the catalyst in a 1:1 water:methanol mixture. The proposed structures of (c) HPN coordination via the alcohol and (d) the *ansa*-molybdocene methanol adduct are also shown. OTs = C_6H_4Me, D = $[C_2Me_4Cp_2Mo(\mu\text{-}OH)]_2[OTs]_2$, M = $[C_2Me_4Cp_2Mo(OH)(OH_2)][OTs]$, and A = $[C_2Me_4Cp_2Mo(OCH_3)(OH_2)][OTs]$

Phosphate Ester Hydrolysis

The rate laws for phosphate hydrolysis using the molybdocene catalysts are pseudo-first order, and a first-order fit of the kinetic data obtained using $Cp'_2Mo(OH)(OH_2)^+$ is shown in Figure 8. The rate constants are shown in Table 6.

Comparison of these data to those in Table 5 shows that the molybdocenes are more reactive toward phosphate substrates than nitriles; however, phosphate hydrolysis (eq 11) is not catalytic.[10] The enhanced rate may be due to the greater stability of the product P=O bonds relative to the C=O product bonds that form in the nitrile hydration reactions. The lack of turnover may be due to the greater stability of the 4-membered Mo-phosphate structure in the product (eqs 12 and 13). Nevertheless, the hydrolysis of p-nitrophenylphosphate (NPP) was examined in order to further investigate the reactivity of the molybdocene molecules toward intramolecular nucleophilic attack.

(11)

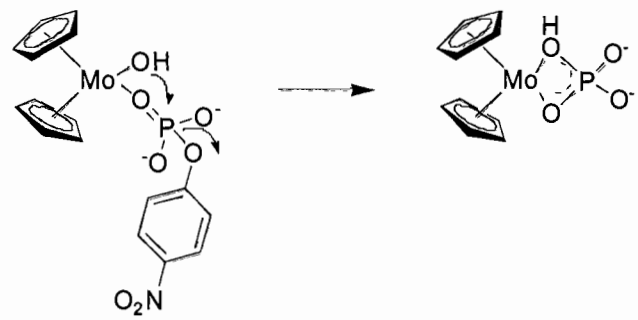

(12)

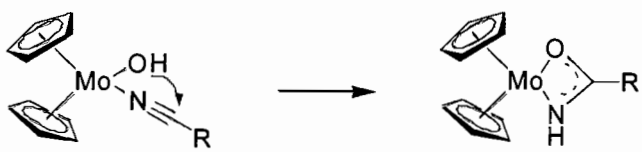

(13)

As shown in Table 6, NPP hydrolysis was most efficient using the unsubstituted molybdocene catalyst $Cp_2Mo(OH)(OH_2)^+$, as the rate constants decrease in the order $Cp_2Mo(OH)(OH_2)^+ > Cp'_2Mo(OH)(OH_2)^+ > C_2Me_4Cp_2Mo(OH)(OH_2)^+$. These results

support the hypothesis that the changes in the electronic environment are counteractive. In other words, the increase in activation of the substrate by the more electrophilic Mo center is offset by deactivation of the hydroxo-leaving group. With the electron-donating Cp′ ligand, the increase in nucleophilicity of the hydroxo ligand is offset by the reduced reactivity of the substrate. It is interesting to note that phosphate ester hydrolysis is much more sensitive to alterations in the electronic environment of the metal center; the rate constant k_{app} is decreased by an order of magnitude as a result of an increase or decrease in the electron density of the Mo center as opposed to a factor of four or less in HPN hydration. In this case, changes in the electronics of the Mo center seem to affect the reactivity of the nucleophile and substrate to the same extent, leading to similar k_{app} values for $Cp'_2Mo(OH)(OH_2)^+$ and $C_2Me_4Cp_2Mo(OH)(OH_2)^+$.

Table 6. Comparison of NPP hydrolysis kinetics at 30 °C

Ligand(s)	**[Monomer] (mM)**	**k_{app} ($M^{-1}s^{-1}$ x 10^2)**
$\{C_2Me_4(C_5H_4)\}$	0.50	1.6 ± 0.3
$(C_5H_5)_2$	0.80	64 ± 9
$(C_5H_4Me)_2$	3.8	5.3 ± 0.7

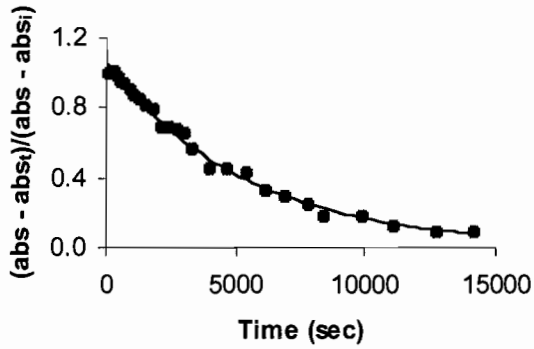

Figure 8. Kinetic data for hydrolysis of *p*-nitrophenyl phosphate promoted by $Cp'_2Mo(OH)(OH_2)^+$ fit to the exponential equation $y = 1.06\ e^{-1.87 \times 10\text{-}4}$, $R^2 = 0.992$.

Carboxylic Ester Hydrolysis

The kinetic data for the hydrolysis of ethyl acetate are summarized in Table 7. Again, when comparing k_{app} values, the $Cp_2Mo(OH)(OH_2)^+$ catalyst is an order of magnitude more reactive than the $C_2Me_4Cp_2Mo(OH)(OH_2)^+$ and $Cp'_2Mo(OH)(OH_2)^+$ catalysts. As with the other catalytic reactions, this trend suggests that $Cp_2Mo(OH)(OH_2)^+$ has optimal electron density on the metal center for reactions proceeding by intramolecular nucleophilic attack.

Table 7. Comparison of ethyl acetate hydrolysis kinetics for listed molybdocenes at 80 °C

Ligand(s)	**[Monomer] (mM)**	**[EtOAc] (M)**	**k_{app} ($M^{-1}s^{-1} \times 10^{-3}$)**
$\{C_2Me_4(C_5H_4)_2\}$	2.2	0.12	4.0 ± 0.2
$(C_5H_5)_2$	2.3	0.43	17 ± 1
$(C_5H_4Me)_2$	9.0	0.50	1.4 ± 0.3

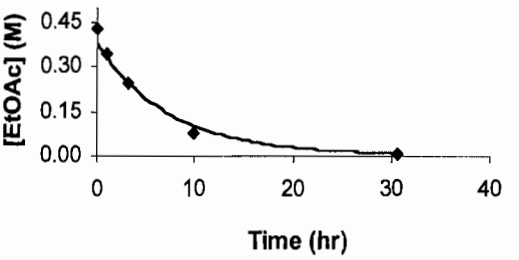

Figure 9. $Cp_2Mo(OH)(OH_2)^+$ catalyzed hydrolysis of ethyl acetate fit to the exponential equation $y = 0.382\ e^{-0.136}$, $R^2 = 0.994$.

2.3.6 Effect of Monomer-Dimer Equilibrium on the Reaction Rate

The formation of an inactive dimeric species was found to be of critical importance in determining the reaction rates for the Cu(II) macrocyclic amine phosphate ester hydrolysis catalysts reported by Burstyn and coworkers.[32] The Cu(II) promoted hydrolysis reactions were shown to exhibit a half order dependence on the total Cu(II) concentration, and the active catalyst was proposed to be a monomer that exists in equilibrium with a dimer (eq 14), analogous to the monomer-dimer equilibrium observed with the molybdocene catalyst (eq 1). In an investigation of the effect of ligand structure on reactions rates in the Cu(II) system, Burstyn and coworkers found that the rate of hydrolysis increased with increasing ligand size due to a resulting destabilization of the inactive dimeric species. Other factors such as the Lewis acidity of the Cu(II) center and steric constraints on the phosphate binding were also proposed to have an affect on the reaction rates but were concluded to be of secondary importance.

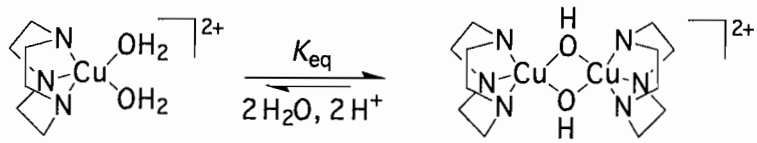

(14)

Because of the monomer-dimer equilibrium in eq 1, the rates of hydrolysis and hydration can be similarly affected by dimerization in the non-*ansa* catalysts, especially in the case of nitrile hydration where changes in the electronics of the metal center resulted in the smallest variations in rate constants. Accordingly, although the unsubstituted $Cp_2Mo(OH)(OH_2)^+$ catalyst is the most reactive toward intramolecular nucleophilic attack, the *rate* of $Cp_2Mo(OH)(OH_2)^+$-catalyzed hydration and hydrolysis reactions per *total* molybdenum concentration may not be fastest due to the extensive dimer formation. Note that because the $C_2Me_4Cp_2Mo(OH)(OH_2)^+$ catalyst is not in apparent equilibrium with a dimeric species the actual rate of hydration or hydrolysis per mole of total Mo(IV) may be increased for the *ansa*-catalyst. Further studies on the effect of catalyst dimerization in these molybdocene systems are underway in our laboratory.

2.4 Summary and Key Insights

A major goal in homogeneous catalysis is identifying specific ligand sets that afford selective catalytic transformations of organic substrates with maximum turnover rates. Molybdocenes have outstanding selectivity and moderate reactivity in the hydration of nitriles in aqueous solution, and they display promise in phosphate ester degradation. In an effort to explore the reactivity of a more electrophilic molybdenum center toward hydrolysis and hydration reactions, the tetramethylethylene-bridged bis(cyclopentadienyl) ligand was employed. The ethylene bridge was shown to alter the

molybdocene catalyst in three significant ways. First, the ethylene bridge greatly reduced the water-solubility of the catalyst. Second, the bridging ring substituents suppressed formation of the inactive μ-hydroxo dimer. Third, the ethylene bridge increased the electrophilicity of the molybdenum center, as shown by the relatively high energy ν(C≡O) stretching frequency in $C_2Me_4Cp_2Mo(CO)H$ compared with the analogous non-*ansa* molybdocenes studied herein.

Although the *ansa*-linkage reduced the electron density at the Mo center, the increase in the Lewis acidity did not increase the reactivity of a bound substrate toward intramolecular nucleophilic attack by the hydroxo ligand. In fact, the observed trends in the rate constants did not correlate with the electron density on the metal center. Instead, the $Cp_2Mo(OH)(OH_2)^+$ catalyst, which has intermediate electron density, was the most reactive toward every substrate examined. These results were interpreted by evaluating the competing effects of changes in the electrophilicity of the Mo center, namely that an increase in the electrophilicity will increase the reactivity of a bound substrate toward nucleophilic attack but will also decrease the reactivity of the bound hydroxo nucleophile.

Although the $Cp_2Mo(OH)(OH_2)^+$ is the most reactive of the selected molybdocenes, it also has the greatest tendency to dimerize to the inactive $[(C_5H_4)_2Mo(\mu\text{-}OH)]_2[OTs]_2$ form. Interestingly, no monomer-dimer equilibrium was detectable in aqueous solutions of $[\{C_2Me_4(\eta^5\text{-}C_5H_4)_2\}Mo(OH)(OH_2)][OTs]$. In Chapter III, the solution-state behavior of $[\{C_2Me_4(\eta^5\text{-}C_5H_4)_2\}Mo(OH)(OH_2)][OTs]$ in a variety of

solvent mixtures is investigated in more detail. Furthermore, the effect of catalyst dimerization on the rate of molybdocene-catalyzed nitrile hydration is examined.

CHAPTER III

EFFECT OF SOLVENT ON THE DIMERIZATION OF THE *ANSA*-MOLYBDOCENE CATALYST $[C_2Me_4Cp_2Mo(OH)(OH_2)][OTs]$

3.1 Introduction

Previous reports showed that the $Cp^{(\prime)}{}_2Mo(OH)(OH_2)^+$ species are in equilibrium with the hydroxo-bridged dimer $[Cp^{(\prime)}{}_2Mo(\mu\text{-}OH)]_2{}^{2+}$, eq 1.[1,11]

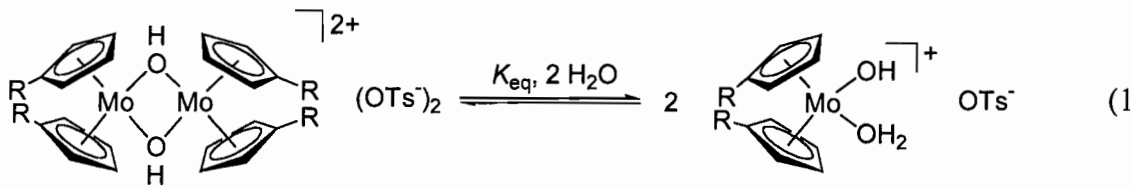

(1)

When R = H, K_{eq} is 2.7 x 10^{-4} M ± 0.1 x 10^{-4} M in MOPS-buffered D_2O (0.13 M, pD 6.8) at 25 °C. The addition of one methyl group to each Cp ring increased the equilibrium constant by two orders of magnitude to 2.5 x 10^{-2} M ± 0.1 x 10^{-2} M. The large increase in K_{eq} in the latter species was attributed primarily to the decrease in the Lewis acidity of the

metal center of the $Cp'Mo^{2+}$ unit (leading to weaker Mo-OH bonds in the dimeric structure) and to unfavorable steric interactions between the Cp′ methyl substituents upon dimerization. Based on the results obtained for the $Cp'_2Mo(OH)(OH_2)^+$ complex, we originally postulated that the equilibrium for *ansa*-$C_2Me_4Cp_2Mo(OH)(OH_2)^+$ would lie in favor of the dimeric $[C_2Me_4Cp_2Mo(\mu\text{-}OH)]_2^{2+}$ species due to the fixed position of the rings and the increased Lewis acidity of the complex. Surprisingly, no [*ansa*-$C_2Me_4Cp_2Mo(\mu\text{-}OH)]_2^{2+}$ was detected by ^1H NMR spectroscopy in pure or buffered water solutions of *ansa*-$C_2Me_4Cp_2Mo(OH)(OH_2)^+$.[1] This result was puzzling because [*ansa*-$C_2Me_4Cp_2Mo(OH)(OH_2)$][OTs] crystallizes as [*ansa*-$C_2Me_4Cp_2Mo(\mu\text{-}OH)]_2[OTs]_2$ from a supersaturated solution in water.

The extent of the monomer-dimer equilibrium has practical consequences. For example, the tendency of molybdocenes to dimerize may adversely affect the rates achieved by $(CpR)_2Mo(OH)(OH_2)^+$-promoted reactions.[12,13] As mentioned above, although the $Cp_2Mo(OH)(OH_2)^+$ complex appeared to be the most reactive toward intramolecular nucleophilic attack, this complex also has the greatest tendency to dimerize, giving rise to large amounts of the catalytically inactive $[Cp_2Mo(\mu\text{-}OH)]_2^{2+}$. As a result, the rate of reaction per molybdenum center obtained using the $Cp_2Mo(OH)(OH_2)^+$ complex may actually be smaller than that obtained for slightly less reactive molybdocene complexes (i.e., *ansa*-$C_2Me_4Cp_2(OH)(OH_2)^+$ and $Cp'_2Mo(OH)(OH_2)^+$) that have a lesser tendency to dimerize. This result suggests that suppressing catalyst dimerization may be a more effective method of achieving faster rates than tuning the electrophilicity of the metal center. Furthermore, if catalyst

dimerization does have a significant effect on the rate of molybdocene-promoted reactions, it is expected to be most significant in the molybdocene-catalyzed hydration of nitriles where the difference in the rate constants for the variously substituted molybdocenes is marginal.[1]

In this paper, we explore the factors that control the monomer-dimer equilibrium for *ansa*-$C_2Me_4Cp_2Mo(OH)(OH_2)^+$. In addition, the consequences of dimer formation with respect to the catalytic hydration activity of water-soluble molybdocene complexes are discussed.

3.2 Experimental

3.2.1 General Procedures

All experiments were performed under a nitrogen atmosphere using standard glove box techniques. Solvents were prepared by purging with nitrogen or using three freeze-pump-thaw cycles. All catalyst mixtures were prepared in J-Young tubes or 9 inch NMR tubes that were subsequently flame-sealed to prevent oxidation. The compounds [*ansa*-$C_2Me_4Cp_2Mo(OH)(OH_2)][OTs]$,[1] $[C_2Me_4Cp_2Mo(\mu\text{-}OH)]_2][OTs]_2$,[1] $[Cp'_2Mo(\mu\text{-}OH)]_2[OTs]_2$,[14] and $[Cp_2Mo(\mu\text{-}OH)]_2[OTs]_2$[15] were prepared as previously described. Nitrile hydration kinetics were modeled using an iterative fitting program, GIT,[16,17] and the following equations.

$$\text{catalyst} + \text{nitrile} \xrightarrow{k_{app}} \text{catalyst} + \text{amide} \qquad (2)$$

$$\text{catalyst} + \text{amide} \xrightarrow{k_2} \text{catalyst} + \text{amide-}d_2 \qquad (3)$$

$$\text{catalyst} + \text{amide-}d_2 \xrightarrow{k_3} \text{catalyst} + \text{amide} \quad (4)$$

A representative GIT fits is shown in Figure 4. The apparent second-order rate constants, k_{app}, obtained for nitrile hydration were used to calculate rates and turnover frequencies. The rate constants obtained for the H/D exchange of the α-hydrogens[1] (k_2 and k_3) are reported in the Supporting Information.

3.2.2 Investigation of Solvent Effects on the Behavior of $C_2Me_4Cp_2Mo(OH)(OH_2)^+$

Crystalline $[C_2Me_4Cp_2Mo(\mu\text{-}OH)]_2]^{2+}$ (0.0045 g) was allowed to hydrolyze in D_2O (1.50 mL) at 70 °C for 3 hours. 250 μL of deuterated acetone, methanol, ethanol, dimethyl sulfoxide, or tetrahydrofuran was added to a 250 μL aliquot of the hydrolyzed solution in a J-Young tube and mixed. The resulting mixture was monitored by ^{1}H NMR spectroscopy until it remained unchanged for at least 10 hours.

3.2.3 Hydration of 3-Hydroxypropionitrile

Stock solutions of $C_2Me_4Cp_2Mo(OH)(OH_2)^+$, $Cp_2Mo(OH)(OH_2)^+$, and $Cp'_2Mo(OH)(OH_2)^+$ were prepared by dissolving the respective dimers in 0.13 M MOPS buffered D_2O. The catalyst concentrations were confirmed using tetrabutylammonium tetrafluoroborate as an internal standard. In an NMR tube, 7 μL of 3-hydroxypropionitrile was added to 0.500 mL of catalyst solution. The tube was then heated to 80 °C for 14 days. Addition of 3-HPN caused the stock solution of $[Cp'_2Mo(OH)(OH_2)][OTs]$ to turn pink, while the other two solutions remained yellow. ^{1}H NMR spectroscopy (D_2O) was used to monitor the disappearance of 3-hydroxypropionitrile at 3.78 ppm (t, J = 6.0 Hz, 2H, $HOCH_2CH_2CN$) and 2.67 ppm (t, J = 6.0 Hz, 2H, $HOCH_2CH_2CN$) and the appearance of 3-hydroxypropionamide at 3.76 ppm

(t, J = 6.0 Hz), 2H, $HOCH_2CH_2CONH_2$) and 2.45 ppm (t, J = 6.0 Hz), 2H, $HOCH_2CH_2CONH_2$).

3.3 Results and Discussion

3.3.1 Investigation of the Equilibrium Behavior of ansa-$C_2Me_4Cp_2Mo(OH)(OH_2)^+$

The *ansa*-$C_2Me_4Cp_2Mo(OH)(OH_2)^+$ monomer exhibits hydrolytic behavior both similar and distinct to the non-*ansa* $Cp'_2Mo(OH)(OH_2)^+$ monomers. An important similarity is that the *ansa*-$C_2Me_4Cp_2Mo(OH)(OH_2)^+$ monomer crystallizes as the *ansa*-$[C_2Me_4Cp_2Mo(\mu\text{-}OH)]_2^{2+}$ dimer. In addition, the *ansa*-$[C_2Me_4Cp_2Mo(\mu\text{-}OH)]_2^{2+}$ dimer dissolves in water to give the *ansa*-$C_2Me_4Cp_2Mo(OH)(OH_2)^+$ monomer (Figure 1). This behavior is also observed for the non-*ansa* complexes and is described by eq 1. However, the behavior of the *ansa*-molybdocene differs from that of the non-*ansa* complexes in two important ways. First, the $[Cp'_2Mo(\mu\text{-}OH)]_2^{2+}$ dimers dissolve readily in water, yet the *ansa*-$[C_2Me_4Cp_2Mo(\mu\text{-}OH)]_2^{2+}$ dimer is only sparingly soluble in H_2O (< 1 mM). Furthermore, as shown in Figure 1, the small amount of *ansa*-$[C_2Me_4Cp_2Mo(\mu\text{-}OH)]_2^{2+}$ dimer that does dissolve, slowly hydrolyzes over hours to the *ansa*-$C_2Me_4Cp_2Mo(OH)(OH_2)^+$ monomer. Second, hydrolysis of the *ansa*-dimer appears to proceed to completion. No $[C_2Me_4Cp_2Mo(\mu\text{-}OH)]_2^{2+}$ is detectable in the aromatic region of the ^1H NMR spectrum once hydrolysis is complete at 25 °C or at elevated temperatures.[a]

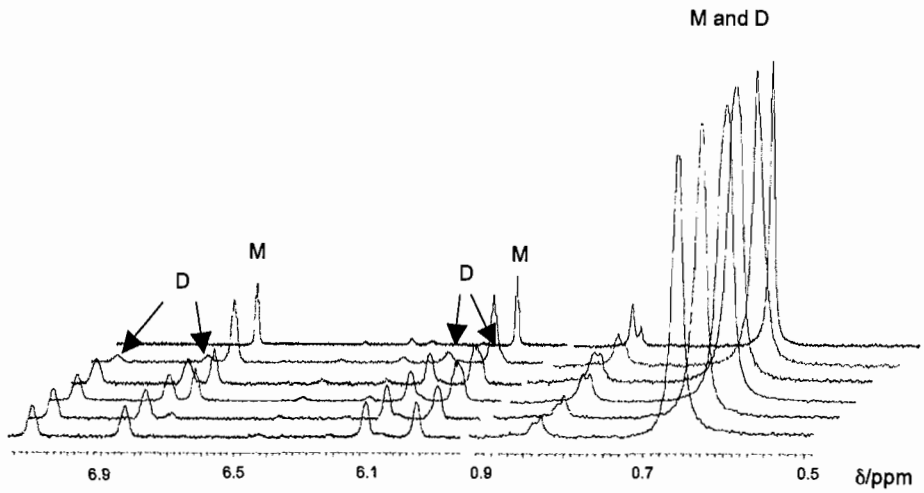

Figure 1. Stacked ^{1}H NMR spectra showing the hydrolysis of $[C_2Me_4Cp_2Mo(\mu\text{-}OH)]_2[OTs]_2$ to $[C_2Me_4Cp_2Mo(\mu\text{-}OH)]_2[OTs]_2$ in D_2O. (From bottom to top: 0 hrs, 23 hrs, 84 hrs, 96 hrs, 108 hrs, and 168 hrs.) D = $[C_2Me_4Cp_2Mo(\mu\text{-}OH)]_2^{2+}$, M = $[C_2Me_4Cp_2Mo(OH)(OH_2)]^+$.

Because [*ansa*-$C_2Me_4Cp_2Mo(\mu\text{-}OH)]_2^{2+}$ was not detectable in solutions of the *ansa*-$C_2Me_4Cp_2Mo(OH)(OH_2)^+$ monomer in water, it was unclear whether the [*ansa*-$C_2Me_4Cp_2Mo(\mu\text{ -}OH)]_2^{2+}$ and *ansa*-$C_2Me_4Cp_2Mo(OH)(OH_2)^+$ species were in an equilibrium analogous to eq 1. Crystallization of [*ansa*-$C_2Me_4Cp_2Mo(\mu\text{-}OH)]_2[OTs]_2$ from supersaturated solutions of [*ansa*-$C_2Me_4Cp_2Mo(OH)(OH_2)][OTs]$ suggests that the two species are in equilibrium; however, dehydration of [*ansa*-$C_2Me_4Cp_2Mo(OH)(OH_2)][OTs]$ upon crystallization to give [*ansa*-$C_2Me_4Cp_2Mo(\mu\text{-}OH)]_2[OTs]_2$ cannot be ruled out. Dimerization of *ansa*-$C_2Me_4Cp_2Mo(OH)(OH_2)^+$ was

observed in aqueous alcoholic solutions to give a mixture of the [*ansa*-$C_2Me_4Cp_2Mo(\mu$-$OH)]_2^{2+}$ dimer and the *ansa*-$C_2Me_4Cp_2Mo(OH)(OH_2)^+$ monomer, which indicates that the monomer and dimer are in equilibrium (eq 5) and the equilbrium has a strong solvent dependence. This observation led us to further investigate the behavior of the *ansa*-complexes in organic solvent mixtures.

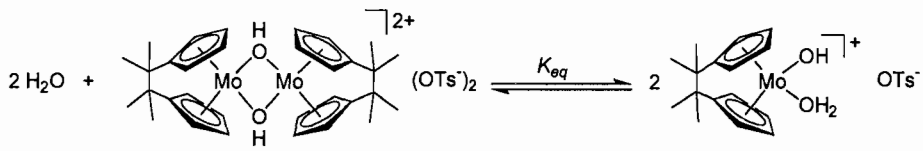

(5)

To explore the behavior of the *ansa*-$C_2Me_4Cp_2Mo(OH)(OH_2)^+$ complex in various solvent mixtures, aqueous solutions containing only *ansa*-$C_2Me_4Cp_2Mo(OH)(OH_2)^+$ (as indicated by the ^1H NMR spectra) were diluted with water-miscible organic solvents. Addition of an equal volume of methanol or ethanol to an aqueous solution of the monomeric species resulted in a mixture of *ansa*-$C_2Me_4Cp_2Mo(OH)(OH_2)^+$, $[C_2Me_4Cp_2Mo(\mu$-$OH)]_2^{2+}$, and a third *ansa*-molybdocene species assigned to [*ansa*-$C_2Me_4Cp_2Mo(OH)(X)]^+$ or [*ansa*-$C_2Me_4Cp_2Mo(X)_2$], where X = OCD_3 or OC_2D_5, respectively (Figure 3). (The resonances for these latter species, labeled A in Figure 2, have been observed before.[1] Because the A resonances are always observed upon addition of an alcohol to *ansa*-$C_2Me_4Cp_2Mo(OH)(OH_2)^+$, assignment to the [*ansa*-$C_2Me_4Cp_2Mo(OH)(X)]^+$ or [*ansa*-$C_2Me_4Cp_2Mo(X)_2$] species is logically suggested.[1] Furthermore, the alkoxide ligands may bridge the *ansa*-$C_2Me_4Cp_2Mo^{2+}$ fragments leading to the formation of [*ansa*-$C_2Me_4Cp_2Mo(\mu$-$X)]_2^{2+}$ instead of [*ansa*-

$C_2Me_4Cp_2Mo(\mu\text{-}OH)]_2^{2+}$ or to an equilibrium mixture of both species. Assignment of the dimeric species formed in aqueous alcohol as [*ansa*-$C_2Me_4Cp_2Mo(\mu\text{-}OH)]_2^{2+}$ instead of [*ansa*-$C_2Me_4Cp_2Mo(\mu\text{-}X)]_2^{2+}$ was based on excellent agreement with the ^1H NMR spectrum of $[C_2Me_4Cp_2Mo(\mu\text{-}OH)]_2^{2+}$ in pure water.) Note that, for the experiment depicted in Figure 2, 76 % of the *ansa*-$C_2Me_4Cp_2Mo(OH)(OH_2)^+$ monomer is converted to the [*ansa*-$C_2Me_4Cp_2Mo(\mu\text{-}OH)]_2^{2+}$ dimer in the presence of methanol, while only 7 % dimerized in the solution containing aqueous ethanol. In contrast, no dimer was observed on addition of an equal volume of THF, DMSO, or acetone to an aqueous solution of *ansa*-$C_2Me_4Cp_2Mo(OH)(OH_2)^+$. In fact, crystals of [*ansa*-$C_2Me_4Cp_2Mo(\mu\text{ -}OH)]_2^{2+}$ are immediately dissolved and completely hydrolyzed to the monomer in slightly wet DMSO or THF as shown by the appearance of resonances at 7.0 ppm and 6.2 ppm in the ^1H NMR spectra, which demonstrates that *ansa*-$C_2Me_4Cp_2Mo(OH)(OH_2)^+$ is the preferred species in these wet solvents as well as in water, i.e., the monomer is more stable than the dimer in these solvents. Such stabilization of the monomeric species is unprecedented using the non-*ansa* molybdocenes. Note that both non-*ansa* $[Cp^{(\prime)}{}_2Mo(\mu\text{ -}OH)]_2^{2+}$ dimers are more stable than their respective $Cp^{(\prime)}{}_2Mo(OH)(OH_2)^+$ monomers (as indicated by the equilibrium constants, see the Introduction) under all aqueous conditions examined thus far.[1,11] Based on the available spectroscopic data, as well as the limit of detection for a 600 MHz NMR spectrometer, $K_{eq} \geq 2$ M for eq 5 in water (25 °C, pD 6.8), which is four orders of magnitude greater than the K_{eq} found for $[Cp_2Mo(\mu\text{-}OH)]_2^{2+}$. In contrast, K_{eq} is approximately 9×10^{-2} M and 7×10^{-6} M at 25 °C in ethanol and methanol, respectively,

based on the ratio of monomer to dimer present in the 50 % aqueous solutions previously discussed.[b]

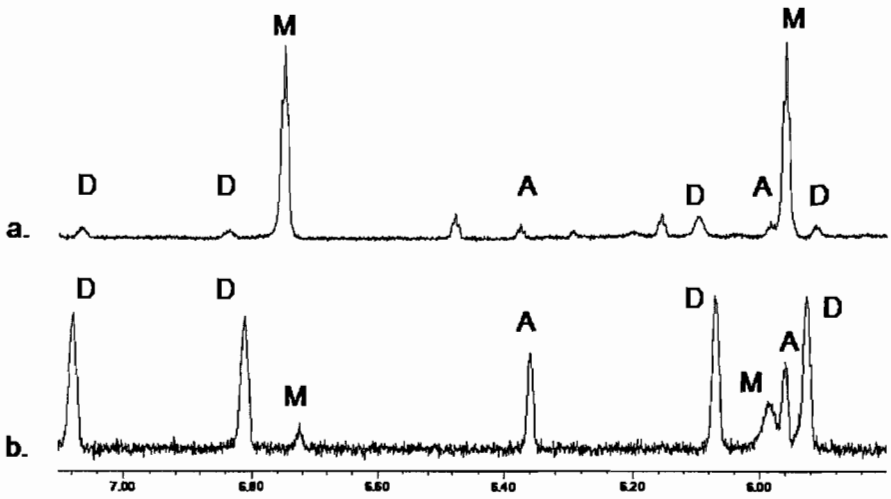

Figure 2. Aromatic region of ^{1}H NMR spectra of *ansa*-$C_2Me_4Cp_2Mo(OH)(OH_2)^+$ dissolved in 1:1 mixtures of (a) D_2O:C_2D_5OD and (b) D_2O:CD_3OD. D = [*ansa*-$C_2Me_4Cp_2Mo(\mu\text{-}OH)]_2^{2+}$, M = [*ansa*-$C_2Me_4Cp_2Mo(OH)(OH_2)]^+$, A = [*ansa*-$C_2Me_4Cp_2Mo(OH)(X)]^+$ or [*ansa*-$C_2Me_4Cp_2Mo(X)_2$], where X = OC_2D_5 or OCD_3.

The large differences in the estimated equilibrium constants for eq 5 illustrates that the equilibrium established by the tetramethylethylene-bridged *ansa*-molybdocenes is not determined by sterics or electronics. The *ansa*-linkage minimizes, if not eliminates, steric interactions between the Cp rings on different Mo centers. Moreover, the increased electrophilicity of the *ansa*-$C_2Me_4Cp_2Mo^{2+}$ cation should promote dimerization of the monomer. This statement is based on the equilibrium data previously measured for the non-*ansa* complexes, which showed more favorable dimerization of the relatively electrophilic Cp complexes compared with the Cp' species due to a larger enthalpic gain achieved upon formation of the Mo-OH bonds in $[Cp_2Mo(\mu\text{-}OH)]_2^{2+}$ compared to $[Cp'_2Mo(\mu\text{-}OH)]_2^{2+}$ ($\Delta H^\circ = 6.2 \pm 0.5$ kcal/mol and 1.5 ± 0.1 kcal/mol for Cp and Cp', respectively, in eq 1). Because the absence of dimerization noted for the *ansa*-$C_2Me_4Cp_2Mo(OH)(OH_2)^+$ monomer cannot be attributed to the steric or electronic effects of the ligand, it is suggested that the equilibrium established by the *ansa*-molybdocenes is largely determined by the ability of the chosen medium to solvate either the *ansa* monomer or dimer species. Effective solvation of the *ansa*-dimer is likely dependant on the solvent polarity, dielectric constant, hydrogen bonding ability, and/or solvent basicity; however, no correlation could be made between the estimated K_{eq} values and any one of these factors. (A table of solvent properties, i.e. dielectric constants, pK_a values, etc., for solvents used in this study is located in Appendix B.)

The strong solvent dependence of K_{eq} in the *ansa* complexes is consistent with prior observations noted in the synthesis of the *ansa*-$C_2Me_4Cp_2Mo(OH)(OH_2)^+$ monomer.[1] The $Cp^{(\prime)}{}_2Mo(OH)(OH_2)^+$ catalysts are accessed by hydrolysis of the

$[Cp^{(\prime)}_2Mo(\mu\text{-}OH)]_2^{2+}$ dimers, which are prepared by reaction of the respective molybdocene dihydride with *p*-toluene sulfonic acid in aqueous acetone (eq 6).[14,15]

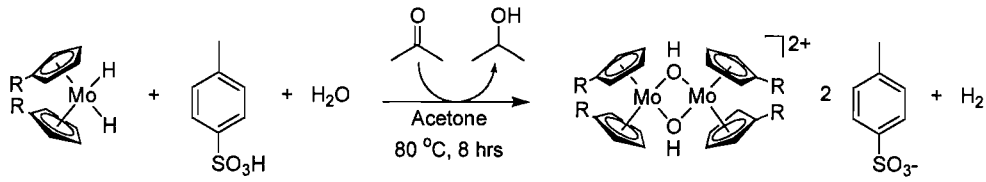

(6)

In contrast, reaction of the analogous tetramethylethylene-bridged *ansa*-molybdocene dihydride with tosic acid did not give the $[ansa\text{-}C_2Me_4Cp_2Mo(\mu\text{-}OH)]_2^{2+}$ dimer. Instead, the monomeric $ansa\text{-}C_2Me_4Cp_2Mo(OH)(OH_2)^+$ species (eq 7) precipitates from this reaction because, as this work has demonstrated, it is the thermodynamically favored product in aqueous acetone.

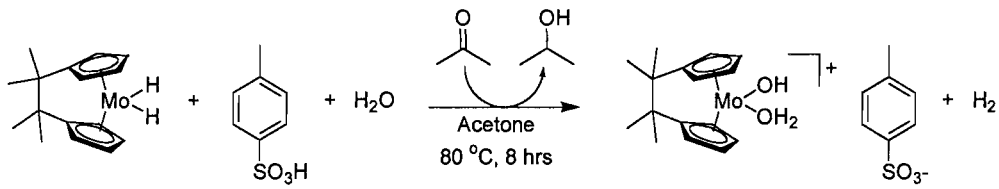

(7)

3.3.2 Effect of Molybdocene Dimerization on the Rate of Catalytic Nitrile Hydration

To investigate the impact of catalyst dimerization on the rate of nitrile hydration, rates for the $Cp'_2Mo(OH)(OH_2)^+$- and $Cp_2Mo(OH)(OH_2)^+$-catalyzed hydration of 3-hydroxypropionitrile (3-HPN) were compared to those obtained with the *ansa*-$C_2Me_4Cp_2Mo(OH)(OH_2)^+$ catalyst. The experimental plan was for each reaction to be

performed using identical concentrations of nitrile and total Mo. Therefore, if dimerization of the non-*ansa* molybdocenes has a significant effect on the reaction rates, the rates will decrease with increasing dimer formation in the order *ansa*-$C_2Me_4Cp_2Mo(OH)(OH_2)^+ > Cp'_2Mo(OH)(OH_2)^+ > Cp_2Mo(OH)(OH_2)^+$ due to a decrease in the concentration of the active monomer. (To summarize why this ordering is predicted: no [*ansa*-$C_2Me_4Cp_2Mo(\mu\text{-}OH)]_2^{2+}$ is observed in solutions of *ansa*-$C_2Me_4Cp_2Mo(OH)(OH_2)^+$ at any temperature. In the case of the Cp'-containing molecule, the $[Cp'_2Mo(\mu\text{-}OH)_2]^{2+}$ dimer is slightly more stable than $Cp'_2Mo(OH)(OH_2)^+$ (eq 2, $\Delta G^\circ = 2.2$ kcal/mol at pH 7.2, 25 °C), and consequently only a small amount of dimerization is observed in aqueous solution. Appreciable catalyst dimerization is only observed for the $Cp_2Mo(OH)(OH_2)^+$ catalyst.) Because of the low solubility of the *ansa*-$C_2Me_4Cp_2Mo(OH)(OH_2)^+$ complex in water (< 5 mM), nitrile hydration was carried out using a total Mo concentration of 0.58 mM in 0.13 M MOPS buffer. The resulting concentration of monomer and the kinetic data for the three catalysts are compared in Table 1. A sample kinetic trace and the calculated fit are shown in Figure 3. The second-order rate constants (k_{app}) for nitrile hydration and the first-order rate constants for H-D exchange (k_2 and k_3) are found in Appendix B.

Table 1. Comparison of kinetic data obtained for the hydration of 0.060 M 3-hydroxypropionitrile at 80 °C using a total Mo concentration of 0.58 mM in 0.13 M MOPS buffered D_2O

Ligand	[Monomer] (mM)	Rate ($Ms^{-1} \times 10^8$)	TOF (mol amide/mol monomer · s x 10^5)
$\{C_2Me_4(C_5H_4)_2\}$	0.58	3.2 ± 0.2	5.6 ± 0.3
$(C_5H_5)_2$	0.39	3.9 ± 0.3	10 ± 1
$(C_5H_4Me)_2$	0.56	3.0 ± 0.2	5.4 ± 0.4

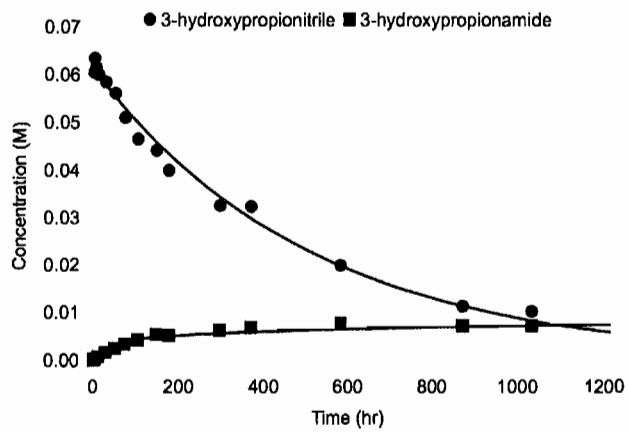

Figure 3. Graph of concentration versus time and the GIT fit for the *ansa*-$C_2Me_4Cp_2Mo(OH)(OH_2)^+$-catalyzed hydration of 3-hydroxypropionitrile.

Comparison of the turnover frequencies in Table 1 shows that $Cp_2Mo(OH)(OH_2)^+$ is almost twice as reactive as the *ansa*-$C_2Me_4Cp_2Mo(OH)(OH_2)^+$ and $Cp'_2Mo(OH)(OH_2)^+$ complexes. However, because of the increased amount of dimer in solution for the $Cp_2Mo(OH)(OH_2)^+$ complex, the net reaction rate is only 22% and 30% faster than the rates for the *ansa*-$C_2Me_4Cp_2Mo(OH)(OH_2)^+$ and $Cp'_2Mo(OH)(OH_2)^+$

catalysts, respectively. These data show that a small increase in reaction rate can be achieved by suppressing catalyst dimerization using the slightly less reactive *ansa*-$C_2Me_4Cp_2Mo(OH)(OH_2)^+$ complex. Note that an equilibrium mixture of $Cp_2Mo(OH)(OH_2)^+$ containing a 0.58 mM concentration of the Cp_2Mo^{2+} unit contains only 17 % of the dimeric $[Cp_2Mo(\mu\text{-}OH)]_2^{2+}$ species at 80 °C. To test whether dimerization affects the reaction rate at higher concentrations of molybdocene, where the percentage of dimer in solution is higher, a second comparison was made using a total molybdenum concentration of 2.8 mM of the non-*ansa* $Cp'_2Mo(OH)(OH_2)^+$ and $Cp_2Mo(OH)(OH_2)^+$ catalysts, which contain approximately 6 % $[Cp'_2Mo(\mu\text{-}OH)_2]_2^{2+}$ and 30 % $[Cp_2Mo(\mu\text{-}OH)_2]_2^{2+}$, respectively. The results are shown in Table 2. Note the rate of $Cp'_2Mo(OH)(OH_2)^+$-catalyzed HPN hydration is virtually identical to the rate obtained using the $Cp_2Mo(OH)(OH_2)^+$ catalyst when the concentration of catalyst and the associated dimer are increased. These data indicate that a significant reduction in catalyst dimerization does counterbalance the slight, yet significant, activity loss exhibited by the $Cp'_2Mo(OH)(OH_2)^+$ complex. It may be inferred by comparison of this trend with that obtained at lower concentrations of catalyst that the effect of dimerization will continue to increase with increasing catalyst concentration.

Table 2. Comparison of kinetic data obtained for the hydration of 0.26 M 3-hydroxypropionitrile at 80 °C using a total Mo concentration of 2.8 mM in 0.13 M MOPS buffered D_2O

Ligand(s)	[Monomer] (mM)	Rate ($Ms^{-1} \times 10^6$)	TOF (mol amide/mol monomer · s x 10^4)
$(C_5H_5)_2$	1.1	1.3 ± 0.1	12 ± 1
$(C_5H_4Me)_2$	2.5	1.3 ± 0.2	5.3 ± 0.4

A comparison of the turnover frequencies in Table 2 indicates that the $Cp_2Mo(OH)(OH_2)^+$ monomer is two times more reactive than the $Cp'_2Mo(OH)(OH_2)^+$ monomer toward the hydration of 3-HPN. Data reported previously[1] found that the rate constants for these reactions are the same within error. The discrepancy can be attributed to a difference in the concentration of total molybdenum and substrate concentration for the two sets of experiments, because both parameters affect k_{app}. Although the trends reported herein are slightly different, all of the data show that $Cp_2Mo(OH)(OH_2)^+$ is more reactive than the Cp-substituted molybdocene complexes. In summary of this section, the dimerization of molybdocene complexes does not have an appreciable effect on the rate of nitrile hydration at low catalyst concentration. However, at high concentrations, the percentage of dimer present in solution becomes significant and the net rate of hydration may be affected.

3.4 Summary

The $[Cp^{(\prime)}{}_2Mo(\mu\text{-}OH)]_2{}^{2+}$ dimers are more thermodynamically stable than two $Cp^{(\prime)}{}_2Mo(OH)(OH_2)^+$ molecules (ΔG^o = 2.2 kcal/mol and 4.9 kcal/mol for Cp and Cp', respectively, at 25 °C) in water. A consequence of this dimer stability is that a significant fraction of the catalytically active $Cp'_2Mo(OH)(OH_2)^+$ monomer is inactive because it is tied up in dimeric form. In contrast, the experiments reported herein demonstrate that the monomeric *ansa*-$C_2Me_4Cp_2Mo(OH)(OH_2)^+$ complex is significantly more stable than the [*ansa*-$C_2Me_4Cp_2Mo(\mu\text{-}OH)]_2{}^{2+}$ dimer in water, as well as in aqueous mixtures of THF, DMSO, and acetone. Experiments showed that the destabilization of *ansa*-$[C_2Me_4Cp_2Mo(\mu\text{-}OH)]_2{}^{2+}$ relative to the monomer is due to solvation changes. Specifically, because the *ansa* dimer crystallizes from aqueous solution at low concentration, it is suggested that in water the dimer is solvated more poorly than the monomer. However, the *ansa* dimer is soluble in DMSO and THF, and it is unclear whether the energy of monomer or dimer is most affected by solvation in these solvents. Overall, these results show that careful solvent selection is an effective method of suppressing catalyst dimerization, which can lead to faster rates of catalytic hydration.

In Chapter IV, the effect of Cp ring substituents on the acidity of the aqua ligands of $Cp_2Mo(OH_2)_2{}^{2+}$ is examined. Potentiometric investigations of the non-*ansa* molybdocenes $[Cp_2Mo(\mu\text{-}OH)]_2[OTs]_2$ and $[Cp'_2Mo(\mu\text{-}OH)]_2[OTs]_2$ confirmed the presence of a third protonation/deprotonation event that was not reported in previous literature. A new scheme is proposed for the aqueous speciation of the molybdocene that

accounts for this additional protic species and the equilibrium data previously reported for Cp_2MoO.

3.5 Notes

(*a*) Note that the other spectroscopic handles in the [*ansa*-$C_2Me_4Cp_2Mo(\mu\text{-}OH)]_2^{2+}$ species, namely the methyl substituents on the bridging atoms, could not be used to detect the dimer because they resonate at the same frequency as in the *ansa*-$C_2Me_4Cp_2Mo(OH)(OH_2)^+$ monomer in D_2O.

(*b*) The K_{eq} values in the aqueous methanol and ethanol solutions were determined using an activity of one for H_2O rather than using the molar concentration of water. This was done to facilitate comparisons with the K_{eq} values for the non-*ansa* complexes obtained in dilute aqueous solution, for which a value of one was used for the activity of water. If the molar concentration of water is used instead of an activity of one then the K_{eq} values for the non-*ansa* complexes are 8.8×10^{-8} $M^{-1} \pm 0.3 \times 10^{-8}$ M^{-1} and 8.1×10^{-6} $M^{-1} \pm 0.3 \times 10^{-6}$ M^{-1} for Cp and Cp', respectively. Using the molar concentration of water for the equilbrium constants measured for the *ansa*-bridged species, K_{eq} is at least 7×10^{-4} M^{-1} in dilute water and approximately 1×10^{-4} M^{-1} and 9×10^{-9} M^{-1} in aqueous ethanol and methanol, respectively.)

CHAPTER IV

AQUEOUS SPECIATION OF *ANSA*- AND NON-*ANSA*- SUBSTITUTED

$[Cp_2Mo(\mu\text{-}OH)]_2[OTs]_2$

This chapter was coauthored with Gregory T. Baxley and David R. Tyler and has been submitted to *Inorganica Chimica Acta*.

4.1 Introduction

In order to understand the catalytic species that may be present in aqueous solutions of *ansa*-molybdocenes, the aqueous speciation of *ansa*-$[C_2Me_4Cp_2Mo(\mu\text{-}OH)]_2[OTs]_2$ (**4**[a]) was investigated. For comparison purposes in this study, titration curves of complex **1** were reinvestigated. An earlier investigation of **1** in aqueous solution found two titratable protons (pK_a = 5.5 and 8.5), assigned to species **2** and **3**. Curiously, a third inflection point was observed for aqueous solutions of **1** in our studies,[1] indicating an additional protonation pathway that is not represented in Scheme 1. In this paper, titration curves generated from aqueous solutions of $[Cp_2Mo(\mu\text{-}OH)]_2[OTs]_2$ (**4**) $[Cp'_2Mo(\mu\text{-}OH)]_2[OTs]_2$ (**4'**, where Cp' = η^5-C_5H_4Me), *ansa*-$[C_2Me_4Cp_2Mo(\mu\text{-}$

OH)]$_2$[OTs]$_2$ (**4**^{a}) and Cp_2MoO (**6**) are compared. The titration and ^{1}H NMR data for **4** are also compared to that previously collected for aqueous solutions of **1** and **6**. These investigations support the equilibria established in Scheme 1, but confirm that an additional protonated species exists at low pH. A protonation step that is consistent with the reactivity and solution state behavior is proposed. These data improve our understanding of the aqueous speciation of molybdocenes. Furthermore, these data show how *ansa* Cp ligands affect the equilibrium processes in comparison to their non-*ansa* analogs.

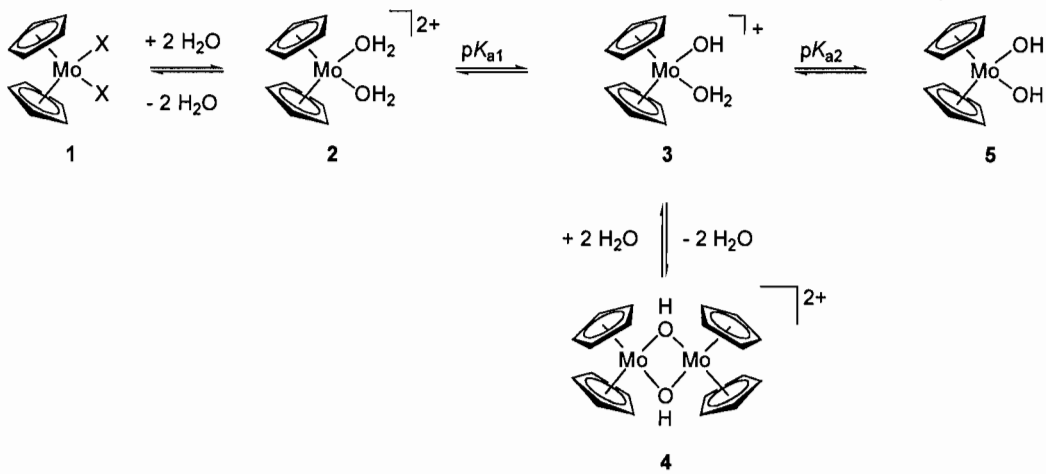

Scheme 1. Equilibria established by molybdocene complexes in water.

4.2 Experimental

$[Cp_2Mo(\mu\text{-}OH)]_2[OTs]_2$ (**4**),[2] $[Cp'_2Mo(\mu\text{-}OH)]_2[OTs]_2$ (**4′**),[3] *ansa*-$[C_2Me_4Cp_2Mo(\mu\text{-}OH)]_2[OTs]_2$ (**4a**),[4] and Cp_2MoO[1] were prepared as reported in the literature. Water and dilute HCl were purged with nitrogen prior to use. The

potentiometric measurements were carried out in a Vacuum Atmospheres Co. glovebox under nitrogen using an Orion model 230A plus pH meter with a Orion 9107BN Triode™ 3-in-1 pH/Automatic Temperature Compensation Probe. The pH adjustments were made using 0.026 M NaOH and 1.2 M HCl. Each titration curve was repeated three times. The variable pH ^{1}H NMR (500 MHz) spectra were obtained by adjusting of the pD of solutions of the dimer in D_2O using concentrated NaOD or DCl. The spectra were referenced to the tosylate counter ion at 7.60 ppm.

4.3 Results and Discussion

4.3.1 The Non-ansa Complexes

Potentiometric studies of the complexes **4**, **4′**, and **4^a** were carried out in order to determine the effect of the Cp ring substituents on the acidity of the aqua ligands of species **2**. To determine the acidity of the hydrolysis products generated from **4**, **4′**, and **4^a**, aqueous solutions of each dimer were acidified to pH 2 using dilute hydrochloric acid and then titrated with NaOH in a nitrogen atmosphere. The non-*ansa* dimers **4** and **4′** gave rise to similar titration curves (Figure 1), with three equivalence points each; the titration curve of **4^a** was distinct from that of the non-*ansa* dimers **4** and **4′** and will be discussed separately below. The pK_a values for **4** and **4′** are listed in Table 1. Note that complex **4** produced the same pK_a values (5.6 ± 0.1 and 8.3 ± 0.2) previously reported for **1**, a result that supports the equilibria shown in Scheme 1.[5]

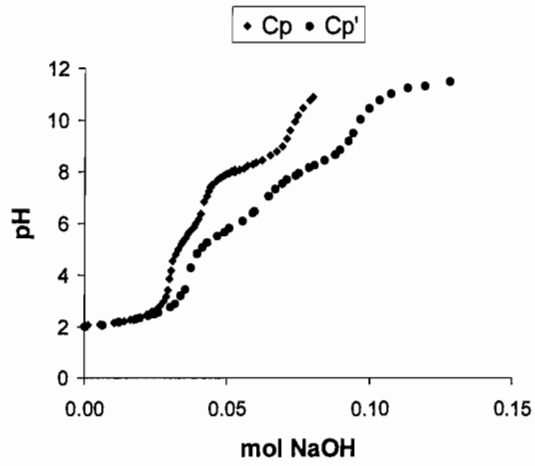

Figure 1. Base titration curves for the non-*ansa* molybdocenes $[Cp_2Mo(\mu\text{-}OH)]_2[OTs]_2$ (**4**) and $[Cp'_2Mo(\mu\text{-}OH)]_2[OTs]_2$ (**4′**).

Potentiometric studies of complexes **1** and **6** in aqueous solution were also carried out. The titration curves obtained in these experiments were essentially identical to those obtained for aqueous solutions of complex **4**, with pK_a values of 2.8, 5.5, and 8.3 (± 0.2) (Table 1).[1] (An acid titration of complex **6** using 0.01 M HCl gave similar results: the pK_a values obtained were 2.5, 5.3, and 8.2 (± 0.2).) The similarities in the pK_a values for **1**, **4**, and **6** suggests that all three complexes hydrolyze to similar species in aqueous solution, as illustrated in Scheme 1 for **1** and **4** and via the initial hydrolysis reaction shown in eq 1 for complex **6**. The pK_a values resulting from hydrolysis of the methyl-substituted dimer **4′** are slightly higher than those of **4** (~ 0.3 pK_a units on average) indicating a decrease in the acidity of the aqua ligands, as expected for the electron-richer Mo center in this molecule.

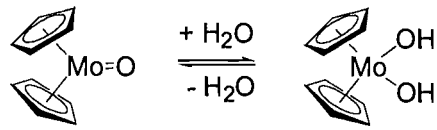

6 5 (1)

Table 1. pK_a values for $[Cp_2Mo(\mu\text{-}OH)]_2[OTs]_2$ (**4**), $[Cp'_2Mo(\mu\text{-}OH)]_2[OTs]_2$ (**4′**), **1**, and **6** in water. Unless indicated otherwise, all data are from this study.

	Complex				
	4	**4′**	**1**	**1**[a]	**6**
pK_{a1}	2.3 ± 0.1	2.5 ± 0.2	2.8 ± 0.2	not reported	2.8 ± 0.2
pK_{a2}	5.6 ± 0.1	6.0 ± 0.1	5.5 ± 0.1	5.5 ± 0.3	5.5 ± 0.1
pK_{a3}	8.3 ± 0.2	8.6 ± 0.2	8.3 ± 0.2	8.5 ± 0.3	8.3 ± 0.2

[a] ref. 5

Previous characterization and reactivity data suggest that the two deprotonation steps of complex **2** (Scheme 1) correspond to the higher pK_a values at approximately pH 5 and 8.[6] It is suggested that the third equivalence point observed for aqueous solutions of **1**, **4**, **4′**, and **6** corresponds to protonation/deprotonation of the dimeric species **4** (or **4′**) according to eq 2. Consistent with this proposal, it is noted that the bridging H_2O ligands in **8** are expected to be more acidic than the terminal H_2O ligand in **2** because the bridging H_2O ligands are bonded to two strongly Lewis acidic metal centers rather than just one.[a]

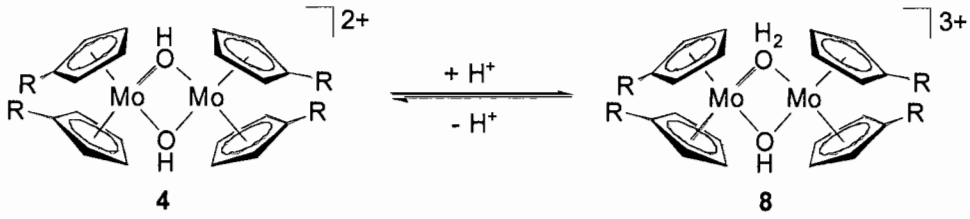

4 8 (2)

In support of the proposal that the most acidic equivalence point is attributable to the reaction in eq 2, the ^{1}H NMR spectra of complex **4** (or **4′**) dissolved in aqueous solutions at pH 2 to pH 4 showed only the presence of the monomers **2** (**2′**) and **3** (**3′**) and the dimer **4** (**4′**), Table 2.[7] Because these species are the only ones present in solution and because the equivalence points at higher pH are attributed to the deprotonations of **2** and **3**, it is reasonable to propose that deprotonation of **4** (or **4′**) gives rise to the third equivalence point. As expected from the equilibria in Scheme 1, the ^{1}H NMR spectrum of **1** at pH 2 to pH 4 is essentially identical to that of **4** at the same pH and also shows only the presence of species **2**, **3**, and **4** (Table 2).

Table 2. ^{1}H NMR data for aqueous solutions of **1**, **4**, and **4′** at pH 2-4.

	Monomers	Dimer
4′	5.82 (m,Cp), 5.55 (m, Cp), 1.72 (s, Me)	5.70 (m, Cp), 5.50 (m, Cp), 1.92 (s, Me)
4	5.98 (s) Cp	5.86 (s) Cp
1[a]	6.05 (s) Cp	5.85 (s) Cp

[a] pH 3

Based on the data presented here, a modified equilibrium scheme for molybdocenes in water is proposed in Scheme 2 that incorporates the protonation of **4** and the hydrolysis of **6**. The reactions in Scheme 2 account for all three pK_a values observed in the titrations of **1**, **4**, **4′**, and **6**.

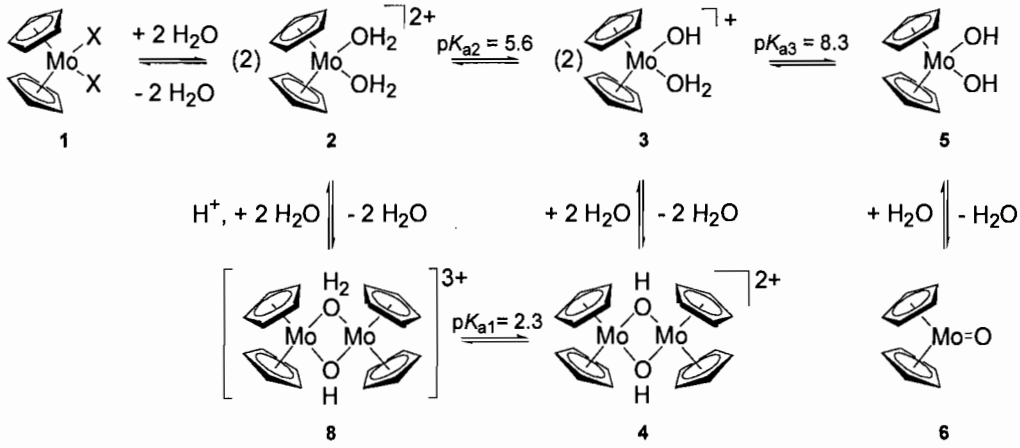

Scheme 2. Equilibrium pathways proposed for **4** and **4′** accounting for all three pK_a values (2.2 ± 0.1, 5.6 ± 0.1, 8.3 ± 0.2). In comparison to Scheme 1, also note the addition of Cp_2MoO to this scheme.

4.3.2 The ansa-Complex

Because the tetramethylethylene *ansa*-linkage leads to a more acidic Cp ligand set,[4,8-9] lower pK_a values were expected for **4**^{a} relative to **4** and **4′**. However, the titration curve of **4**^{a} was not simply a shifted version of the curves in Figure 2. Rather, a distinctly different curve with only two discernable equivalence points (pK_a = 2.2 ± 0.2 and 9.8 ± 0.2) with a shape indicative of a strong and a weak Bronstead acid was obtained (Figure

2). Although the second equivalence point is barely discernable, the derived (derivative) inflection point is clear and reproducible. Furthermore, titration of a basic solution of **4**^{a} with dilute HCl gave an identical curve. It is noted that previous work has shown that the aqueous behavior and reactivity of **4**^{a} is similar to that of **4** and **4′**.[4,10] For example, **4**^{a} undergoes hydrolysis in water to give the monomeric species **3**^{a},[10] which catalyzes hydration and hydrolysis reactions at rates comparable to **4** and **4′**.[4] An investigation of the effect of solvent medium on the equilibrium behavior of **3**^{a} demonstrated that **3**^{a} is in equilibrium with **4**^{a}; however, the monomer **3**^{a} is significantly more stable than the dimer **4**^{a} in water. As a result, aqueous solutions are mostly monomer (~ 99 % **3**^{a}). Note that the equilibrium established by the *ansa*-molybdocenes can be shifted in favor of **4**^{a} by adding alcoholic solvents to give a desired mixture of **3**^{a} and **4**^{a}.

Given this similar aqueous behavior and reactivity for **4**^{a} compared to that of **4** and **4′**, it is suggested that similar protonation pathways exist in solution. Two possible equilibrium schemes are proposed for the *ansa*-molybdocene (shown as equilibria A and B in Scheme 3). In both cases, protonation of **5**^{a} ($pK_a = 9.8 \pm 0.2$) most likely occurs first, followed by protonation of either the monomeric **3**^{a} (equilibrium A) or the dimeric **4**^{a} (equilibrium B) at $pK_a = 2.2 \pm 0.2$. As discussed above, **4**^{a} should be harder to protonate because the ligand is being shared by two high oxidation state metals, which suggests that the protonation having an equivalence point at $pK_a = 2.2 \pm 0.2$ is of **3**^{a} (equilibrium A). However, this pK_a is close to that obtained for protonation of the analogous non-*ansa* dimers **4** and **4′** and therefore may correspond to protonation of **4**^{a} (equilibrium B).

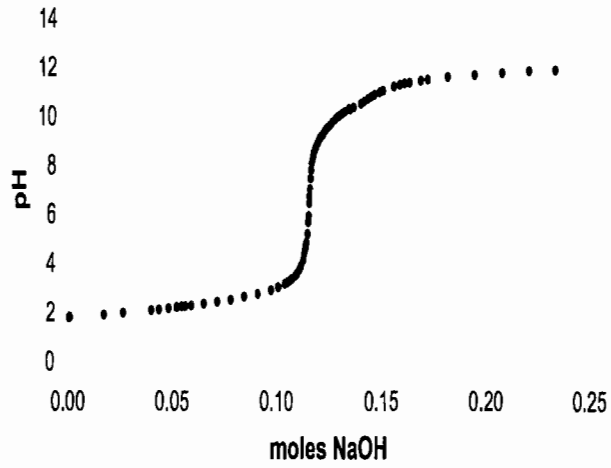

Figure 2. Base titration curve measured for an aqueous solution of $\mathbf{4}^{a}$.

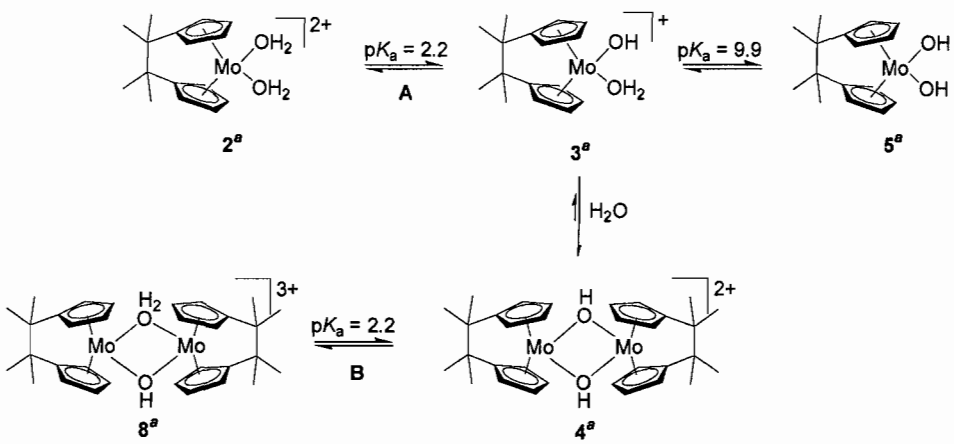

Scheme 3. Equilibrium pathways for the hydrolysis products of $\mathbf{4}^{a}$ involving the protonation of $\mathbf{3}^{a}$ (equilibrium A) and the protonation of $\mathbf{4}^{a}$ (equilibrium B).

4.4 Summary

The hydrolysis products of the molybdocene dimers **4**, **4′**, and **4^a** were titrated with base in water. Dimers **4** and **4′** gave rise to three titratable protons: two from the aqua ligands of $Cp^{(\prime)}Mo(OH)_2^{2+}$ and one from $[Cp^{(\prime)}_2Mo(OH_2)(OH)MoCp^{(\prime)}_2]^{3+}$. Comparison of the titration and ^{1}H NMR data for **4** to that for complexes **1** and **6** demonstrated that all three species give rise to the same hydrolysis products. The equilibria in Scheme 2 account for all of the titratable protons observed experimentally. Addition of a methyl substituent to the Cp ring increased each pK_a value by approximately 0.3 pK_a units compared to the unsubstituted complex. This increase in pK_a (decrease in acidity) is attributed to the greater electron density on the Mo center in **4′** compared to **4**. In contrast, the tetramethylethylene *ansa*-linkage in **4^a** led to a totally different base titration curve with only two inflection points. Despite this difference, the aqueous speciation of complex **4^a** was shown to be analogous to that of the non-*ansa* species **4** and **4′**. This conclusion is based on NMR data showing monomer-dimer equilibrium behavior analogous to the non-*ansa* dimers **4** and **4^a**.[11] It remains unclear why the titration curve is different.

In Chapter V, the reactivity of $Cp_2Mo(OH)(OH_2)^+$ and the Pt phosphinito complex $[PtCl(PMe_2OH)\{(PMe_2O)_2H\}]$ with ketone- and aldehyde-derived cyanohydrins is recorded.

4.5 Notes

a. Direct comparison of the pK_a values for **2**, **2′**, **8**, and **8′** to values for other bridging and terminal aqua ligands of small molecule analogs cannot be made due to the lack of suitable systems for comparison in the literature. However, in general, geometric and electronic modifications that increase the Lewis acidity of the transition metal center or otherwise remove electron density from the water ligand also increase the acidity of the aqua ligand. These modifications include electronic-withdrawing ancillary ligands, an unsaturated coordination environment, or secondary hydrogen bonding interactions. Interaction with a second metal center would exert a similar electron withdrawing effect on an aqua ligand, thus rendering a bridging aqua ligand even more easily deprotonated than a terminal aqua ligand.

CHAPTER V

AN INVESTIGATION OF THE REACTIVITY OF PT PHOSPHINITO AND MOLYBDOCENE NITRILE HYDRATION CATALYSTS TOWARD CYANOHYDRINS

Sections of this work will be submitted for publication to the *Journal of the American Chemical Society* with coauthors Brandy R. Fox, Spring Melody M. Knapp, J. Jerrick Juliette, and David R. Tyler[†,*]

5.1 Introduction

The catalytic hydration of cyanohydrins (eq 1) provides an atom economical route to high-value α-hydroxyamides, α-hydroxycarboxylic acids, and α-hydroxycarboxylic esters, and is therefore an important transformation in many chemical and pharmaceutical industries.

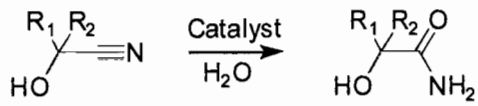

(1)

Industrial practices to hydrate cyanohydrins most heavily rely on sulfuric acid catalysis and generate the amide sulfate salt, as opposed to affording direct access to the α-hydroxyamide.[1] The amide sulfate product can then be hydrolyzed or esterified to afford value-added carboxylic acids and esters in high yield (> 92 %) for the generation of useful polymeric materials. However, the mass balance includes undesired sulfonates, oligomers, polymers, and ammonium bisulfate generated as a result of the strongly acidic reaction conditions. The production of ammonium bisulfate is a major economic and environmental drawback of a large-scale sulfuric acid mediated process, because its disposal requires additional processing steps. (For a more detailed discussion of cyanohydrin hydration, see Chapter I Section 1.2). We aim to develop a sulfuric acid-free process for the hydration of cyanohydrins using a low-cost homogeneous, transition metal catalyst that will enable direct access to the α-hydroxyamide product. The electronic and structural environment of such a catalytic system can be tailored to afford a general synthetic route by which a range of chiral and achiral α-hydroxyamides, α-hydroxycarboxylic acids, and α-hydroxycarbocylic esters can be accessed.

It is noteworthy that Cu salts and metal oxides that have found use in the industrial-scale synthesis of amides (such as Cu/Cr oxides, Cu/Mo oxides, and Raney Cu) were found to be ineffective in the hydrolytic conversion of cyanohydrins. Interestingly, even the MnO_2 must be treated to modify its structure for optimal activity, which adds to overall manufacturing cost. Because mechanistic investigations of heterogeneous catalytic systems are often ambiguous, the factors that affect the reactivity of these complexes toward cyanohydrins have not been delineated.

A host of organometallic and coordination complexes of early and late transition metals have been shown to catalyze the chemoselective conversion of nitriles to amides.[2] However, none of these systems have been applied to cyanohydrins. Herein, the reactivity of the water-soluble nitrile hydration catalysts $Cp_2Mo(OH)(OH_2)^+$ and $[PtCl(PR_2OH)\{(PR_2O)_2H\}]$ toward aldehyde- and ketone derived cyanohydrins is described. Previous studies demonstrated that the molybdocene catalysts are the most reactive toward nitriles bearing electron-withdrawing substituents, which boded well for molybdocene-catalyzed cyanohydrin hydration. The Pt phosphinito catalyst, first developed by Parkins and coworkers,[3-5] was chosen because it is one of the most reactive and versatile homogeneous nitrile hydration catalysts reported in the literature to date.[3-7] The broad applicability and high activity of the Pt phosphinito complexes toward nitrile substrates makes them excellent candidates for catalytic conversions of cyanohydrins.

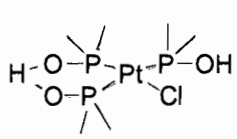

1

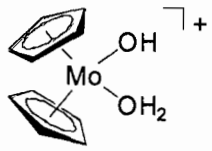

2

5.2 Experimental

5.2.1 General Considerations

Experiments were performed using standard air-free techniques in an atmosphere of N_2 unless otherwise stated. The complexes $[PtCl(PMe_2OH)\{(PMe_2O)_2H\}]$,[4] $[Cp_2Mo(\mu\text{-}OH)]_2[OTs]_2$,[8] 2-methoxypriopionitrile,[9] and 2-methoxyisobutyronitrile[9] were

synthesized according to procedures previously reported in the literature. Reagent grade nitriles (> 97 % purity) were purchased from Sigma Aldrich. Cyanohydrins were distilled before use, except cyclohexanone cyanohydrin (a solid) and glycolonitrile (purchased as a 55 % solution in water). Glycolamide was purchased from Sigma-Aldrich, and 2-hydroxyisobutyramide was purchased from TCI Japan Organic Chemicals. All hydrolysis and hydration reaction samples were prepared in a glovebox under an atmosphere of N_2 in Wilmad 9 in. precision NMR tubes or Wilmad J-Young screw cap NMR tubes, except when noted in the text. Reactions carried out in the Wilmad 9 in. NMR tubes were flame sealed while frozen. Reaction tubes were heated in an oil bath. ^{1}H NMR spectra were obtained using a Varian Inova 500 MHz (500.104 MHz for ^{1}H and 125.764 MHz for ^{13}C) or 600 MHz NMR spectrometer (599.982 MHz for ^{1}H and 150.879 MHz for ^{13}C). Cyanohydrin hydration reactions were performed using a plethora of reaction conditions. Representative procedures that yielded the best results are given below.

5.2.2 Preparation of Stock Solutions of 1

Stock solutions of **1** were prepared by adding [PtCl(PMe$_2$OH){(PMe$_2$O)$_2$H}] and Tl triflate to 10 mL of D_2O and heating to 80 °C. After 8 hours, the solutions were allowed to cool to room temperature and filtered using 0.22 μm filters to remove grey or white precipitate. The concentration of [PtX(PMe$_2$OH){(PMe$_2$O)$_2$H}] and degraded Pt was determined using an using a known amount of tetrabutylphosphonium bromide as an internal standard.

5.2.3 General procedures for the hydration of cyanohydrins catalyzed by 1

Note that procedure using the molybdocene catalyst (**2**) were identical to those described below, however, no Tl salt was added.

Glycolonitrile

Catalyst **1** (0.0054 g, 0.012 mmol) and TlOTf (0.0036 g, 0.010 mmol) was added to a solution of 55 % glyconitrile (3.55 mmol) in H_2O and allowed to react at 25 °C. After 3 days, the ^1H NMR spectrum showed a mixture of glycolonitrile at 4.50 ppm (s, 2H, (HO)C*H*$_2$CN), glycolamide at 4.30 ppm (s, 2H, (HO)C*H*$_2$C(O)NH$_2$).

Lactonitrile

Lactonitrile (250 μL, 3.49 mmol), catalyst **1** (0.0102 g, 0.0220 mmol), and TlOTf (0.0110 g, 0.0311 mmol) were added to 250 μL of D_2O. The mixture was allowed to react at 25 °C for 13 days over which time 69.0 % of lactonitrile was hydrated to 2-hydroxypropionamide. In the ^1H NMR spectrum, resonances (D_2O) for lactonitrile were observed at 4.66 ppm (q, J = 6.5 Hz, 1H, (HO)(CH$_3$)C*H*CN) and 1.48 ppm (d, J = 6.5 Hz, 3H, (HO)(C*H*$_3$)CHCN), and resonances for 2-hydroxypropionamide were apparent at 4.4 ppm (m, 1H, (HO)(CH$_3$)C*H*C(O)ND$_2$) and 1.29 ppm (d, 3H, (HO)(CH$_3$)C*H*C(O)ND$_2$)..

2-Hydroxybutyronitrile

A solution containing catalyst **1** (0.0165 g, 0.0356 mmol), TlOTf (0.0150 g, 0.0424 mmol), 2-hydroxybutyronitrile (250 μL, 2.83 mmol), 50 μL H_2O, and 200 μL methanol was prepared. Over 60 days at 25 °C, ^1H NMR resonances for 2-hydroxybutyronitrile at 4.57 ppm (t, J = 6.9 Hz, 1H, CH$_3$(HO)(CH$_2$)C*H*CN) and 1.91 ppm (quintet, J = 7.0 Hz, 2H, CH$_3$(HO)(CH$_2$)C*H*CN) and 1.14 ppm (t, J = 7.2 Hz, 3H,

CH_3(HO)(CH_2)CHCN) disappeared, and the appearance of 2-hydroxybutyramide at 7.52 ppm (s, 1H, CH_3(HO)(CH_2)CHCONH_2), 7.11 ppm (s, 1H, CH_3(HO)(CH_2)CHCONH_2), 4.12 ppm (m, 1H, CH_3(HO)(CH_2)CHCONH$_2$), 1.74 ppm (m, 2H, CH_3(HO)(CH_2)CHCN), and 1.06 ppm (t, J = 7.0 Hz, 3H, CH_3(HO)(CH_2)CHCN) was observed.

Mandelonitrile

A solution containing catalyst **1** (0.0183 g, 0.0395 mmol), TlOTf (0.0170 g, 0.0481 mmol), mandelonitrile (250 μL, 2.10 mmol), 50 μL H_2O, and 200 μL methanol was prepared. Initially, ^{1}H NMR resonances for mandelonitrile appeared at 7.46 ppm (m, 2H, C_5H_5(HO)CHCN), 7.32 ppm (m, 3H, C_5H_5(HO)CHCN), and 5.59 ppm (s, 1H, C_5H_5(HO)CHCN) After 3 days at 25 °C, benzaldehdye was noted at 9.77 ppm (s, 1H, C_5H_5(HO)C(O)H). A resonance of very low intensity was observable in the ^{13}C NMR spectrum at 183 ppm, which corresponds to the carbonyl C of the amide product and indicates a very small amount of hydration.

Cyclohexanone Cyanohydrin

Cyclohexanone cyanohydrin (0.0901 g, 0.720 mmol), catalyst **1** (0.0162 g, 0.0349 mmol), TlOTf (0.0150 g, 0.0424 mmol) were added to a mixture of 50 μL H_2O and 450 μL methanol. After 3 days at 25 °C, amide protons were apparent at 7.59 ppm and 7.01 ppm in the ^{1}H NMR spectrum.

Acetone Cyanohydrin

A solution containing catalyst **1** (0.0232 g, 0.0500 mmol), TlOTf (0.0200 g, 0.0566 mmol), acetone cyanohydrin (500 μL, 5.48 mmol), and 500 μL D_2O was prepared. The mixture was allowed to react for 7 days at 25 °C. During this time, the

acetone cyanohydrin was hydrated to 2-hydroxyisobutyramide (2.73 % yield) and dissociated to give 0.93 % of acetone. ^{1}H NMR resonances for the acetone cyanohydrin appeared at 1.65 ppm (s, 6H, HO(CH_3)$_2$CCN) and 2-hydroxyisobutyramide was observable at 1.44 ppm (s, 6H, HO(CH_3)$_2$CCOND$_2$). A less intense resonance was observed for acetone at 2.01 ppm (s, 6H, (CH_3)$_2$CO. The amide deuterium atoms were observable in the ^{2}H spectrum at 7.46 ppm and 6.76 ppm.

5.2.4 Hydration of Various Nitriles Catalyzed by 1

3-Hydroxypropionitrile

3-Hydroxypropionitrile (16 μL, 0.24 mmol) was added to 0.60 mL of catalyst solution (0.24 μmol) and 0.10 mL of PBu$_4$Br (0.32 μmol). Over 10 hours at 43 °C, ^{1}H NMR resonances (D$_2$O) for the 3-hydroxypropionitrile at 3.78 ppm (t, J = 6.0 Hz, 2H, HOCH_2CH$_2$CN) and 2.67 ppm (t, J = 6.0 Hz, 2H, HOCH$_2$$CH_2$CN) disappeared, and the appearance of 3-hydroxypropionamide at 3.76 ppm (t, J = 6.0 Hz), 2H, HOCH$_2$$CH_2$CONH$_2$) and 2.45 ppm (t, J = 6.0 Hz), 2H, HOCH_2CH$_2$CONH$_2$) was observed.

2-Methoxypropionitrile

Catalyst stock solution (0.60 mL, 0.24 μmol), PBu$_4$Br (0.10 mL, 0.32 μmol), and 2-methoxypropionitrile (22 μL, 0.24 mmol) were added to a nine-inch NMR tube. The ^{1}H NMR resonances (D$_2$O) before heating appeared at 4.39 ppm (q, J = 6.8 Hz, 1H, (CH_3O)(CH_3)CHCN), 3.44 ppm (s, 3H, (CH_3O)(CH_3)CHCN), and 1.49 (d, J = 6.8 Hz, 3H, (CH_3O)(CH_3)CHCN). Over 15 hours at 43 °C, the ^{1}H NMR resonances corresponding to 2-methoxypropionitrile decreased in intensity, and resonances for 2-

methoxypropionamide increased at 3.82 ppm (q, J = 6.8 Hz, 1H, $(CH_3O)(CH_3)CHC(O)ND_2$), 3.33 ppm (s, 3H, $(CH_3O)(CH_3)CHC(O)ND_2$), and 1.29 (d, J = 6.8 Hz, 3H, $(CH_3O)(CH_3)CHC(O)ND_2$).

2-Bromopropionitrile

2-Bromopropionitrile (21 μL, 0.24 mmol) was added to a mixture of catalyst stock solution (0.60 mL, 0.24 μmol) and PBu_4Br (0.10 mL, 0.32 μmol). 2-bromopropionitrile was sparingly soluble in D_2O and formed a white layer at the bottom of the NMR tube. The sample was heated at 43 °C for 24 hours. During this time all of the 2-bromoproionitrile dissolved and the ^1H NMR resonances (D_2O) for the 2-bromopropionitrile at 4.69 ppm (q, J = 7.2 Hz, 1H, $(Br)(CH_3)CHCN$) and 1.90 ppm (d, J = 7.1 Hz, 3H, $(Br)(CH_3)CHCN$) were replaced by resonances for 2-bromopropionamide at 4.49 ppm (q, J = 6.9 Hz, 1H, $(Br)(CH_3)CHC(O)ND_2$) and 1.71 ppm (d, J = 6.9 Hz, 3H, $(Br)(CH_3)CHC(O)ND_2$). Less intense resonances attributed to 2-hydroxypropionamide were also observed at 4.37 ppm and 1.33 pppm.

Acetonitrile

Acetonitrile (12.5 μL, 0.24 mmol) was added to a mixture of catalyst stock solution (0.60 mL, 0.24 μmol) and PBu_4Br (0.10 mL, 0.32 μmol). The resulting mixture was heated on an oil bath at 43 °C for 45 hours. During this time, acetonitrile was converted to acetamide. The production of acetamide was monitered in ^1H NMR spectrum (D_2O) by disppearance of the acetonitrile protons at 2.01 (s, CH_3CN) and the appearance of acetamide at 1.93 ppm (s, $CH_3C(O)ND_2$).

Propionitrile

Catalyst stock solution (0.60 mL, 0.24 μmol), PBu_4Br (0.10 mL, 0.32 μmol), and propionitrile (17 μL, 0.24 mmol) were added to a nine-inch NMR tube. Over 3 days at 43 °C, ^1H NMR resonances (D_2O) for the propionitrile at 2.38 ppm (q, J = 7.6 Hz, 2H, CH_3CH_2CN) and 1.18 ppm (t, J = 7.6 Hz, 3H, CH_3CH_2CN) disappeared, and the appearance of propionamide at 2.21 ppm (q, J = 7.6 Hz), 2H, $CH_3CH_2C(O)ND_2$) and 1.05 ppm (t, J = 7.7 Hz), 3H, $CH_3CH_2C(O)ND_2$) was observed.

Isobutyronitrile

Catalyst stock solution (0.600 mL, 0.24 μmol), PBu_4Br (0.10 mL, 0.32 μmol), and isobutyronitrile (22 μL, 0.24 mmol) were added to a nine-inch NMR tube. The ^1H NMR resonances (D_2O) at 2.81 ppm (heptet, J = 7.0 Hz, 1H, $(CH_3)_2CHCN$) and 1.26 ppm (d, J = 7.0 Hz, 6H, $(CH_3)_2CHCN$) before heating. Over three weeks at 43 °C, the ^1H NMR resonances corresponding to isobutyronitrile decreased in intensity, and resonances for 2-isobutyroamide appeared at 2.49 ppm (heptet, J = 7.0 Hz, 1H, $(CH_3)_2CHC(O)ND_2$) and 1.07 ppm (d, J = 7.0 Hz, 6H, $(CH_3)_2CHC(O)ND_2$).

Trimethylacetonitrile

Catalyst stock solution (0.60 mL, 0.24 μmol), PBu_4Br (0.10 mL, 0.32 μmol), and 2-methoxypropionitrile (26 μL, 0.24 mmol) were added to a nine-inch NMR tube. The resulting mixture was heated on an oil bath at 80 °C two days. During this time, trimethylacetonitrile was converted to trimethylacetamide. The production of trimethylacetamide was monitered in ^1H NMR spectrum (D_2O) by disppearance of the

trimethylacetonitrile protons at 1.31 (s, $(CH_3)_3CN$) and the appearance of trimethylacetamide at 1.35 ppm (s, $(CH_3)_3C(O)ND_2$).

2-Methoxyisobutyronitrile

2-methoxyisobutyronitrile (35 μL, 0.34 mmol) and **1** (0.0010 g, 2.2 μmol) and excess $NaBPh_4$ were added D_2O in to a nine-inch NMR tube. The solution was heated to 60 °C for 14 hours, during which time the 2-methoxyisobutyronitrile was hydrated. The hydration was monitored by the disappearance of ^1H NMR resonances (D_2O) at 3.36 ppm (s, 3H, $(CH_3O)(CH_3)_2CCN$) and 1.51 ppm (s, 6H, $(CH_3O)(CH_3)_2CCN$), and the appearance of resonancs at 3.18 (s, 3H, $(CH_3O)(CH_3)_2CC(O)ND_2$) and 1.28 (s, 6H, $(CH_3O)(CH_3)_2CC(O)ND_2$).

5.2.5 Control Experiment for H/D Exchange Reaction

7.00 μL of acetone cyanohydrin (77.0 μmol) was added to 0.800 mL od D_2O containing NBu_4BF_4 (6.96 μmol) and CD_3SO_3D (1.13 μmol) internal standards (pH 3.5). The dissapearance of ACH was monitored at 1.62 ppm (s, 6H, $HO(CH_3)_2CCN$), and the appearance of acetone and HCN were monitored at 2.23 ppm (s, 6H, $(CH_3)_2CO$) and 5.29 ppm (*H*CN) in the ^1H NMR spectrum. The appearance of deuterated ACH, acetone, and hydrocyanic acid were monitored in the ^2H NMR spectra at 1.62 ppm ($DO(CD_3)_2CCN$), 2.25 ppm ($(CD_3)_2CO$), and 5.28 ppm (*D*CN). After 25 days, 90.5 % of the ACH was fully deuterated, and a total of 43.3 % of the ACH was dissociation to acetone and HCN.

5.2.6 Tests for Substrate Inhibition

PBu_4Br (100 μL, 0.398 μmol), an aliquot of stock solution of **1** (400 μL, 0.195 μmol), and 3-hydroxyproponitrile (17.0 μL, 0.250 mmol) were added to each of three

nine-inch NMR tubes. After 50 minutes of reaction, one reaction mixture was spiked with lactonitrile (18.0 μL, 0.250 mmol), and acetone cyanohydrin (23.0 μL, 0.250 mmol) was added to a second. Reaction solutions spiked with lactonitrile and ACH showed an abrupt halt in reactivity.

5.2.7 Tests for Product Inhibition

Acetonitrile (28.0 mL, 0.536 mmol), 2-hydroxyisobutryonitrile (0.0135 g, 0.184 μmol), and PBu_4Br (100 μL, 0.44 μmol) were added to 400 μL of **1** (0.24 μmol) in D_2O and heated to 35 °C in oil bath and monitored for three days. In a separate trial, acetonitrile (12.5 μL, 0.239 mmol), glycolamide (0.0244 g, 0.325 mmol), and PBu_4Br (100 μL, 0.32 μmol) were added to 600 μL of **1** (0.24 μmol) in D_2O and heated to 35 °C in oil bath and monitored for three days. In both cases, the acetonitrile hydration was monitored by ^1H NMR spectroscopy as noted above. The rate of acetamide production was identical to that observed for the control reactions performed using identical concentrations of reactants (and internal standard) and no added amide.

5.2.8 Titration with KCN

Aliquots of KCN dissolved in D_2O (2 – 60 μL; 8.91 μmol – 0.913 mmol) were added to reaction mixtures containing 28.0 μL acetonitrile (0.536 mmol), 400 μL of **1** (0.205 μmol), and 100 μL of PBu_4Br (0.398 μmol) in 9 inch NMR tubes. The mixtures were heated at 35 °C in an oil bath for three days over which time the production of acetamide was monitored as noted above. Complete cessation of catalytic was observed above 3.5 equivalents. The rate of acetonitrile hydration was calculated from the %

conversion at 22 hours of reaction and plotted as a function of KCN equivalents with respect to dissolved Pt, which gives a linear plot described by ($y = -0.012x + 0.033$).

5.2.9 Hg Poisoning Test

1 (13 mg, 0.028 mmol) was added to a stirred mixture of acetonitrile (6.5 mL, 0.12 mol) and H_2O (4.0 mL, 0.22 mol). $AgBF_4$ (7.4 mg, 0.038 mmol) was added to the reaction mixture, and the mixture was refluxed at 85 °C for 3 hours. Hg^0 (3drops) was added to the reaction mixture, and the reaction was stirred under reflux for another 21 hours. Aliquots (0.25mL) of the reaction were taken at over twenty three hours, being careful not to remove any Hg^0. Aliquots were added to internal standard (3.32mM NMe_4PF_6 in D_2O, 0.25mL) in an NMR tube, and ^1H NMR was taken. When the reaction was stopped (at 24 hours), the Hg^0 was still shiny (no amalgam was observed). The conversion of acetonitrile to the acetamide occurred at the same rate as previously noted for a control reaction, indicating that the addition of Hg^0 did not suppress the activity of the Pt catalyst. Thus, the addition of Hg^0 had no effect on the catalyst, which leads to the conclusion that $[PtCl(DMPO)_3]$ is not a heterogeneous catalyst

5.3 Results and Discussion

5.3.1 Reactivity of Transition Metal Complexes with Cyanohydrins

Cyanohydrins were reacted with $[PtCl(PMe_2OH)\{(PMe_2O)_2H\}]$ (**1**) and $Cp_2Mo(OH)(OH_2)^+$ (**2**) nitrile hydration catalysts under a variety of reaction conditions. Selected reaction conditions and results illustrating the range of reactivity observed are listed in Table 1. Note that the results varied greatly with catalyst concentration,

substrate concentration, and volume of diluent. In general, the substrates reacted slowly to give poor yields of α-hydroxy acid amide product, if at all. Lactonitrile and 2-hydroxybutryonitrile produced the highest yields of amide product (> 48 %); while, glycolonitrile and cyclohexanone cyanohydrin yielded only 3 % and 14 % of the respective α-hydroxyamides. Acetone cyanohydrin (ACH) and mandelonitrile showed the least reactivity with the Pt catalyst, producing only few percent of α-hydroxyisobutyramide (< 3 %) and trace amounts of α-mandelamide, respectively. Lactonitrile and acetone cyanohdyrin were even less reactive with the strongly Lewis acidic molybdocene nitrile hydration catalyst **2**, producing only a couple percent of amide, at best. In many cases, dissociation of the cyanohydrin to give an equilibrium mixture of the cyanohydrin, hydrocyanic acid, and the parent aldehyde or ketone (eq 2) was the only reactivity observed.

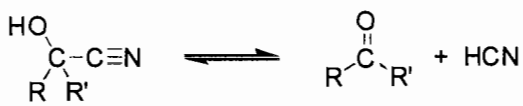

(2)

The extent of dissociation observed in the dilute reaction mixtures was more than expected, since the mixtures were acidified using triflic, methyl sulfonic, or tosic acid. It was expected that acidic conditions would help to stabilize the cyanohydrin species because acid is produced upon dissociation (eq 2). However, even at pH 1, extensive dissociation (> 80 %) was observed in several dilute reaction mixtures of ACH. This dissociation does not appear to be metal mediated on the basis of two results: First,

controls set up without Pt or Mo species present demonstrated that water (as well as other cosolvents) encourages the cyanohydrin dissociation, even when kept acidic. Specifically, at pH 3, 76.1 % dissociation of ACH was observed in five days without either catalyst present. Second, much less degradation was observed in reaction solutions maintained at room temperature, indicating thermal degradation as opposed to a metal-mediated mechanism. In contrast, if the metal center mediated dehydrocyanation of the cyanohydrin, dissociation would occur to the same degree at low temperature at a slower rate. The unfavorable effect of cosolvents observed in this study is consistent with the reports by Stewart and Fontana[10] who demonstrated that the equilibrium in eq 2 shifts toward the dissociation products at low concentrations of ACH. As shown in Table 1, carrying the reactions out at room temperature and high concentration of cyanohydrin minimized the dissociation. However, varying amounts of aldehyde or ketone due to dissociation were always observable by ^{1}H NMR spectroscopy in all of the reaction mixtures.

Table 1. Summary of cyanohydrin hydration results using $PtCl(PMe_2OH)\{(PMe_2O)_2H\}$ (**1**) and $Cp_2Mo(OH)(OH_2)^+$ (**2**) Nitrile Hydration Catalysts

Cyanohydrin	Catalyst	Cosolvent	mL Cyanohdyrin	mL water	mL Other Cosolvent	[Cyanohydrin] (M)	% Catalyst	Reaction Temp (°C)	% Dissociation	% Hydration	Rxn Time (hrs)
Glycolonitrile	1	H_2O	0.275	0.225	0.000	8.68	0.06%	25	1.00%	3.98%	52.6
Lactonitrile	1	D_2O	0.025	1.000	0.000	0.34	0.29%	80	1.07%	68.00%	1896.0
Lactonitrile	1	D_2O	0.250	0.250	0.000	6.97	0.63%	25	0.25%	68.95%	143.8
Lactonitrile	2	H_2O	0.250	0.25	0.000	6.97	1.04%	25	0.21%	0.82%	74.8
2-Hydroxybutyronitrile	1	D_2O	0.500	0.100	0.000	9.42	0.20%	50	< 0.5 %	0.00%	24.0
2-Hydroxybutyronitrile	1	H_2O, CH_3OH	0.250	0.050	0.200	5.65	1.26%	25	< 0.5 %	51.35%	99.5
Mandelonitrile	1	D_2O	0.500	0.100	0.000	7.01	0.20%	50	2.86%	0.00%	24.0
Mandelonitrile	1	H_2O, CH_3OH	0.200	0.050	0.250	3.36	2.35%	25	2.86%	Trace	74.4
Cyclohexanone Cyanohydrin	1	D_2O	0.0300	0.500	0.000	0.40	0.20%	50	--	0.00%	24.0
Cyclohexanone Cyanohydrin	1	H_2O, CH_3OH	0.0901	0.450	0.050	1.26	4.71%	25	--	14.00%	74.4
Acetone Cyanohydrin	1	D_2O	0.032	1.000	0.000	0.34	0.33%	25	5.30%	0.00%	24.2
Acetone Cyanohydrin	1	D_2O, $(CH_3)_2CO_2H$	1.000	0.426	1.000	4.51	0.05%	80	47.85%	0.00%	24.0
Acetone Cyanohydrin	1	D_2O, $(CH_3)_2CO$	0.640	0.426	0.815	3.73	0.08%	80	68.60%	0.00%	24.0
Acetone Cyanohydrin	1	D_2O	0.500	0.100	0.000	9.13	0.20%	50	25.00%	0.00%	328.2
Acetone Cyanohydrin	1	CH_3OH	0.500	0.000	0.100	9.13	0.19%	50	1.57%	0.00%	328.6
Acetone Cyanohydrin	1	IPA	0.500	0.000	0.100	9.13	0.10%	50	0.90%	0.00%	328.5
Acetone Cyanohydrin	1	D_2O	0.900	0.100	0.000	9.86	0.02%	25	0.32%	0.00%	170.7
Acetone Cyanohydrin	1	D_2O	0.500	0.500	0.000	5.48	0.04%	25	0.60%	0.00%	170.7
Acetone Cyanohydrin	1	D_2O	0.100	0.900	0.000	1.10	0.20%	25	2.98%	0.00%	170.7
Acetone Cyanohydrin	1	D_2O	0.500	0.500	0.000	5.48	0.91%	25	0.93%	2.72%	144.8
Acetone Cyanohydrin	1	H_2O, CH_3OH	0.250	0.050	0.200	5.48	1.34%	25	0.90%	2.00%	163.9
Acetone Cyanohydrin	1	H_2O, CH_3OH	0.250	0.250	0.000	5.48	1.34%	25	1.27%	1.06%	163.9
Acetone Cyanohydrin	2	D_2O, Acetic Acid	0.500	0.200	0.500	4.56	0.19%	80	80.00%	0.52%	38.6
Acetone Cyanohydrin	2	H_2O	0.250	0.250	0.000	5.48	1.76%	25	6.42%	1.00%	75.0

While the metal complex does not appear to mediate degradation, it does influence the position of the cyanohydrin-carbonyl equilibrium. A higher percentage of degradation was observable when a higher concentration of catalyst was used, even though all other conditions remained identical (i.e. solvent composition, reaction temperature, and substrate concentration). Over time, the percentage of degradation always approached or exceeded the percent catalyst. In general, more dissociation was observed in the presence of the molybdocene catalyst. The implications of these results will be discussed later in the text.

In several of the ACH reaction mixtures where no reactivity was observed, scrambling of the ketone and cyanohydrin protons with solvent deuterium was evident in the ^{1}H NMR spectrum by the appearance of triplet and quintet resonances on the shoulder of the parent resonance. The presence of the deuterated species was also confirmed in the ^{2}H spectrum. Exchange of the cyanohydrin protons with the deuterium oxide solvent was intriguing, because β-hydride elimination of the tertiary alcohol is not possible. However, H/D exchange was also observed in a control reaction performed at pH 3 without the Pt complex, indicating that the H/D exchange most likely proceeds via the keto-enol tautomerism of the parent carbonyl species under acidic conditions. It follows that deuterated cyanohydrin resulted from reversible addition of HCN to the ketone (Scheme 1). Indeed, at high ACH concentration when no acid was added to the reaction mixture, no deuterated acetone or cyanohydrin was observed.

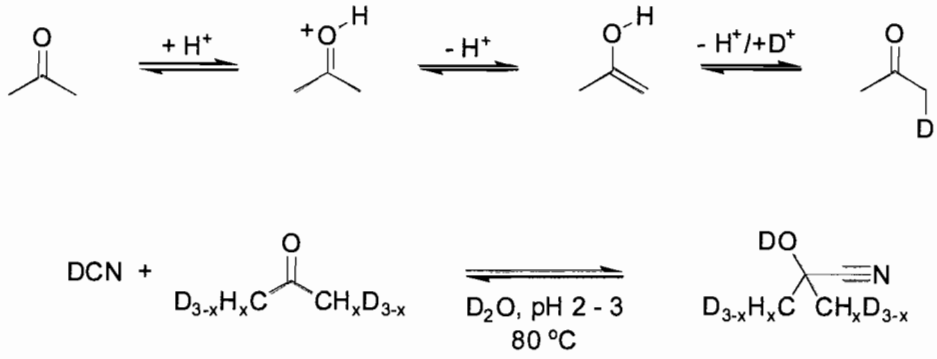

Scheme 1. Proposed mechanism of H/D exchange for cyanohydrins under acidic reaction conditions.

5.3.2 Comparison of Cyanohydrins to Other Nitriles

Based on the fact the cyanohydrins readily release cyanide, it was speculated that the nitrile carbon of cyanohydrins may be much more nucleophilic (or have more cyanide character) than other nitrile substrates. Such an electron rich carbon center will be much less susceptible to attack by an incoming nucleophile and may, therefore, be relatively unreactive by typical metal-mediated nitrile hydration pathways. However, comparison of the ^{13}C resonate frequencies of selected nitriles suggests that the cyanohydrin carbon is not unique (Table 2).

Table 2. Comparison of nitrile ^{13}C NMR resonate frequencies for selected nitriles

Nitrile	δ (NCR)
acetonitirile	118.1
3-hydroxypropionitrile	120.7
2-hydroxypropionitrile	121.5
acetone cyanohydrin	123.3
propionitrile	123.7

To gain further insight into the electronic and steric influence of the α-hydroxy group, an investigation of variously substituted nitriles was conducted. A summary of these results appears in Table 3. The rates shown were calculated for the nitrile substrates based on the percent conversion after two hours of reaction. No carboxylic acid product was observed in the reaction mixtures of this system, even after prolonged heating. Note that all reactions proceeded to completion displaying first or zero order dependencies on substrate, except for the hydration of lactonitrile (Figure 1). The rate of lactonitrile hydration declines rapidly from 0.062 M/hr to 1.9×10^{-4} M/hr within nine hours of reaction, which is typical of product inhibition. Interestingly, the substrates 2-methoxypropionitrile and 2-methoxyisobutyronitrile, which are electronically very similar to the cyanohydrins lactonitrile and acetone cyanohydrin (σ_m = 0.10 and 0.13 for MeO and OH, respectively) and even more sterically encumbered, reacted rapidly in excellent yield showing no signs of inhibition activity. Based on the results listed in Table 3, it is clear that the electron-withdrawing substituents actually facilitate the hydration reaction, and cyanohydrins are equally susceptible to Pt-mediated hydration as compared to the other nitriles tested. The lack of reactivity noted for the cyanohydrins is due to acute catalyst inhibition, which is unique to the cyanohydrins. Possible causes of inhibition are entertained in the following section.

Table 3. Rate data for hydration of various nitriles catalyzed by **1**

Substrate	[Substrate] (M)	% Catalyst	Rxn Temp. (°C)	Rate (M/hr)	% Conversion
3-hydroxypropionitrile[a]	0.34	0.10	43	9.4×10^{-2}	100
2-methyoxypropionitrile[a]	0.34	0.10	43	5.5×10^{-2}	100
2-bromopropionitrile[a]	0.34	0.10	43	2.5×10^{-2}	90
2-hydroxypropionitrile[a]	0.34	0.10	43	2.2×10^{-2}	12
acetonitrile[a]	0.34	0.10	43	1.3×10^{-2}	100
propionitrile[a]	0.34	0.10	43	8.0×10^{-3}	100
isobutyronitrile[a]	0.34	0.10	43	2.2×10^{-3}	100
Trimethylacetonitrile[b]	0.34	0.25	80	1.1×10^{-1}	100

[a] Reaction mixtures also contained 0.45 mM PBu_4Br as an internal standard.

[b] The hydration of $(CH_3)_3CCN$ was too slow at 43 °C to compare to other reaction rates listed in Table 3.

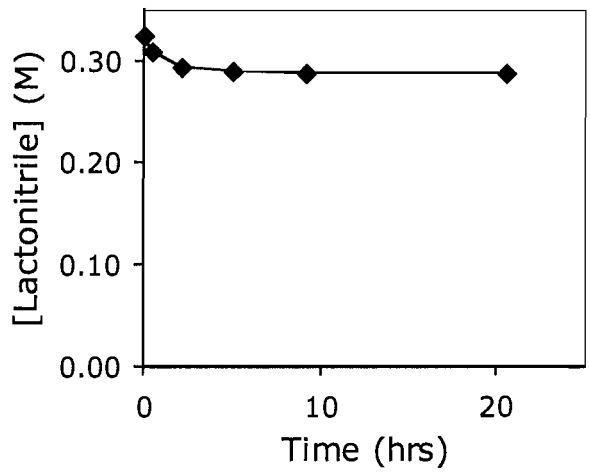

Figure 1. Plot of [Lactonitrile] versus time for the hydration of lactonitrile (0.34 M) catalyzed by **1**.

Note that molybdocene catalyzed nitrile hydration is facilitated by e^- withdrawing substituents, as well. In the case of molybdocenes, less than 1 % of lactonitrile was hydrated, suggesting more rapid catalyst inhibition for the molybdocene catalyst.

5.3.3 Catalyst Inhibition Tests

Although the cyanohydrins are electronically similar to the α-methoxy analogs, the substrates differ in that the cyanohydrins can be deprotonated. The consequences of deprotonation of the cyanohydrin are formation of a superior alkoxide ligand and dissociation of the cyanohydrin to generate the parent aldehyde or ketone and prussic acid. Based on these unique possibilities, three hypotheses were formulated to explain the observed inhibition of catalytic activity in the cyanohydrin substrate: 1.) Catalysis may be inhibited by irreversible formation of inert metallocyclic iminol or carboxamide structures. Such products would result from chelation or the partially or fully hydrated nitrile. It is well documented that coordination of amides to the transition metals stabilizes the iminol tautomer (Figure 2).[2] If fact, molybdocene-catalyzed nitrile hydration is known to be inhibited by irreversible coordination of amide products.[11] The α-hydroxy group of an α-hydroxyamide enables the formation of a more stable five-membered structure that may be even more inert to substitution. 2.) The cyanohydrin preferentially binds through the alcohol functionality leading to formation of an alkoxide ligand. Perhaps, binding of the cyanohydrin through the oxygen may lead to inadequate activation of the nitrile carbon and compromised activity. Furthermore, if the resulting alkoxide ligand is relatively inert, the formation of the metal-alkoxide complex will be a

thermodynamic sink resulting in acute substrate inhibition. 3.) The prussic acid produced in the dissociation of the cyanohydrin may poison the catalyst.

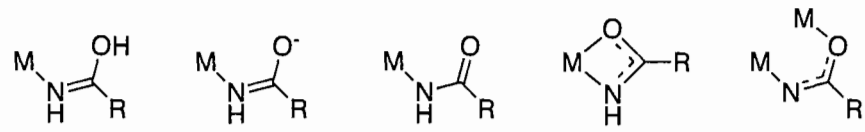

Figure 2. Stabilization of iminolato tautomers via metal coordination

To test for substrate and product inhibitition, acetone cyanohydrin, lactonitrile, α-hydroxyisobutyramide, and glycolamide were added to reaction mixtures containing 3-hydrxypropionitrile (3-HPN) or acetonitrile and complex **1**. Addition of the one equivalent of the α-hydroxyamides (with respect to the nitrile) to a reaction mixture of acetonitrile and **1** did not effect the rate of acetamide production, which suggests that product inhibition does not occur and hypothesis one was inaccurate for the Pt catalyst. Secondly, even though molybdocene mediated nitrile hydration tested positive for product inhibition in other experiments, the low levels of amide detected in those reaction mixtures could not be solely responsible for inactivating the catalyst. Thus, even though product inhibition does occur in the case of catalyst **2** other factors must be contributing to the low reactivity observed. Note that an abrupt halt in reactivity was observed when either acetone cyanohydrin or lactonitrile were added to a mixture of 3-HPN and **1**, which is superficially consistent with hypothesis two. However, because the cyanohydrins

dissociate to give HCN, this cessation in catalytic activity could be due to either the cyanohydrin (hypothesis 2) or the cyanic acid (hypothesis 3).

Results previously obtained for the molybdocene-catalyzed hydration of 3-hydroxypropionitrile (3-HPN) are inconsistent with the second hypothesis. The β-hydroxynitrile 3-HPN undergoes H/D exchange of the protons α to the alcohol and hydration of the nitrile in the presence of molybdocene catalysts in D_2O solvent (eq 3).[12]

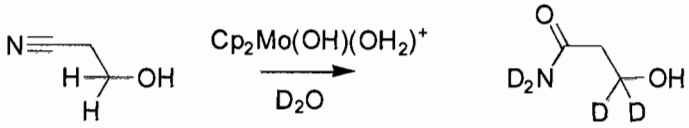

(3)

The accepted pathway of molybdocene catalyzed H/D exchange of alcohols involves β-hydride elimination of the coordinated alkoxide,[13,14] which indicates oxygen-coordination of the 3-HPN substrate. Coordination of 3-HPN does not compromise the reactivity of its nitrile functionality; on the contrary, the hydration of 3-HPN is one of the fastest nitrile hydration reactions noted for the molydbocene catalysts. If the nitrile carbon of β-hydroxynitrile is aptly activated for hydration despite preferential binding through the alcohol group, O-coordination of α-hydroxynitriles should not be problematic. Accordingly, hypothesis two can be ruled out.

Hypothesis three suggests that free cyanide generated from dissociation of the cyanohydrin may bind irreversibly to the Pt center and deactivate the catalyst. Indeed, the addition of excess KCN to 3-hydroxypropionitrile prevented hydration of nitrile. Instead, substitution of the hydroxy group occurred to give succinonitrile. In order to

determine the efficiency of cyanide poisoning, substoichiometric aliquots of potassium cyanide were added to reaction mixtures containing acetonitrile substrate (Figure 3). Interestingly, catalytic activity did not cease until the $[CN]/[Pt]_{total}$ ratio reached 3:1. Note that the concentration of **1** does not account for all of the Pt in solution, as some free ligand is observed in solution due to degradation of the Pt complex. (The aqueous behavior of $[PtCl(PMe_2OH)\{(PMe_2O)_2H\}]$ is described in more detail in the following section.) The identity of the resulting Pt cyanide complex(es) was not determined; however, it is obvious that three cyanide ligands are required to deactivate the catalyst. Furthermore, the rate of acetonitrile hydration versus cyanide equivalents gives a linear relationship, which indicates that cyanide binding is irreversible.

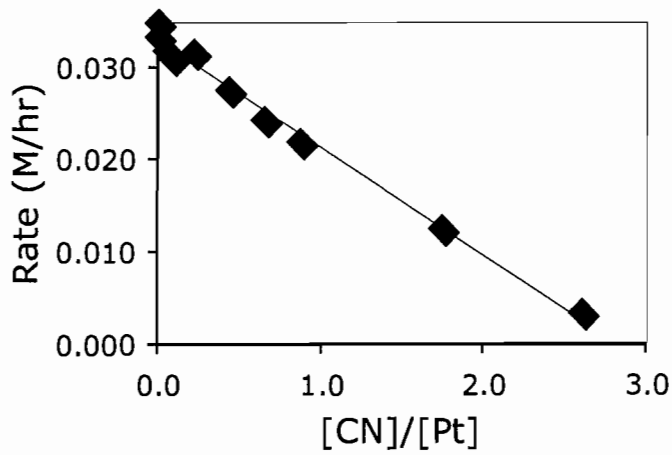

Figure 3. Plot of acetonitrile hydration rate versus [CN]/[Pt] showing the effect of CN on the catalytic activity of the $[PtCl(PMe_2OH)\{(PMe_2O)_2H\}]$ ($y = -0.012x + 0.033$).

Hypothesis three is also consistent with the results summarized in Table 1. As noted previously, at least trace amounts of ketone or aldehyde were detected in the ^{1}H NMR spectra of all of the reaction mixtures indicating equivalent levels of hydrocyanic acid. The highest percent of hydration was observed using the lactonitrile and 2-hydroxybutyronitrile, which are naturally more robust to dissocation than the acetone cyanohydrin and mandelonitrile substrates that showed little reactivity.[15] Close scrutiny of Table 1 shows that hydration was only observed when the percent dissociation was less than the percent of catalyst in solution, except in the cases of lactonitrile and glycolonitrile. This result may be rationalized after consideration that equilibration of cyanohydrins in solution occurs at different rates. The apparent inconsistency in the partial hydration of glycolonitrile and lactontrile is most likely due to slower dissociation of the more robust substrates leading to slower catalyst poisoning. Faster dissociation was observed at high temperatures leading to faster catalyst poisoning and lower yields (or none in the case of ACH). However, when left to react for over two and a half months, over 60 % conversion lactonitrile was observed. This may be due to very low levels of Pt or general acid catalysis.

It is interesting that three equivalents of HCN were not required to inhibit hydration of the cyanohydrins as in the case of acetonitrile hydration. The relative acuteness of cyanide poisoning in the cyanohydrin reaction mixtures may be due the inferiority of the cyanohydrins as ligands in comparison to acetonitrile. That is, acetonitrile is sterically less hindered and electron donating relative to the α-hydroxynitriles. As such, the acetonitrile substrate will be more competitive versus

cyanide for Pt binding than the cyanohydrins. These electronic and steric factors may also contribute to the partial hydration observed for glycolonitrile and lactonitrile; acetone cyanohydrin, on the other hand, is effectively poisoned at one equivalent of HCN. Furthermore, because the percent of hydrocyanic acid generated increases with increasing percent catalyst (presumably due to removal of cyanide in the form of a metal-CN complex), the number of catalytic turnovers possible will always be limited. The high oxidation state molybdocene catalyst is even more susceptible to cyanide poisoning because it is a much stronger Lewis acid.

5.4 Aqueous Behavior of [PtCl(PMe$_2$OH){(PMe$_2$O)$_2$H}]

The catalyst **1** was treated with a Ag^+, Tl^+, or Na^+ salt in water in order to abstract the chloro ligand from the Pt center. Partial to complete degradation of the [PtCl(PMe$_2$OH){(PMe$_2$O)$_2$H}] complex,due to dissociation of the dimethyl phosphinito ligands was always observed. Upon treatment of complex **1** with one of the aforementioned salts, the complex becomes slightly more water-soluble. The resonances in the ^{31}P NMR spectrum sharpen (δ 96 (d, 2 P) and δ 58 (t, 1 P)) and new resonances appear at δ 35 (t) and δ 53 (s), due to free ligand and dimethyl phosphinic acid, respectively. Note that dimethylphosphinic acid is generated by disproportionation of dimethylphoshine oxide, the tautomer of the dimetylphoshinito ligand. The gaseous dimethylphoshine byproduct is typically not observed; however, spiking with an authentic sample decisively identified the dimethylphosphinic acid. Addition of dimethylphosphinic acid to a solution of Pt stock solution after treatment with AgOTf

resulted in an increase in the resonance at δ 53 and no additional resonances. Little or no dimethylphosphinic acid was observed when oxygen was excluded from the reaction vessel.

Degradation of the catalyst is more extensive at high temperatures or when using Ag^+ salts. In fact, no resonances due to **1** were detectable by ^{31}P NMR spectroscopy after 12 hours at reflux in the presence of AgOTf or $AgBF_4$. Quantification of the resulting phosphine oxide and/or dimethylphosphinic acid only accounted for 67 % of the parent Pt complex, however analysis of the remaining solid indicated undissolved Pt starting material. Note that stock solutions prepared using Ag^+ salts were less reactive toward nitriles in general, especially the bulky 2° and 3° nitriles. Furthermore, in some cases, the reaction mixtures changed colors after several hours of reaction time. The color changes were inconsistent and appeared blue, pink, purple, red, yellow, and amber in different trials, and several reaction mixtures turned continued to change in color from colorless to blue to pink if left on the heat source. Additionally, in many of the instances where the solid formed upon treatment with Ag (presumed to be AgCl) was removed prior to addition of the nitrile, an abrupt halt in the hydration of the substrate accompanied this color change. The reaction rates were also inconsistent when Ag salts were used to abstract the chloride from **1**, which is suggestive of heterogeneous catalysis. However, no evidence was collected in support of heterogeneous catalysis, and addition of mercury to acetonitrile hydration reaction catalyzed by **1** did not affect the rate of the reaction. Further, treatment of the complex with AgOTf as a chloride abstraction in water agent led to formation of small amounts of acetic acid (< 10 %) in the subsequent hydration of

acetonitrile at 80 °C. The catalytic activity of **1** after treatment with Ag salts is discussed in further detail in Appendix D.

It was not possible to determine the identity of the active catalyst. Repeated attempts to crystallize the catalyst from stock solutions after treatment with a chloride abstraction agent resulted in crystallization of $[PtCl(PMe_2OH)\{(PMe_2O)_2H\}]\cdot 0.5H_2O$. (The crystallographic data for the hydrate appears in Appendic C.) Only one Pt phosphinito species is observable by ^{31}P NMR spectroscopy in the catalyst stock solution, so it may be assumed that the crystal structure is identical to the species observed in solution. However, the $[PtCl(PMe_2OH)\{(PMe_2O)_2H\}]$ species may be a relatively insoluble component that is only present in very small concentration.

5.5 Summary and Key Insights

Comparison of the reactivity of the cyanohydrins with that of other nitriles shows that the low reactivity of the α-hydroxynitrile substrates is not due to the steric or electronic consequences of the hydroxy group in the α position. In fact, the cyanohydrin lactonitrile exhibits initial rates that are comparable to that of other nitriles containing electron-withdrawing substituents, demonstrating that this subset of nitriles is not unique with regard to the electronic character of the nitrile carbon. Instead, the low activity observed is due to liberation of the hydrogen cyanide from the cyanohydrin substrate, which leads to deactivation of the catalyst. Unfortunately, because water is necessary for the hydration reaction, generation of some small equilibrium amount of HCN is inevitable. No evidence of metal-mediated hydrodecyanation was observed, however

coordination of the free cyanide to the transition metal encourages greater dissociation by removing HCN from the equilibrium. Irreversible binding of cyanide ensures complete catalyst poisoning. Deactivation due to cyanide poisoning was general for the low oxidation state, late transition metal Pt catalyst and the high oxidation state early transition metal Mo catalyst tested, and it may explain the lack of reactivity noted for other highly reactive, transition metal nitrile hydration catalysts. This work provides a thorough explanation of the challenges associated with transition metal catalyzed nitrile hydration. The knowledge gained can be used to develop new innovative nitrile hydration catalysts that are less susceptible to cyanide poisoning for this important transformation. The outlook for transition metal-catalyzed cyanohydrin hydration is discussed in Chapter VI.

5.6 Notes

a. For the reaction performed at 43 °C, nitriles containing electron withdrawing groups displayed psuedo-first order kinetics. While, psuedo-zero order kinetics were observed for electron donating nitriles, indicating a change in rate determining step. This inconsistency precluded generation of a Hammett plot. Kinetic traces for each substrate are available in Appendix C.

b. Unfortunately, rate data was not obtained for the 2-methoxyisobutyronitrile. However, the reaction of ~0.50 M 2-methoxyisobutyronitrile did proceed to completion.

CHAPTER VI

SUMMARY AND OUTLOOK

Molybdocene complexes mediate hydrolysis of organic substrates by facilitating addition of a hydroxo ligand to a coordinated substrate. The investigations outlined herein demonstrate that altering the electron density on the metal center using Cp ring substituents does not enhance the reactivity of the complex. Substitution of electron-withdrawing or donating groups to the Cp rings results in slower reactivity due to opposing electronic effects on the bound substrate and nucleophile. Although the *ansa* and methyl substituents did not enhance the reactivity of the molybdenum center, the substituents did significantly reduce the tendency of the monomeric catalyst to dimerize to an inactive form. This decrease in dimerization can lead to faster rates of hydration, especially at high catalyst concentrations. The extent of dimerization can also be manipulated by addition of water-miscible organic solvents, which suggests that faster rates may be achieved by carrying out the reactions in mixed solvent systems.

The hydration of nitriles catalyzed by $Cp_2Mo(OH)(OH_2)^+$ or $PtCl(PMe_2OH)\{(PMe_2O)_2H\}$ complexes is facilitated by the addition of electron withdrawing groups (on the nitrile). However, both catalysts gave unsatisfactory results when reacted with nitriles containing an α-hydroxy substituent. The results chronicled in

Chapter V demonstrate that the cyanohydrin substrates react equally as fast toward nucleophilic attack as do other nitriles. However, cyanohydrins poison the transition metal catalysts readily by releasing hydrocyanic acid upon dissociation. Dissociation is minimized at low temperature and high substrate concentration; however, irreversible binding of cyanide to the substrate removes cyanide from the equilibrium, which ensures complete catalyst poisoning over time. These results may explain the lack of reactivity noted previously for Cu nitrile hydration catalysts.

In order to circumvent cyanide poisoning, a more labile catalytic system must be developed. Unfortunately, cyanide is a good σ donor and an excellent π acceptor, and thus attracted to both hard and soft metal centers. As demonstrated in the work herein, cyanide poisoning was more acute using the Mo(IV) centered catalyst than the Pt(II) complex, due to the increased Lewis acidic of the Mo(IV). However, both the second and third row transition metals bind cyanide irreversibly. First-row transition metal complexes are more labile, in general, and may be less susceptible to cyanide poisoning. An ideal catalytic system should bind cyanide reversibly, which will prevent complete poisoning of the catalyst. If a cyanide bound species were in equilibrium with the catalytically active species, such a system can be optimized (by modulation of its steric and electronic environment) to favor the active species, thereby further improving reaction rates.

Most nitrile hydration catalysts in the literature employ second- and third-row transition metals. However, a few nitrile hydration catalysts incorporating Ni, Cr, and Co

have been developed. A new homogeneous catalyst with an Fe(II) center was recently reported. This system may be worthy of investigation.

APPENDIX A

SUPPORTING INFORMATION FOR CHAPTER II

A.1 Crystallographic Data for [{$C_2Me_4(\eta^5\text{-}C_5H_4)_2$}Mo(μ-OH)]$_2$[OTs]$_2$·2$H_2O$ (tak1)

Table 1. Crystal data and structure refinement for [{$C_2Me_4(\eta^5\text{-}C_5H_4)_2$}Mo(μ-OH)]$_2$[OTs]$_2$·2$H_2O$ (tak1).

Identification code	tak1	
Empirical formula	C23 H30 Mo O5 S	
Formula weight	514.47	
Temperature	293(2) K	
Wavelength	0.71073 Å	
Crystal system	Triclinic	
Space group	P-1	
Unit cell dimensions	a = 7.7452(4) Å	a= 76.2590(10)°.
	b = 10.5132(5) Å	b= 75.3250(10)°
	c = 14.7256(7) Å	g = 84.3120(10)°
Volume	1125.78(10) Å^3	
Z	2	
Density (calculated)	1.518 Mg/m^3	
Absorption coefficient	0.707 mm^{-1}	
F(000)	532	
Crystal size	0.48 x 0.23 x 0.04 mm^3	
Theta range for data collection	2.00 to 28.54°	
Index ranges	-10<=h<=10, -13<=k<=13, -19<=l<=19	

Reflections collected	13033
Independent reflections	5203 [R(int) = 0.0135]
Completeness to theta = 28.54°	90.6 %
Absorption correction	Semi-empirical from equivalents
Max. and min. transmission	1.000 and 0.903
Refinement method	Full-matrix least-squares on F^2
Data / restraints / parameters	5203 / 0 / 391
Goodness-of-fit on F^2	1.012
Final R indices [I>2sigma(I)]	R1 = 0.0203, wR2 = 0.0524
R indices (all data)	R1 = 0.0211, wR2 = 0.0531
Largest diff. peak and hole	0.397 and -0.274 e.$Å^{-3}$

Table 2. Atomic coordinates (x 10^4) and equivalent isotropic displacement parameters ($Å^2$ x 10^3) for $[\{C_2Me_4(\eta^5\text{-}C_5H_4)_2\}Mo(\mu\text{-}OH)]_2[OTs]_2\cdot 2H_2O$ (tak1). U(eq) is defined as one third of the trace of the orthogonalized U^{ij} tensor.

	x	y	z	U(eq)
Mo(1)	284(1)	3763(1)	5995(1)	23(1)
S(1)	2847(1)	7465(1)	6611(1)	34(1)
O(1)	257(1)	5792(1)	5377(1)	27(1)
O(2)	2638(2)	7311(1)	5686(1)	49(1)
O(3)	3353(2)	8777(1)	6556(1)	55(1)
O(4)	3984(2)	6445(1)	7032(1)	52(1)
O(5)	6767(3)	136(2)	5808(2)	82(1)
C(1)	2960(2)	3879(2)	6299(1)	32(1)
C(2)	3258(2)	3922(2)	5297(1)	35(1)
C(3)	2864(2)	2705(2)	5176(1)	35(1)
C(4)	2280(2)	1898(2)	6085(1)	32(1)
C(5)	2372(2)	2602(1)	6797(1)	29(1)
C(6)	1986(2)	2075(2)	7880(1)	34(1)
C(7)	-38(2)	1711(2)	8210(1)	36(1)
C(8)	-1013(2)	2629(1)	7513(1)	31(1)
C(9)	-1843(2)	2244(2)	6856(1)	34(1)
C(10)	-2817(2)	3342(2)	6456(1)	36(1)
C(11)	-2560(2)	4420(2)	6813(1)	36(1)
C(12)	-1414(2)	4009(2)	7452(1)	32(1)
C(13)	3278(3)	891(2)	8096(2)	48(1)
C(14)	2395(3)	3128(2)	8354(2)	48(1)
C(15)	-943(3)	1898(3)	9233(1)	55(1)
C(16)	-297(3)	288(2)	8199(2)	50(1)
C(17)	680(2)	7277(2)	7390(1)	35(1)
C(18)	455(3)	6636(2)	8346(1)	44(1)

C(19)	-1253(3)	6509(2)	8940(2)	55(1)
C(20)	-2741(3)	7023(2)	8595(2)	59(1)
C(21)	-2495(3)	7668(2)	7642(2)	54(1)
C(22)	-804(2)	7801(2)	7034(2)	44(1)
C(23)	-4616(5)	6902(6)	9231(3)	101(1)

Table 3. Bond lengths [Å] and angles [°] for [{$C_2Me_4(\eta^5$-$C_5H_4)_2$}Mo(μ-OH)]$_2$[OTs]$_2$·2H_2O (tak1)

Mo(1)-O(1)#1	2.1009(10)
Mo(1)-O(1)	2.1117(10)
Mo(1)-C(1)	2.2491(14)
Mo(1)-C(12)	2.2727(15)
Mo(1)-C(2)	2.2778(15)
Mo(1)-C(8)	2.2931(14)
Mo(1)-C(9)	2.3173(15)
Mo(1)-C(5)	2.3220(14)
Mo(1)-C(11)	2.3513(15)
Mo(1)-C(4)	2.3728(14)
Mo(1)-C(3)	2.3793(15)
Mo(1)-C(10)	2.3803(15)
S(1)-O(4)	1.4433(13)
S(1)-O(3)	1.4495(12)
S(1)-O(2)	1.4589(13)
S(1)-C(17)	1.7762(17)
O(1)-Mo(1)#1	2.1009(10)
O(1)-H(1O)	0.72(2)
O(5)-H(5OA)	0.69(3)
O(5)-H(5OB)	0.81(4)
C(1)-C(5)	1.425(2)
C(1)-C(2)	1.426(2)
C(1)-H(1)	0.92(2)
C(2)-C(3)	1.406(2)
C(2)-H(2)	0.947(19)
C(3)-C(4)	1.395(2)
C(3)-H(3)	0.89(2)
C(4)-C(5)	1.439(2)
C(4)-H(4)	0.883(19)

C(5)-C(6)	1.521(2)
C(6)-C(14)	1.536(2)
C(6)-C(13)	1.542(2)
C(6)-C(7)	1.576(2)
C(7)-C(8)	1.528(2)
C(7)-C(16)	1.533(2)
C(7)-C(15)	1.542(2)
C(8)-C(9)	1.437(2)
C(8)-C(12)	1.440(2)
C(9)-C(10)	1.406(2)
C(9)-H(9)	0.887(19)
C(10)-C(11)	1.407(2)
C(10)-H(10)	0.917(19)
C(11)-C(12)	1.418(2)
C(11)-H(11)	0.91(2)
C(12)-H(12)	0.90(2)
C(13)-H(13A)	1.00(3)
C(13)-H(13B)	0.94(2)
C(13)-H(13C)	0.97(2)
C(14)-H(14A)	0.95(3)
C(14)-H(14B)	0.92(2)
C(14)-H(14C)	0.96(2)
C(15)-H(15A)	0.91(3)
C(15)-H(15B)	0.96(3)
C(15)-H(15C)	0.95(2)
C(16)-H(16A)	0.92(3)
C(16)-H(16B)	0.92(2)
C(16)-H(16C)	1.00(2)
C(17)-C(18)	1.383(2)
C(17)-C(22)	1.394(2)
C(18)-C(19)	1.388(3)
C(18)-H(18)	0.88(2)
C(19)-C(20)	1.386(3)
C(19)-H(19)	0.90(2)

C(20)-C(21)	1.379(3)
C(20)-C(23)	1.515(4)
C(21)-C(22)	1.385(3)
C(21)-H(21)	0.84(3)
C(22)-H(22)	0.93(2)
C(23)-H(23A)	0.93(5)
C(23)-H(23B)	0.81(6)
C(23)-H(23C)	0.91(4)

O(1)-Mo(1)-O(1)	66.90(5)
O(1)-Mo(1)-C(1)	125.45(5)
O(1)-Mo(1)-C(1)	90.40(5)
O(1)-Mo(1)-C(12)	131.64(5)
O(1)-Mo(1)-C(12)	93.93(5)
C(1)-Mo(1)-C(12)	97.08(6)
O(1)-Mo(1)-C(2)	89.67(5)
O(1)-Mo(1)-C(2)	82.24(5)
C(1)-Mo(1)-C(2)	36.71(6)
C(12)-Mo(1)-C(2)	133.13(6)
O(1)-Mo(1)-C(8)	137.49(5)
O(1)-Mo(1)-C(8)	130.68(5)
C(1)-Mo(1)-C(8)	95.41(6)
C(12)-Mo(1)-C(8)	36.75(5)
C(2)-Mo(1)-C(8)	127.17(5)
O(1)-Mo(1)-C(9)	102.00(5)
O(1)-Mo(1)-C(9)	135.83(5)
C(1)-Mo(1)-C(9)	125.73(6)
C(12)-Mo(1)-C(9)	60.62(6)
C(2)-Mo(1)-C(9)	141.80(6)
C(8)-Mo(1)-C(9)	36.32(5)
O(1)1-Mo(1)-C(5)	140.13(5)
O(1)-Mo(1)-C(5)	126.05(5)
C(1)-Mo(1)-C(5)	36.29(5)
C(12)-Mo(1)-C(5)	87.53(5)

C(2)-Mo(1)-C(5)	59.71(5)
C(8)-Mo(1)-C(5)	67.56(5)
C(9)-Mo(1)-C(5)	90.68(6)
O(1)-Mo(1)-C(11)	96.01(5)
O(1)-Mo(1)-C(11)	79.34(5)
C(1)-Mo(1)-C(11)	129.10(6)
C(12)-Mo(1)-C(11)	35.67(6)
C(2)-Mo(1)-C(11)	156.74(6)
C(8)-Mo(1)-C(11)	59.39(5)
C(9)-Mo(1)-C(11)	58.73(6)
C(5)-Mo(1)-C(11)	122.41(5)
O(1)-Mo(1)-C(4)	107.84(5)
O(1)-Mo(1)-C(4)	140.56(5)
C(1)-Mo(1)-C(4)	59.84(6)
C(12)-Mo(1)-C(4)	113.59(5)
C(2)-Mo(1)-C(4)	58.37(6)
C(8)-Mo(1)-C(4)	80.98(5)
C(9)-Mo(1)-C(4)	83.46(6)
C(5)-Mo(1)-C(4)	35.68(5)
C(11)-Mo(1)-C(4)	138.96(6)
O(1)-Mo(1)-C(3)	81.67(5)
O(1)-Mo(1)-C(3)	109.97(5)
C(1)-Mo(1)-C(3)	59.67(6)
C(12)-Mo(1)-C(3)	145.59(5)
C(2)-Mo(1)-C(3)	35.05(6)
C(8)-Mo(1)-C(3)	115.10(5)
C(9)-Mo(1)-C(3)	110.29(6)
C(5)-Mo(1)-C(3)	58.52(5)
C(11)-Mo(1)-C(3)	168.21(6)
C(4)-Mo(1)-C(3)	34.13(5)
O(1)-Mo(1)-C(10)	81.05(5)
O(1)-Mo(1)-C(10)	101.81(5)
C(1)-Mo(1)-C(10)	153.50(6)
C(12)-Mo(1)-C(10)	59.06(6)

C(2)-Mo(1)-C(10)	167.31(6)
C(8)-Mo(1)-C(10)	58.82(5)
C(9)-Mo(1)-C(10)	34.80(6)
C(5)-Mo(1)-C(10)	123.91(5)
C(11)-Mo(1)-C(10)	34.60(6)
C(4)-Mo(1)-C(10)	116.29(6)
C(3)-Mo(1)-C(10)	133.86(6)
O(4)-S(1)-O(3)	113.59(9)
O(4)-S(1)-O(2)	112.87(9)
O(3)-S(1)-O(2)	111.64(9)
O(4)-S(1)-C(17)	106.36(8)
O(3)-S(1)-C(17)	106.50(8)
O(2)-S(1)-C(17)	105.15(8)
Mo(1)-O(1)-Mo(1)	113.10(5)
Mo(1)-O(1)-H(1O)	122.1(15)
Mo(1)-O(1)-H(1O)	118.4(15)
H(5OA)-O(5)-H(5OB)	103(4)
C(5)-C(1)-C(2)	106.89(14)
C(5)-C(1)-Mo(1)	74.64(8)
C(2)-C(1)-Mo(1)	72.74(8)
C(5)-C(1)-H(1)	126.3(12)
C(2)-C(1)-H(1)	126.7(13)
Mo(1)-C(1)-H(1)	121.2(13)
C(3)-C(2)-C(1)	109.03(14)
C(3)-C(2)-Mo(1)	76.43(9)
C(1)-C(2)-Mo(1)	70.55(8)
C(3)-C(2)-H(2)	125.4(11)
C(1)-C(2)-H(2)	125.5(12)
Mo(1)-C(2)-H(2)	120.2(12)
C(4)-C(3)-C(2)	108.26(14)
C(4)-C(3)-Mo(1)	72.68(8)
C(2)-C(3)-Mo(1)	68.53(8)
C(4)-C(3)-H(3)	125.3(13)
C(2)-C(3)-H(3)	126.4(12)

Mo(1)-C(3)-H(3)	121.7(13)
C(3)-C(4)-C(5)	108.39(14)
C(3)-C(4)-Mo(1)	73.19(8)
C(5)-C(4)-Mo(1)	70.23(8)
C(3)-C(4)-H(4)	126.3(12)
C(5)-C(4)-H(4)	125.3(12)
Mo(1)-C(4)-H(4)	124.7(12)
C(1)-C(5)-C(4)	107.37(13)
C(1)-C(5)-C(6)	125.88(13)
C(4)-C(5)-C(6)	126.71(13)
C(1)-C(5)-Mo(1)	69.07(8)
C(4)-C(5)-Mo(1)	74.09(8)
C(6)-C(5)-Mo(1)	123.95(10)
C(5)-C(6)-C(14)	108.87(14)
C(5)-C(6)-C(13)	108.58(13)
C(14)-C(6)-C(13)	106.93(15)
C(5)-C(6)-C(7)	106.29(12)
C(14)-C(6)-C(7)	112.83(14)
C(13)-C(6)-C(7)	113.23(14)
C(8)-C(7)-C(16)	109.14(14)
C(8)-C(7)-C(15)	107.69(14)
C(16)-C(7)-C(15)	106.91(16)
C(8)-C(7)-C(6)	107.28(12)
C(16)-C(7)-C(6)	112.63(14)
C(15)-C(7)-C(6)	113.06(16)
C(9)-C(8)-C(12)	107.29(13)
C(9)-C(8)-C(7)	125.82(14)
C(12)-C(8)-C(7)	126.66(14)
C(9)-C(8)-Mo(1)	72.76(8)
C(12)-C(8)-Mo(1)	70.85(8)
C(7)-C(8)-Mo(1)	125.93(10)
C(10)-C(9)-C(8)	107.73(14)
C(10)-C(9)-Mo(1)	75.05(9)
C(8)-C(9)-Mo(1)	70.92(8)

C(10)-C(9)-H(9)	124.2(12)
C(8)-C(9)-H(9)	128.0(12)
Mo(1)-C(9)-H(9)	122.8(12)
C(9)-C(10)-C(11)	108.94(14)
C(9)-C(10)-Mo(1)	70.15(9)
C(11)-C(10)-Mo(1)	71.57(9)
C(9)-C(10)-H(10)	124.4(12)
C(11)-C(10)-H(10)	126.5(12)
Mo(1)-C(10)-H(10)	120.5(12)
C(10)-C(11)-C(12)	108.63(14)
C(10)-C(11)-Mo(1)	73.83(9)
C(12)-C(11)-Mo(1)	69.14(8)
C(10)-C(11)-H(11)	127.2(12)
C(12)-C(11)-H(11)	124.1(12)
Mo(1)-C(11)-H(11)	120.3(12)
C(11)-C(12)-C(8)	107.27(14)
C(11)-C(12)-Mo(1)	75.18(9)
C(8)-C(12)-Mo(1)	72.39(8)
C(11)-C(12)-H(12)	124.8(12)
C(8)-C(12)-H(12)	127.3(13)
Mo(1)-C(12)-H(12)	125.2(13)
C(6)-C(13)-H(13A)	109.9(14)
C(6)-C(13)-H(13B)	115.2(14)
H(13A)-C(13)-H(13B)	107.6(19)
C(6)-C(13)-H(13C)	111.4(14)
H(13A)-C(13)-H(13C)	107.3(19)
H(13B)-C(13)-H(13C)	105.1(19)
C(6)-C(14)-H(14A)	110.7(14)
C(6)-C(14)-H(14B)	109.5(13)
H(14A)-C(14)-H(14B)	108.7(19)
C(6)-C(14)-H(14C)	113.0(13)
H(14A)-C(14)-H(14C)	108.3(19)
H(14B)-C(14)-H(14C)	106.4(18)
C(7)-C(15)-H(15A)	109.0(15)

C(7)-C(15)-H(15B)	111.1(16)
H(15A)-C(15)-H(15B)	108(2)
C(7)-C(15)-H(15C)	113.7(13)
H(15A)-C(15)-H(15C)	109(2)
H(15B)-C(15)-H(15C)	106(2)
C(7)-C(16)-H(16A)	109.6(15)
C(7)-C(16)-H(16B)	110.7(15)
H(16A)-C(16)-H(16B)	109(2)
C(7)-C(16)-H(16C)	114.1(13)
H(16A)-C(16)-H(16C)	108.2(19)
H(16B)-C(16)-H(16C)	105.5(19)
C(18)-C(17)-C(22)	119.83(17)
C(18)-C(17)-S(1)	120.80(13)
C(22)-C(17)-S(1)	119.36(14)
C(17)-C(18)-C(19)	119.61(19)
C(17)-C(18)-H(18)	120.7(13)
C(19)-C(18)-H(18)	119.6(13)
C(18)-C(19)-C(20)	121.2(2)
C(18)-C(19)-H(19)	120.6(17)
C(20)-C(19)-H(19)	118.2(16)
C(21)-C(20)-C(19)	118.59(19)
C(21)-C(20)-C(23)	119.3(3)
C(19)-C(20)-C(23)	122.1(3)
C(20)-C(21)-C(22)	121.3(2)
C(20)-C(21)-H(21)	117.5(17)
C(22)-C(21)-H(21)	121.2(17)
C(21)-C(22)-C(17)	119.55(19)
C(21)-C(22)-H(22)	119.8(14)
C(17)-C(22)-H(22)	120.7(15)
C(20)-C(23)-H(23A)	112(3)
C(20)-C(23)-H(23B)	115(4)
H(23A)-C(23)-H(23B)	117(5)
C(20)-C(23)-H(23C)	107(3)
H(23A)-C(23)-H(23C)	99(4)

H(23B)-C(23)-H(23C)	105(4)

Symmetry transformations used to generate equivalent atoms: #1 -x,-y+1,-z+1

Table 4. Anisotropic displacement parameters ($Å^2 x\ 10^3$) for [{$C_2Me_4(\eta^5\text{-}C_5H_4)_2$}Mo(μ-OH)]$_2$[OTs]$_2$·2$H_2O$ (tak1). The anisotropic displacement factor exponent takes the form: $-2p^2[\ h^2\ a^{*2}U^{11} + ... + 2\ h\ k\ a^*\ b^*\ U^{12}\ ]$

	U^{11}	U^{22}	U^{33}	U^{23}	U^{13}	U^{12}
Mo(1)	22(1)	22(1)	25(1)	-5(1)	-7(1)	1(1)
S(1)	32(1)	30(1)	44(1)	-14(1)	-11(1)	-1(1)
O(1)	30(1)	24(1)	29(1)	-5(1)	-12(1)	-2(1)
O(2)	44(1)	65(1)	43(1)	-19(1)	-7(1)	-14(1)
O(3)	50(1)	36(1)	81(1)	-23(1)	-8(1)	-10(1)
O(4)	40(1)	50(1)	66(1)	-12(1)	-16(1)	11(1)
O(5)	83(1)	77(1)	85(1)	9(1)	-38(1)	-24(1)
C(1)	27(1)	31(1)	39(1)	-5(1)	-15(1)	1(1)
C(2)	22(1)	40(1)	37(1)	1(1)	-7(1)	2(1)
C(3)	29(1)	45(1)	31(1)	-12(1)	-8(1)	12(1)
C(4)	32(1)	29(1)	37(1)	-10(1)	-10(1)	7(1)
C(5)	28(1)	28(1)	32(1)	-6(1)	-12(1)	6(1)
C(6)	41(1)	32(1)	30(1)	-6(1)	-15(1)	6(1)
C(7)	44(1)	32(1)	28(1)	-1(1)	-9(1)	2(1)
C(8)	31(1)	30(1)	27(1)	-4(1)	-3(1)	-1(1)
C(9)	31(1)	33(1)	36(1)	-4(1)	-5(1)	-8(1)
C(10)	24(1)	46(1)	34(1)	-2(1)	-6(1)	-6(1)
C(11)	26(1)	37(1)	36(1)	-3(1)	-2(1)	5(1)
C(12)	34(1)	32(1)	30(1)	-9(1)	-4(1)	3(1)
C(13)	53(1)	45(1)	42(1)	1(1)	-20(1)	14(1)
C(14)	60(1)	52(1)	40(1)	-17(1)	-23(1)	2(1)
C(15)	61(1)	66(1)	29(1)	-4(1)	-6(1)	6(1)
C(16)	61(1)	31(1)	52(1)	6(1)	-15(1)	-5(1)
C(17)	35(1)	32(1)	42(1)	-16(1)	-10(1)	0(1)
C(18)	49(1)	44(1)	45(1)	-16(1)	-15(1)	2(1)
C(19)	65(1)	58(1)	42(1)	-17(1)	-2(1)	-6(1)

C(20)	46(1)	69(1)	62(1)	-32(1)	3(1)	-9(1)
C(21)	35(1)	67(1)	67(1)	-28(1)	-13(1)	3(1)
C(22)	38(1)	49(1)	49(1)	-16(1)	-14(1)	2(1)
C(23)	57(2)	140(4)	94(3)	-37(3)	19(2)	-17(2)

Table 5. Hydrogen coordinates (x 10^4) and isotropic displacement parameters ($Å^2$x 10 ^{3}) for [{$C_2Me_4(\eta^5$-$C_5H_4)_2$}Mo(μ-OH)]$_2$[OTs]$_2$·$2H_2O$ (tak1)

	x	y	z	U(eq)
H(1)	3180(30)	4530(20)	6572(14)	44(5)
H(2)	3680(30)	4649(19)	4792(14)	39(5)
H(3)	2910(30)	2494(19)	4621(14)	40(5)
H(4)	1960(20)	1080(19)	6207(13)	34(4)
H(9)	-1830(20)	1454(19)	6737(13)	36(5)
H(10)	-3440(30)	3352(18)	6000(14)	38(5)
H(11)	-2990(30)	5260(19)	6648(14)	40(5)
H(12)	-1150(30)	4504(19)	7813(14)	41(5)
H(13A)	4530(40)	1180(20)	7893(17)	67(7)
H(13B)	3230(30)	200(20)	7799(16)	53(6)
H(13C)	3040(30)	490(20)	8782(17)	59(6)
H(14A)	3600(30)	3360(20)	8112(17)	60(7)
H(14B)	2190(30)	2810(20)	9011(16)	49(5)
H(14C)	1650(30)	3910(20)	8258(15)	51(6)
H(15A)	-2080(30)	1610(20)	9400(17)	59(7)
H(15B)	-320(40)	1390(30)	9696(19)	74(8)
H(15C)	-980(30)	2780(20)	9297(15)	50(6)
H(16A)	-1500(40)	140(20)	8335(17)	62(7)
H(16B)	190(30)	-280(20)	8654(17)	58(6)
H(16C)	290(30)	40(20)	7575(17)	58(6)
H(18)	1370(30)	6283(19)	8574(14)	40(5)
H(19)	-1420(30)	6090(20)	9562(18)	65(7)
H(21)	-3410(30)	7980(20)	7444(18)	64(7)
H(22)	-670(30)	8240(20)	6398(17)	57(6)
H(23A)	-5060(70)	7680(50)	9410(40)	180(20)
H(23B)	-5280(70)	6520(60)	9060(40)	200(30)

H(23C)	-4530(50)	6410(40)	9820(30)	108(13)
H(1O)	790(30)	6200(19)	5516(14)	35(5)
H(5OA)	5990(40)	-150(30)	5820(20)	85(12)
H(5OB)	6760(50)	810(40)	5400(30)	116(14)

Table 6. Hydrogen bonds for [{$C_2Me_4(\eta^5\text{-}C_5H_4)_2$}Mo(μ-OH)]$_2$[OTs]$_2$·2$H_2O$ (tak1) [Å and °]

D-H...A	d(D-H)	d(H...A)	d(D...A)	<(DHA)
O(1)-H(1O)...O(2)	0.72(2)	2.03(2)	2.7412(16)	169(2)
O(5)-H(5OA)...O(3)#2	0.69(3)	2.32(3)	2.962(3)	156(4)
O(5)-H(5OB)...O(2)#3	0.81(4)	2.24(4)	3.031(3)	167(4)

Symmetry transformations used to generate equivalent atoms:

#1 -x,-y+1,-z+1 #2 x,y-1,z #3 -x+1,-y+1,-z+1

A.2 Crystallographic Data for $[\{C_2Me_4(\eta^5\text{-}C_5H_4)_2\}Mo(\mu\text{-}OH)]_2[OTs]_2\cdot 2H_2O$ (tak2)

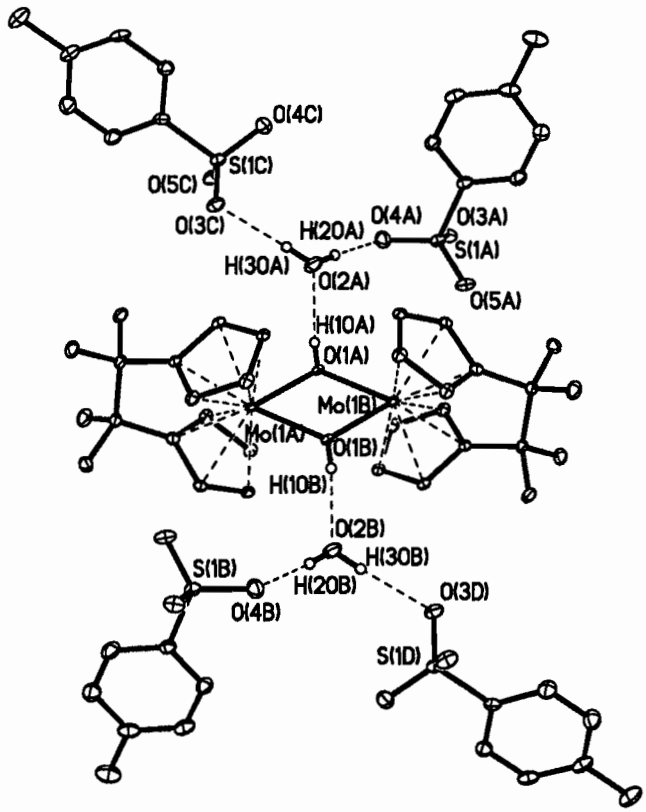

Figure 1. X-ray crystal structure of the second polymorph of $[\{C_2Me_4(\eta^5\text{-}C_5H_4)_2\}Mo(\mu\text{-}OH)]_2[OTs]_2\cdot 2H_2O$ (tak2). The Cp and bridge protons were omitted for clarity. Thermal ellipsoids are drawn at the 50% probability level.

Table 7. Crystal data and structure refinement for $[\{C_2Me_4(\eta^5\text{-}C_5H_4)_2\}Mo(\mu\text{-}OH)]_2[OTs]_2\cdot 2H_2O$ (tak2)

Identification code	tak2	
Empirical formula	C23 H30 Mo O5 S	
Formula weight	514.47	
Temperature	153(2) K	
Wavelength	0.71073 Å	
Crystal system	Monoclinic	
Space group	P2(1)/n	
Unit cell dimensions	a = 17.207(2) Å	α= 90°.
	b = 7.7689(11) Å	β= 110.320(3)°.
	c = 17.786(3) Å	γ = 90°.
Volume	2229.7(5) $Å^3$	
Z	4	
Density (calculated)	1.533 Mg/m^3	
Absorption coefficient	0.714 mm^{-1}	
F(000)	1064	
Crystal size	0.32 x 0.12 x 0.03 mm^3	
Theta range for data collection	1.42 to 28.19°.	
Index ranges	-19<=h<=21, -10<=k<=10, -23<=l<=18	
Reflections collected	13693	
Independent reflections	5118 [R(int) = 0.0409]	
Completeness to theta = 28.19°	93.1 %	
Absorption correction	Semi-empirical from equivalents	
Max. and min. transmission	1.000 and 0.577	
Refinement method	Full-matrix least-squares on F^2	
Data / restraints / parameters	5118 / 0 / 283	
Goodness-of-fit on F^2	1.084	
Final R indices [I>2sigma(I)]	R1 = 0.0499, wR2 = 0.1218	

R indices (all data)	R1 = 0.0599, wR2 = 0.1282
Largest diff. peak and hole	2.065 and -1.484 e.Å^{-3}

Table 8. Atomic coordinates (x 10^4) and equivalent isotropic displacement parameters ($Å^2$x 10^3) for $[\{C_2Me_4(\eta^5\text{-}C_5H_4)_2\}Mo(\mu\text{-}OH)]_2[OTs]_2 \cdot 2H_2O$ (tak2). U(eq) is defined as one third of the trace of the orthogonalized U^{ij} tensor

	x	y	z	U(eq)
Mo(1)	9153(1)	4333(1)	260(1)	12(1)
S(1)	1329(1)	8685(1)	2950(1)	19(1)
O(1)	10447(2)	4542(3)	618(2)	16(1)
O(2)	1368(2)	1994(4)	1484(2)	33(1)
O(3)	692(2)	9444(3)	2253(2)	26(1)
O(4)	2027(2)	8039(4)	2746(2)	30(1)
O(5)	1560(2)	9811(4)	3644(2)	29(1)
C(1)	8048(2)	2420(4)	-393(2)	17(1)
C(2)	8641(2)	2228(4)	-766(2)	19(1)
C(3)	9393(2)	1695(4)	-178(2)	18(1)
C(4)	9266(2)	1505(4)	580(2)	18(1)
C(5)	8422(2)	1945(4)	441(2)	14(1)
C(6)	7997(2)	1855(4)	1059(2)	17(1)
C(7)	7676(2)	3748(5)	1128(2)	18(1)
C(8)	8273(2)	4981(4)	941(2)	18(1)
C(9)	9104(2)	5361(5)	1445(2)	18(1)
C(10)	9383(2)	6776(4)	1096(2)	17(1)
C(11)	8758(2)	7232(4)	376(2)	17(1)
C(12)	8072(2)	6127(4)	255(2)	16(1)
C(13)	8627(3)	1218(5)	1859(2)	24(1)
C(14)	7293(3)	506(5)	791(3)	26(1)
C(15)	7669(3)	4161(5)	1974(3)	29(1)
C(16)	6780(2)	4060(5)	541(3)	25(1)
C(17)	867(2)	6843(5)	3226(2)	20(1)
C(18)	1087(3)	5188(5)	3084(2)	26(1)

C(19)	727(3)	3774(5)	3313(3)	29(1)
C(20)	161(3)	3976(5)	3707(2)	29(1)
C(21)	-57(3)	5657(6)	3842(3)	34(1)
C(22)	294(3)	7073(5)	3608(3)	32(1)
C(23)	-225(3)	2445(6)	3966(3)	40(1)

Table 9. Bond lengths [Å] and angles [°] for [{$C_2Me_4(\eta^5$-$C_5H_4)_2$}Mo(μ-OH)]$_2$[OTs]$_2$·2H_2O (tak2)

Mo(1)-O(1)	2.099(3)
Mo(1)-O(1)#1	2.104(3)
Mo(1)-C(4)	2.262(3)
Mo(1)-C(3)	2.280(3)
Mo(1)-C(9)	2.284(4)
Mo(1)-C(8)	2.299(4)
Mo(1)-C(12)	2.321(3)
Mo(1)-C(5)	2.326(3)
Mo(1)-C(10)	2.359(3)
Mo(1)-C(1)	2.374(3)
Mo(1)-C(2)	2.380(3)
Mo(1)-C(11)	2.381(3)
S(1)-O(5)	1.451(3)
S(1)-O(4)	1.459(3)
S(1)-O(3)	1.464(3)
S(1)-C(17)	1.787(4)
O(1)-Mo(1)#1	2.104(3)
C(1)-C(2)	1.406(5)
C(1)-C(5)	1.444(5)
C(2)-C(3)	1.414(5)
C(3)-C(4)	1.446(5)
C(4)-C(5)	1.429(5)
C(5)-C(6)	1.518(5)
C(6)-C(13)	1.541(5)
C(6)-C(14)	1.547(5)
C(6)-C(7)	1.591(5)
C(7)-C(8)	1.524(5)
C(7)-C(15)	1.542(5)
C(7)-C(16)	1.551(5)

C(8)-C(9)	1.430(5)
C(8)-C(12)	1.452(5)
C(9)-C(10)	1.426(5)
C(10)-C(11)	1.402(5)
C(11)-C(12)	1.414(5)
C(17)-C(18)	1.387(5)
C(17)-C(22)	1.389(6)
C(18)-C(19)	1.391(6)
C(19)-C(20)	1.390(6)
C(20)-C(21)	1.402(6)
C(20)-C(23)	1.511(6)
C(21)-C(22)	1.386(6)

O(1)-Mo(1)-O(1)#1	66.85(12)
O(1)-Mo(1)-C(4)	90.50(11)
O(1)#1-Mo(1)-C(4)	124.65(12)
O(1)-Mo(1)-C(3)	82.79(12)
O(1)#1-Mo(1)-C(3)	88.56(11)
C(4)-Mo(1)-C(3)	37.12(13)
O(1)-Mo(1)-C(9)	93.87(12)
O(1)#1-Mo(1)-C(9)	131.84(11)
C(4)-Mo(1)-C(9)	97.74(13)
C(3)-Mo(1)-C(9)	134.30(13)
O(1)-Mo(1)-C(8)	130.23(12)
O(1)#1-Mo(1)-C(8)	138.23(11)
C(4)-Mo(1)-C(8)	95.46(13)
C(3)-Mo(1)-C(8)	127.38(13)
C(9)-Mo(1)-C(8)	36.36(13)
O(1)-Mo(1)-C(12)	135.92(11)
O(1)#1-Mo(1)-C(12)	102.50(11)
C(4)-Mo(1)-C(12)	125.71(13)
C(3)-Mo(1)-C(12)	141.11(13)
C(9)-Mo(1)-C(12)	60.49(13)
C(8)-Mo(1)-C(12)	36.64(12)

O(1)-Mo(1)-C(5)	125.96(11)
O(1)#1-Mo(1)-C(5)	140.04(11)
C(4)-Mo(1)-C(5)	36.26(12)
C(3)-Mo(1)-C(5)	60.07(12)
C(9)-Mo(1)-C(5)	87.48(12)
C(8)-Mo(1)-C(5)	67.37(12)
C(12)-Mo(1)-C(5)	90.51(12)
O(1)-Mo(1)-C(10)	79.49(11)
O(1)#1-Mo(1)-C(10)	96.18(11)
C(4)-Mo(1)-C(10)	129.92(13)
C(3)-Mo(1)-C(10)	158.08(14)
C(9)-Mo(1)-C(10)	35.72(12)
C(8)-Mo(1)-C(10)	59.24(13)
C(12)-Mo(1)-C(10)	58.55(13)
C(5)-Mo(1)-C(10)	122.35(12)
O(1)-Mo(1)-C(1)	141.42(11)
O(1)#1-Mo(1)-C(1)	108.08(11)
C(4)-Mo(1)-C(1)	59.97(13)
C(3)-Mo(1)-C(1)	58.65(13)
C(9)-Mo(1)-C(1)	112.98(13)
C(8)-Mo(1)-C(1)	80.39(12)
C(12)-Mo(1)-C(1)	82.53(13)
C(5)-Mo(1)-C(1)	35.77(12)
C(10)-Mo(1)-C(1)	137.98(13)
O(1)-Mo(1)-C(2)	110.92(11)
O(1)#1-Mo(1)-C(2)	81.11(11)
C(4)-Mo(1)-C(2)	60.14(13)
C(3)-Mo(1)-C(2)	35.24(13)
C(9)-Mo(1)-C(2)	145.69(13)
C(8)-Mo(1)-C(2)	114.76(13)
C(12)-Mo(1)-C(2)	109.12(13)
C(5)-Mo(1)-C(2)	58.94(12)
C(10)-Mo(1)-C(2)	166.68(13)
C(1)-Mo(1)-C(2)	34.40(12)

O(1)-Mo(1)-C(11)	101.80(11)
O(1)#1-Mo(1)-C(11)	81.28(11)
C(4)-Mo(1)-C(11)	154.07(13)
C(3)-Mo(1)-C(11)	166.01(13)
C(9)-Mo(1)-C(11)	59.09(12)
C(8)-Mo(1)-C(11)	59.19(12)
C(12)-Mo(1)-C(11)	34.97(12)
C(5)-Mo(1)-C(11)	123.95(12)
C(10)-Mo(1)-C(11)	34.41(12)
C(1)-Mo(1)-C(11)	115.51(13)
C(2)-Mo(1)-C(11)	132.52(13)
O(5)-S(1)-O(4)	114.43(18)
O(5)-S(1)-O(3)	112.39(17)
O(4)-S(1)-O(3)	111.54(18)
O(5)-S(1)-C(17)	105.40(18)
O(4)-S(1)-C(17)	106.00(18)
O(3)-S(1)-C(17)	106.33(17)
Mo(1)-O(1)-Mo(1)#1	113.16(12)
C(2)-C(1)-C(5)	108.7(3)
C(2)-C(1)-Mo(1)	73.02(19)
C(5)-C(1)-Mo(1)	70.28(19)
C(1)-C(2)-C(3)	108.0(3)
C(1)-C(2)-Mo(1)	72.58(19)
C(3)-C(2)-Mo(1)	68.53(18)
C(2)-C(3)-C(4)	109.0(3)
C(2)-C(3)-Mo(1)	76.23(19)
C(4)-C(3)-Mo(1)	70.74(18)
C(5)-C(4)-C(3)	106.7(3)
C(5)-C(4)-Mo(1)	74.32(19)
C(3)-C(4)-Mo(1)	72.14(18)
C(4)-C(5)-C(1)	107.6(3)
C(4)-C(5)-C(6)	125.4(3)
C(1)-C(5)-C(6)	126.9(3)
C(4)-C(5)-Mo(1)	69.43(18)

C(1)-C(5)-Mo(1)	73.95(19)
C(6)-C(5)-Mo(1)	123.8(2)
C(5)-C(6)-C(13)	108.8(3)
C(5)-C(6)-C(14)	109.3(3)
C(13)-C(6)-C(14)	106.9(3)
C(5)-C(6)-C(7)	106.3(3)
C(13)-C(6)-C(7)	112.2(3)
C(14)-C(6)-C(7)	113.2(3)
C(8)-C(7)-C(15)	108.4(3)
C(8)-C(7)-C(16)	110.0(3)
C(15)-C(7)-C(16)	106.4(3)
C(8)-C(7)-C(6)	106.6(3)
C(15)-C(7)-C(6)	112.9(3)
C(16)-C(7)-C(6)	112.5(3)
C(9)-C(8)-C(12)	107.2(3)
C(9)-C(8)-C(7)	126.5(3)
C(12)-C(8)-C(7)	126.0(3)
C(9)-C(8)-Mo(1)	71.2(2)
C(12)-C(8)-Mo(1)	72.5(2)
C(7)-C(8)-Mo(1)	126.5(2)
C(10)-C(9)-C(8)	107.5(3)
C(10)-C(9)-Mo(1)	75.0(2)
C(8)-C(9)-Mo(1)	72.4(2)
C(11)-C(10)-C(9)	109.0(3)
C(11)-C(10)-Mo(1)	73.67(19)
C(9)-C(10)-Mo(1)	69.27(19)
C(10)-C(11)-C(12)	108.7(3)
C(10)-C(11)-Mo(1)	71.92(19)
C(12)-C(11)-Mo(1)	70.17(19)
C(11)-C(12)-C(8)	107.6(3)
C(11)-C(12)-Mo(1)	74.9(2)
C(8)-C(12)-Mo(1)	70.9(2)
C(18)-C(17)-C(22)	119.5(4)
C(18)-C(17)-S(1)	121.1(3)

C(22)-C(17)-S(1)	119.4(3)
C(17)-C(18)-C(19)	120.1(4)
C(18)-C(19)-C(20)	121.3(4)
C(19)-C(20)-C(21)	117.9(4)
C(19)-C(20)-C(23)	121.6(4)
C(21)-C(20)-C(23)	120.5(4)
C(22)-C(21)-C(20)	121.1(4)
C(21)-C(22)-C(17)	120.1(4)

Symmetry transformations used to generate equivalent atoms: #1 -x+2,-y+1,-z

Table 10. Anisotropic displacement parameters ($Å^2 x\ 10^3$) for [{$C_2Me_4(\eta^5$-$C_5H_4)_2$}Mo(μ-OH)]$_2$[OTs]$_2$·2H_2O (tak2). The anisotropic displacement factor exponent takes the form: $-2p^2[\ h^2\ a^{*2}U^{11} + ... + 2\ h\ k\ a^*\ b^*\ U^{12}\ ]$

	U^{11}	U^{22}	U^{33}	U^{23}	U^{13}	U^{12}
Mo(1)	16(1)	6(1)	14(1)	0(1)	6(1)	0(1)
S(1)	23(1)	13(1)	19(1)	-1(1)	4(1)	0(1)
O(1)	19(1)	9(1)	19(1)	4(1)	7(1)	1(1)
O(2)	26(2)	29(2)	37(2)	18(1)	1(1)	-2(1)
O(3)	26(2)	21(1)	24(1)	5(1)	0(1)	-2(1)
O(4)	25(2)	29(2)	38(2)	1(1)	13(1)	2(1)
O(5)	38(2)	17(1)	25(1)	-3(1)	4(1)	-6(1)
C(1)	22(2)	12(2)	19(2)	-3(1)	8(1)	-4(1)
C(2)	26(2)	11(2)	20(2)	-7(1)	10(2)	-7(1)
C(3)	29(2)	4(1)	29(2)	-3(1)	19(2)	1(1)
C(4)	22(2)	6(1)	26(2)	1(1)	11(2)	-1(1)
C(5)	18(2)	6(1)	20(2)	-1(1)	9(1)	-1(1)
C(6)	24(2)	12(2)	20(2)	0(1)	13(2)	-1(1)
C(7)	22(2)	14(2)	22(2)	-1(1)	13(2)	-1(1)
C(8)	21(2)	12(2)	22(2)	-3(1)	10(2)	1(1)
C(9)	24(2)	16(2)	16(2)	-3(1)	9(2)	-3(1)
C(10)	23(2)	12(2)	17(2)	-4(1)	7(1)	-4(1)
C(11)	26(2)	8(2)	21(2)	-2(1)	13(2)	3(1)
C(12)	19(2)	10(2)	22(2)	-2(1)	10(2)	3(1)
C(13)	32(2)	20(2)	24(2)	8(2)	16(2)	2(2)
C(14)	30(2)	15(2)	39(2)	-4(2)	21(2)	-5(2)
C(15)	44(3)	22(2)	32(2)	-3(2)	26(2)	-3(2)
C(16)	18(2)	19(2)	41(2)	1(2)	13(2)	0(2)
C(17)	20(2)	14(2)	22(2)	0(1)	2(2)	3(1)
C(18)	30(2)	20(2)	29(2)	0(2)	12(2)	2(2)
C(19)	39(2)	11(2)	31(2)	1(2)	5(2)	3(2)

C(20)	37(2)	19(2)	24(2)	4(2)	2(2)	-7(2)
C(21)	39(3)	28(2)	42(3)	-2(2)	22(2)	-3(2)
C(22)	45(3)	17(2)	41(2)	-3(2)	23(2)	0(2)
C(23)	48(3)	29(2)	36(3)	10(2)	6(2)	-12(2)

Table 11. Hydrogen coordinates (x 10^4) and isotropic displacement parameters ($Å^2$x 10 ^{3}) for $[\{C_2Me_4(\eta^5\text{-}C_5H_4)_2\}Mo(\mu\text{-}OH)]_2[OTs]_2\cdot 2H_2O$ (tak2)

	x	y	z	U(eq)
H(1A)	7455	2756	-667	21
H(2A)	8544	2399	-1349	22
H(3A)	9906	1356	-284	22
H(4A)	9664	981	1080	21
H(9A)	9398	4860	1988	22
H(10A)	9925	7384	1340	20
H(11A)	8785	8205	18	20
H(12A)	7522	6224	-185	20
H(13A)	8808	51	1790	36
H(13B)	8366	1207	2269	36
H(13C)	9107	1989	2027	36
H(14A)	7528	-630	761	38
H(14B)	6898	822	263	38
H(14C)	7007	472	1181	38
H(15A)	7467	5337	1983	44
H(15B)	8233	4060	2364	44
H(15C)	7304	3349	2112	44
H(16A)	6611	5239	605	38
H(16B)	6403	3244	658	38
H(16C)	6762	3892	-11	38
H(18A)	1483	5022	2829	31
H(19A)	870	2648	3199	35
H(21A)	-453	5828	4097	41
H(22A)	142	8202	3709	39
H(23A)	1	1381	3829	60
H(23B)	-827	2468	3691	60

H(23C)	-100	2493	4547	60
H(1O)	10680(30)	3900(70)	890(30)	26(14)
H(2O)	1870(30)	2280(60)	1740(30)	27(12)
H(3O)	1210(40)	1310(90)	1750(40)	55(18)

Table 12. Hydrogen bonds for [{$C_2Me_4(\eta^5$-$C_5H_4)_2$}Mo(μ-OH)]$_2$[OTs]$_2$·2H_2O (tak2) [Å and °]

D-H...A	d(D-H)	d(H...A)	d(D...A)	<(DHA)
O(1)-H(1O)...O(2)#2	0.72(5)	1.95(5)	2.666(4)	170(5)
O(2)-H(2O)...O(4)#3	0.85(5)	1.89(5)	2.745(4)	176(5)
O(2)-H(3O)...O(3)#4	0.81(7)	2.07(7)	2.873(4)	171(6)

Symmetry transformations used to generate equivalent atoms:

#1 -x+2,-y+1,-z #2 x+1,y,z #3 -x+1/2,y-1/2,-z+1/2

#4 x,y-1,z

A.3 Crystallographic Data for [{$C_2Me_4(\eta^5\text{-}C_5H_4)_2$}$MoH_2$] (tak3)

Table 13. Crystal data and structure refinement for [{$C_2Me_4(\eta^5\text{-}C_5H_4)_2$}$MoH_2$] (tak3)

Identification code	tak3	
Empirical formula	C16 H22 Mo	
Formula weight	310.28	
Temperature	173(2) K	
Wavelength	0.71073 Å	
Crystal system	Monoclinic	
Space group	C2/c	
Unit cell dimensions	a = 32.751(10) Å	α= 90°.
	b = 7.589(2) Å	β= 106.612(5)°.
	c = 10.966(3) Å	γ = 90°.
Volume	2611.8(14) $Å^3$	
Z	8	
Density (calculated)	1.578 Mg/m^3	
Absorption coefficient	0.979 mm^{-1}	
F(000)	1280	
Crystal size	0.23 x 0.11 x 0.04 mm^3	
Theta range for data collection	2.60 to 27.00°.	
Index ranges	-39<=h<=40, -9<=k<=7, -14<=l<=12	
Reflections collected	7050	
Independent reflections	2791 [R(int) = 0.0317]	
Completeness to theta = 27.00°	98.3 %	
Absorption correction	Semi-empirical from equivalents	
Max. and min. transmission	1.000 and 0.737	
Refinement method	Full-matrix least-squares on F^2	
Data / restraints / parameters	2791 / 0 / 162	
Goodness-of-fit on F^2	1.035	
Final R indices [I>2sigma(I)]	R1 = 0.0639, wR2 = 0.1597	
R indices (all data)	R1 = 0.0815, wR2 = 0.1779	
Largest diff. peak and hole	6.041 and -1.236 e.$Å^{-3}$	

Table 14. Atomic coordinates (x 10^4) and equivalent isotropic displacement parameters ($Å^2$x 10^3) for [{$C_2Me_4(\eta^5$-$C_5H_4)_2$}MoH_2] (tak3). U(eq) is defined as one third of the trace of the orthogonalized U^{ij} tensor

	x	y	z	U(eq)
Mo(1)	1825(1)	2496(1)	1933(1)	13(1)
C(1)	1483(2)	1830(7)	3416(4)	15(1)
C(2)	1889(2)	1028(7)	3861(4)	19(1)
C(3)	1933(2)	-213(7)	2959(5)	22(1)
C(4)	1552(2)	-226(7)	1933(5)	18(1)
C(5)	1270(2)	1053(6)	2199(4)	14(1)
C(6)	826(2)	1510(7)	1331(4)	16(1)
C(7)	823(2)	3465(7)	839(4)	17(1)
C(8)	1265(2)	3914(6)	718(4)	16(1)
C(9)	1481(2)	3156(7)	-134(4)	16(1)
C(10)	1885(2)	3958(7)	113(5)	19(1)
C(11)	1931(2)	5207(7)	1089(5)	22(1)
C(12)	1549(2)	5212(6)	1467(4)	18(1)
C(13)	721(2)	211(8)	205(5)	27(1)
C(14)	491(2)	1180(8)	2037(5)	26(1)
C(15)	489(2)	3788(8)	-430(5)	27(1)
C(16)	721(2)	4765(8)	1787(5)	24(1)

Table 15. Bond lengths [Å] and angles [°] for [{$C_2Me_4(\eta^5$-$C_5H_4)_2$}MoH_2] (tak3)

Mo(1)-C(8)	2.212(5)
Mo(1)-C(5)	2.213(5)
Mo(1)-C(12)	2.250(5)
Mo(1)-C(4)	2.251(5)
Mo(1)-C(9)	2.280(4)
Mo(1)-C(1)	2.279(5)
Mo(1)-C(11)	2.322(5)
Mo(1)-C(3)	2.322(5)
Mo(1)-C(10)	2.341(5)
Mo(1)-C(2)	2.346(5)
Mo(1)-H(1)	1.68(7)
Mo(1)-H(2)	1.70(6)
C(1)-C(2)	1.415(7)
C(1)-C(5)	1.445(6)
C(1)-H(1A)	1.0000
C(2)-C(3)	1.403(7)
C(2)-H(2A)	1.0000
C(3)-C(4)	1.421(7)
C(3)-H(3A)	1.0000
C(4)-C(5)	1.428(7)
C(4)-H(4A)	1.0000
C(5)-C(6)	1.532(6)
C(6)-C(14)	1.533(7)
C(6)-C(13)	1.540(7)
C(6)-C(7)	1.578(8)
C(7)-C(15)	1.523(6)
C(7)-C(8)	1.532(7)
C(7)-C(16)	1.537(7)
C(8)-C(12)	1.439(7)
C(8)-C(9)	1.442(7)
C(9)-C(10)	1.412(7)
C(9)-H(9A)	1.0000

C(10)-C(11)	1.406(7)
C(10)-H(10A)	1.0000
C(11)-C(12)	1.426(8)
C(11)-H(11A)	1.0000
C(12)-H(12A)	1.0000
C(13)-H(13A)	0.9800
C(13)-H(13B)	0.9800
C(13)-H(13C)	0.9800
C(14)-H(14A)	0.9800
C(14)-H(14B)	0.9800
C(14)-H(14C)	0.9800
C(15)-H(15A)	0.9800
C(15)-H(15B)	0.9800
C(15)-H(15C)	0.9800
C(16)-H(16A)	0.9800
C(16)-H(16B)	0.9800
C(16)-H(16C)	0.9800

C(8)-Mo(1)-C(5)	75.49(17)
C(8)-Mo(1)-C(12)	37.62(17)
C(5)-Mo(1)-C(12)	101.03(19)
C(8)-Mo(1)-C(4)	100.74(19)
C(5)-Mo(1)-C(4)	37.30(18)
C(12)-Mo(1)-C(4)	135.0(2)
C(8)-Mo(1)-C(9)	37.40(18)
C(5)-Mo(1)-C(9)	92.78(18)
C(12)-Mo(1)-C(9)	61.36(18)
C(4)-Mo(1)-C(9)	96.82(19)
C(8)-Mo(1)-C(1)	92.67(18)
C(5)-Mo(1)-C(1)	37.49(16)
C(12)-Mo(1)-C(1)	96.78(19)
C(4)-Mo(1)-C(1)	61.35(18)
C(9)-Mo(1)-C(1)	123.68(17)
C(8)-Mo(1)-C(11)	61.43(18)

C(5)-Mo(1)-C(11)	135.50(18)
C(12)-Mo(1)-C(11)	36.31(19)
C(4)-Mo(1)-C(11)	156.62(18)
C(9)-Mo(1)-C(11)	59.80(18)
C(1)-Mo(1)-C(11)	129.9(2)
C(8)-Mo(1)-C(3)	135.06(19)
C(5)-Mo(1)-C(3)	61.00(18)
C(12)-Mo(1)-C(3)	156.49(19)
C(4)-Mo(1)-C(3)	36.15(17)
C(9)-Mo(1)-C(3)	129.79(19)
C(1)-Mo(1)-C(3)	59.71(19)
C(11)-Mo(1)-C(3)	163.35(18)
C(8)-Mo(1)-C(10)	60.90(18)
C(5)-Mo(1)-C(10)	128.31(17)
C(12)-Mo(1)-C(10)	59.92(18)
C(4)-Mo(1)-C(10)	124.43(18)
C(9)-Mo(1)-C(10)	35.55(18)
C(1)-Mo(1)-C(10)	153.16(18)
C(11)-Mo(1)-C(10)	35.09(18)
C(3)-Mo(1)-C(10)	142.60(19)
C(8)-Mo(1)-C(2)	128.25(18)
C(5)-Mo(1)-C(2)	60.74(17)
C(12)-Mo(1)-C(2)	124.50(19)
C(4)-Mo(1)-C(2)	59.80(17)
C(9)-Mo(1)-C(2)	153.12(19)
C(1)-Mo(1)-C(2)	35.60(17)
C(11)-Mo(1)-C(2)	142.65(18)
C(3)-Mo(1)-C(2)	34.97(18)
C(10)-Mo(1)-C(2)	170.43(17)
C(8)-Mo(1)-H(1)	121(2)
C(5)-Mo(1)-H(1)	128(2)
C(12)-Mo(1)-H(1)	84(2)
C(4)-Mo(1)-H(1)	131(2)
C(9)-Mo(1)-H(1)	132(2)

C(1)-Mo(1)-H(1)	91(2)
C(11)-Mo(1)-H(1)	72(2)
C(3)-Mo(1)-H(1)	96(2)
C(10)-Mo(1)-H(1)	99(2)
C(2)-Mo(1)-H(1)	74(2)
C(8)-Mo(1)-H(2)	128(2)
C(5)-Mo(1)-H(2)	126(2)
C(12)-Mo(1)-H(2)	127(2)
C(4)-Mo(1)-H(2)	89(2)
C(9)-Mo(1)-H(2)	91(2)
C(1)-Mo(1)-H(2)	135(2)
C(11)-Mo(1)-H(2)	91(2)
C(3)-Mo(1)-H(2)	76(2)
C(10)-Mo(1)-H(2)	71(2)
C(2)-Mo(1)-H(2)	101(2)
H(1)-Mo(1)-H(2)	85(3)
C(2)-C(1)-C(5)	107.6(4)
C(2)-C(1)-Mo(1)	74.8(3)
C(5)-C(1)-Mo(1)	68.8(3)
C(2)-C(1)-H(1A)	126.1
C(5)-C(1)-H(1A)	126.1
Mo(1)-C(1)-H(1A)	126.1
C(3)-C(2)-C(1)	108.7(4)
C(3)-C(2)-Mo(1)	71.6(3)
C(1)-C(2)-Mo(1)	69.6(3)
C(3)-C(2)-H(2A)	125.6
C(1)-C(2)-H(2A)	125.6
Mo(1)-C(2)-H(2A)	125.6
C(2)-C(3)-C(4)	108.6(5)
C(2)-C(3)-Mo(1)	73.5(3)
C(4)-C(3)-Mo(1)	69.2(3)
C(2)-C(3)-H(3A)	125.7
C(4)-C(3)-H(3A)	125.7
Mo(1)-C(3)-H(3A)	125.7

C(3)-C(4)-C(5)	107.9(4)
C(3)-C(4)-Mo(1)	74.7(3)
C(5)-C(4)-Mo(1)	69.9(3)
C(3)-C(4)-H(4A)	125.9
C(5)-C(4)-H(4A)	125.9
Mo(1)-C(4)-H(4A)	125.9
C(4)-C(5)-C(1)	107.1(4)
C(4)-C(5)-C(6)	125.6(4)
C(1)-C(5)-C(6)	127.2(4)
C(4)-C(5)-Mo(1)	72.8(3)
C(1)-C(5)-Mo(1)	73.8(3)
C(6)-C(5)-Mo(1)	118.4(3)
C(5)-C(6)-C(14)	109.7(4)
C(5)-C(6)-C(13)	107.9(4)
C(14)-C(6)-C(13)	105.9(4)
C(5)-C(6)-C(7)	109.7(4)
C(14)-C(6)-C(7)	113.0(4)
C(13)-C(6)-C(7)	110.5(4)
C(15)-C(7)-C(8)	109.5(4)
C(15)-C(7)-C(16)	106.1(4)
C(8)-C(7)-C(16)	108.0(4)
C(15)-C(7)-C(6)	113.4(4)
C(8)-C(7)-C(6)	108.9(4)
C(16)-C(7)-C(6)	110.8(4)
C(12)-C(8)-C(9)	106.7(4)
C(12)-C(8)-C(7)	125.1(4)
C(9)-C(8)-C(7)	128.2(4)
C(12)-C(8)-Mo(1)	72.6(3)
C(9)-C(8)-Mo(1)	73.9(3)
C(7)-C(8)-Mo(1)	118.8(3)
C(10)-C(9)-C(8)	108.1(4)
C(10)-C(9)-Mo(1)	74.6(3)
C(8)-C(9)-Mo(1)	68.7(2)
C(10)-C(9)-H(9A)	125.9

C(8)-C(9)-H(9A)	125.9
Mo(1)-C(9)-H(9A)	125.9
C(11)-C(10)-C(9)	109.0(5)
C(11)-C(10)-Mo(1)	71.7(3)
C(9)-C(10)-Mo(1)	69.9(3)
C(11)-C(10)-H(10A)	125.5
C(9)-C(10)-H(10A)	125.5
Mo(1)-C(10)-H(10A)	125.5
C(10)-C(11)-C(12)	108.2(5)
C(10)-C(11)-Mo(1)	73.2(3)
C(12)-C(11)-Mo(1)	69.1(3)
C(10)-C(11)-H(11A)	125.9
C(12)-C(11)-H(11A)	125.9
Mo(1)-C(11)-H(11A)	125.9
C(11)-C(12)-C(8)	108.0(4)
C(11)-C(12)-Mo(1)	74.6(3)
C(8)-C(12)-Mo(1)	69.8(3)
C(11)-C(12)-H(12A)	125.9
C(8)-C(12)-H(12A)	125.9
Mo(1)-C(12)-H(12A)	125.9
C(6)-C(13)-H(13A)	109.5
C(6)-C(13)-H(13B)	109.5
H(13A)-C(13)-H(13B)	109.5
C(6)-C(13)-H(13C)	109.5
H(13A)-C(13)-H(13C)	109.5
H(13B)-C(13)-H(13C)	109.5
C(6)-C(14)-H(14A)	109.5
C(6)-C(14)-H(14B)	109.5
H(14A)-C(14)-H(14B)	109.5
C(6)-C(14)-H(14C)	109.5
H(14A)-C(14)-H(14C)	109.5
H(14B)-C(14)-H(14C)	109.5
C(7)-C(15)-H(15A)	109.5
C(7)-C(15)-H(15B)	109.5

H(15A)-C(15)-H(15B)	109.5
C(7)-C(15)-H(15C)	109.5
H(15A)-C(15)-H(15C)	109.5
H(15B)-C(15)-H(15C)	109.5
C(7)-C(16)-H(16A)	109.5
C(7)-C(16)-H(16B)	109.5
H(16A)-C(16)-H(16B)	109.5
C(7)-C(16)-H(16C)	109.5
H(16A)-C(16)-H(16C)	109.5
H(16B)-C(16)-H(16C)	109.5

Symmetry transformations used to generate equivalent atoms:

Table 16. Anisotropic displacement parameters ($Å^2 x\ 10^3$) for [{$C_2Me_4(\eta^5$-$C_5H_4)_2$}MoH_2] (tak3). The anisotropic displacement factor exponent takes the form: $-2p^2[\ h^2\ a^{*2}U^{11} + ... + 2\ h\ k\ a^*\ b^*\ U^{12}\ ]$

	U^{11}	U^{22}	U^{33}	U^{23}	U^{13}	U^{12}
Mo(1)	13(1)	12(1)	15(1)	2(1)	4(1)	0(1)
C(1)	17(3)	16(2)	14(2)	0(2)	6(2)	-2(2)
C(2)	20(3)	18(3)	17(2)	8(2)	3(2)	-1(2)
C(3)	21(3)	18(3)	26(3)	7(2)	6(2)	2(2)
C(4)	22(3)	13(2)	22(2)	0(2)	11(2)	-2(2)
C(5)	12(2)	14(2)	17(2)	3(2)	4(2)	0(2)
C(6)	15(3)	22(3)	12(2)	1(2)	6(2)	-1(2)
C(7)	11(2)	23(3)	18(2)	4(2)	5(2)	3(2)
C(8)	14(2)	15(2)	19(2)	4(2)	4(2)	4(2)
C(9)	16(3)	21(3)	11(2)	2(2)	1(2)	3(2)
C(10)	18(3)	18(3)	24(2)	10(2)	10(2)	3(2)
C(11)	21(3)	16(3)	27(3)	9(2)	2(2)	0(2)
C(12)	24(3)	9(2)	20(2)	0(2)	6(2)	3(2)
C(13)	21(3)	32(3)	26(3)	-9(2)	2(2)	-9(2)
C(14)	18(3)	39(3)	22(3)	4(2)	6(2)	-4(2)
C(15)	17(3)	48(4)	17(2)	8(2)	5(2)	8(3)
C(16)	22(3)	24(3)	28(3)	-1(2)	11(2)	7(2)

Table 17. Hydrogen coordinates (x 10^4) and isotropic displacement parameters ($Å^2$x 10 ^{3}) for [{$C_2Me_4(\eta^5$-$C_5H_4)_2$}MoH_2] (tak3)

	x	y	z	U(eq)
H(1A)	1357	2695	3895	19
H(2A)	2106	1287	4689	23
H(3A)	2184	-1002	3045	26
H(4A)	1483	-1070	1202	22
H(9A)	1357	2285	-825	20
H(10A)	2102	3697	-346	23
H(11A)	2182	6000	1427	27
H(12A)	1479	6053	2080	21
H(13A)	725	-996	526	41
H(13B)	934	325	-261	41
H(13C)	438	476	-366	41
H(14A)	508	-49	2322	39
H(14B)	206	1416	1465	39
H(14C)	545	1963	2777	39
H(15A)	503	5020	-684	41
H(15B)	205	3539	-345	41
H(15C)	545	3013	-1079	41
H(16A)	720	5970	1464	36
H(16B)	937	4664	2611	36
H(16C)	440	4492	1889	36
H(1)	2210(20)	3570(90)	3040(60)	60(20)
H(2)	2237(19)	1600(90)	1490(60)	43(18)

A.4 ^{1}H NMR Spectra for [{$C_2Me_4(\eta^5$-$C_5H_4)_2$}MoH_2]

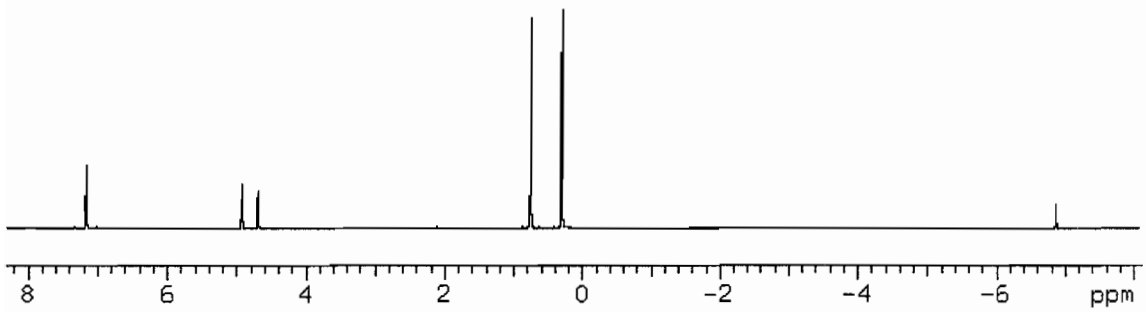

Figure 2. ^{1}H NMR spectrum of {$C_2Me_4(\eta^5$-$C_5H_4)_2$}MoH_2 in benzene-d_6: δ 4.92 (m, 4, C_5H_4), 4.69 (m, 4, C_5H_4), 0.75 (s, 12, C_2Me_4), -6.88 (2, s, MoH_2), (0.29, Si grease in benzene-d_6 solvent). This spectrum is presented as proof of spectroscopic purity.

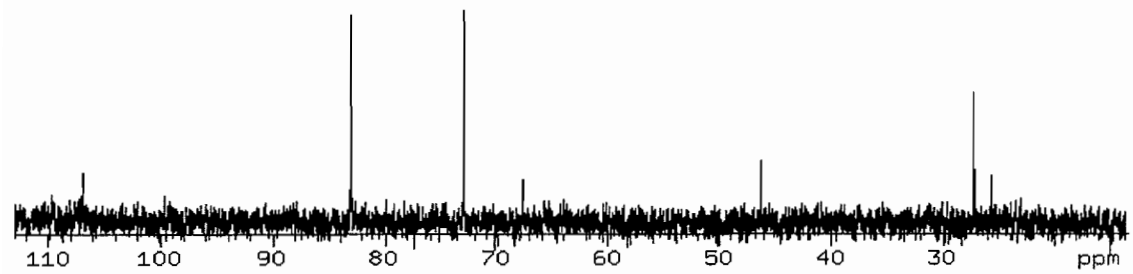

Figure 3. ^{13}C NMR spectrum of {$C_2Me_4(\eta^5$-$C_5H_4)_2$}MoH_2 THF-d_8: δ 106.82 (s, C_5H_4, C_{ipso}), 82.99 (s, C_5H_4), 72.94 (s, C_5H_4), 46.32 (s,C_2Me_4) , 27.23(C_2Me_4)

APPENDIX B

SUPPORTING INFORMATION FOR CHAPTER III

B.1 Kinetic Data for Hydration of Selected Nitriles Catalyzed by Selected Nitriles

Table 1. Rate constants for the hydration of 3-hydroxypropionitrile using molybdocene catalysts bearing selected Cp ligands

Ligand(s)	[Monomer] (mM)	[HPN] (M)	k_1 ($Ms^{-1} \times 10^4$)	k_2 ($Ms^{-1} \times 10^2$)	k_3 ($Ms^{-1} \times 10^3$)
$C_2Me_4(C_5H_4)_2$	0.58	0.060	9.3 ± 0.5	1.2 ± 0.1	1.7 ± 0.1
$(C_5H_5)_2$	0.38	0.060	17 ± 1	4.5 ± 0.5	3.7 ± 0.4
	1.1	0.26	47 ± 2	0.46 ± 0.07	5.5 ± 0.8
$(C_5H_4Me)_2$	0.56	0.060	9.1 ± 0.7	58 ± 8	8.5×10^{-5} ± 0.9 $\times 10^{-5}$
	2.5	0.26	21 ± 3	0.085 ± 0.009	1.5 ± 0.1

B.2 Pertinent Solvent Properties

Table 2. Comparison of various solvent properties for solvents used to investigate the monomer-dimer equilibrium for *ansa*-$C_2Me_4(C_5H_4)_2Mo(OH)(OH_2)^+$

Solvent	$\beta^{a, 1}$	$E_T^{(30), 2}$	pK_a^b	Dielectric Constants[c]
Tetrahydrofuran	0.51	37.4	-2.05	7.52
Ethanol	0.44	51.9	--	25.3
Methanol	0.41	55.4	-2.2	33.0
Acetone	0.50	42.2	-7.2[3]	21.0
Dimethyl sulfoxide	0.78	45.1	-1.8	47.2
Water	0.38	63.1	-1.74	80.1

a. β is a measure of hydrogen bonding acceptor ability
b. pK_a values were taken from the Evans' pK_a table, found at http://daecr1.harvard.edu/pdf/evans_pKa_table.pdf, unless otherwise referenced
c. All dielectric constants were taken from the CRC Handbook of Chemistry and Physics 82nd Ed.

Additional References for Solvent Properties

(1) Abraham, M. H.; Grellier, P. L.; Prior, D. V.; Morris, J. J.; Taylor, P. J. *J. Chem. Soc., Perkin Trans. 2* **1990**, 521-9.

(2) Reichardt, C. *Solvents and Solvent Effects in Organic Chemistry*, 2003.

(3) McTigue, P. T.; Sime, J. M. *Aust. J. Chem.* **1963**, *16*, 592-5.

APPENDIX C

SUPPORTING INFORMATION FOR CHAPTER V

C.1 Kinetic Data for [PtCl(PMe$_2$OH){(PMe$_2$O)$_2$H}]-Catalyzed Hydration of Selected Nitriles

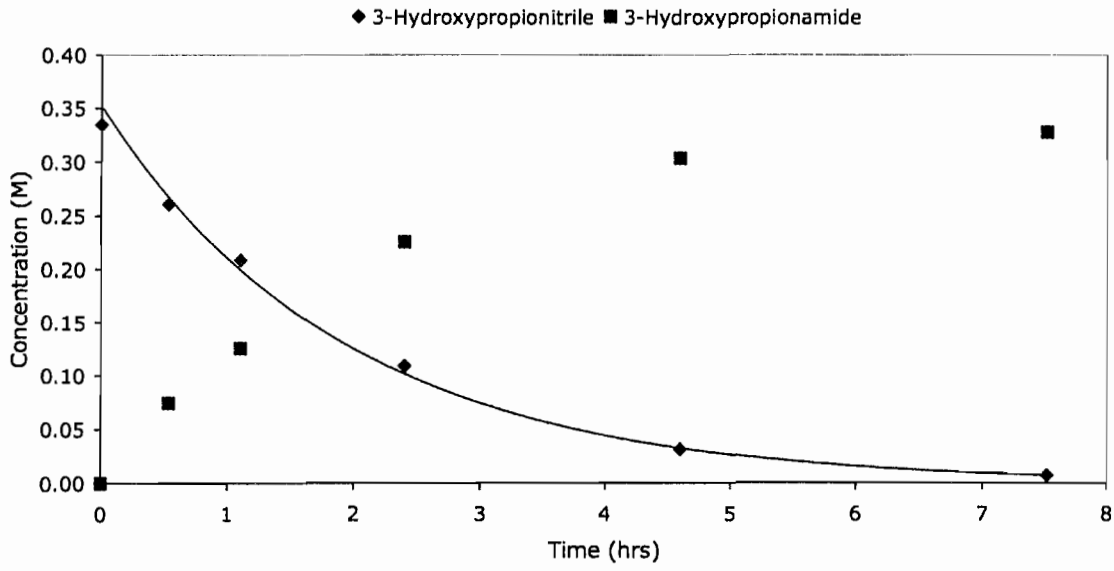

Figure 1. Plot of concentration versus time for the hydration of 3-hydroxypropionitrile catalyzed by [PtCl(PMe$_2$OH){(PMe$_2$O)$_2$H}] at 43 °C ($y = 0.353e^{-0.518}x$; $R^2 = 0.999$)

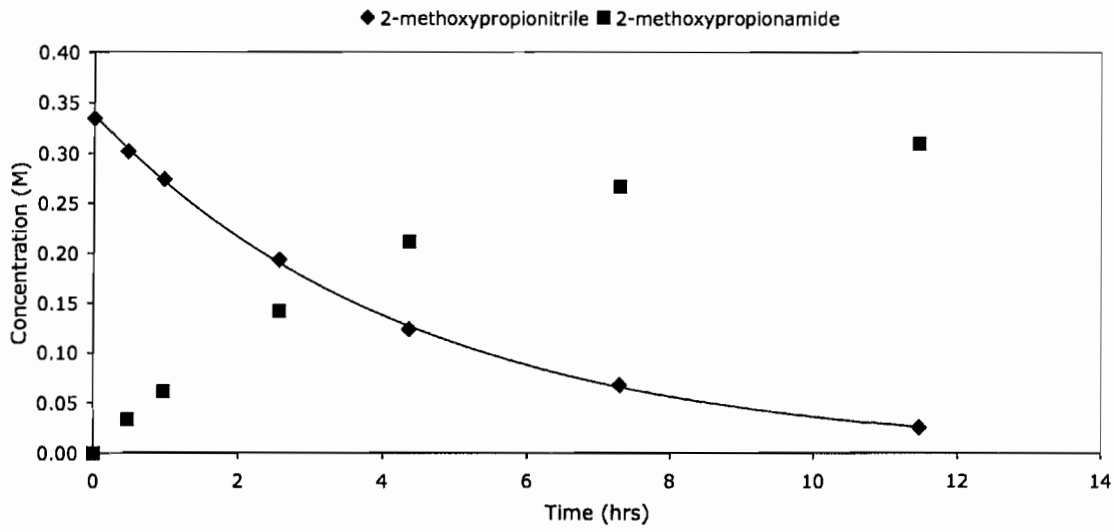

Figure 2. Plot of concentration versus time for the hydration of 2-methoxypropionitrile catalyzed by $[PtCl(PMe_2OH)\{(PMe_2O)_2H\}]$ at 43 °C ($y = 0.338e^{-0.225}x$; $R^2 = 0.9995$)

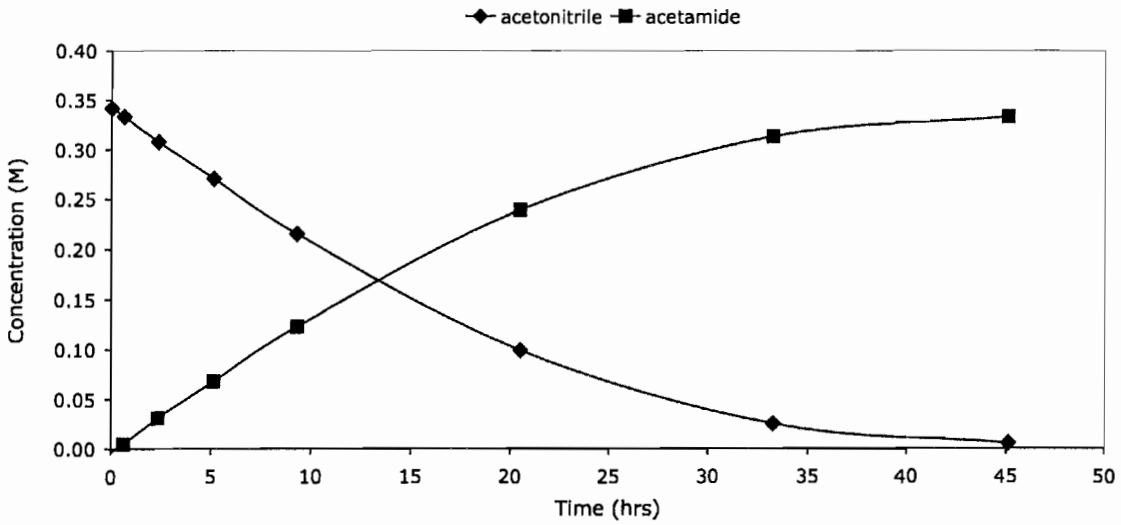

Figure 3. Plot of concentration versus time for the hydration of acetonitrile catalyzed by $[PtCl(PMe_2OH)\{(PMe_2O)_2H\}]$ at 43 °C (does not fit to first or second order decay)

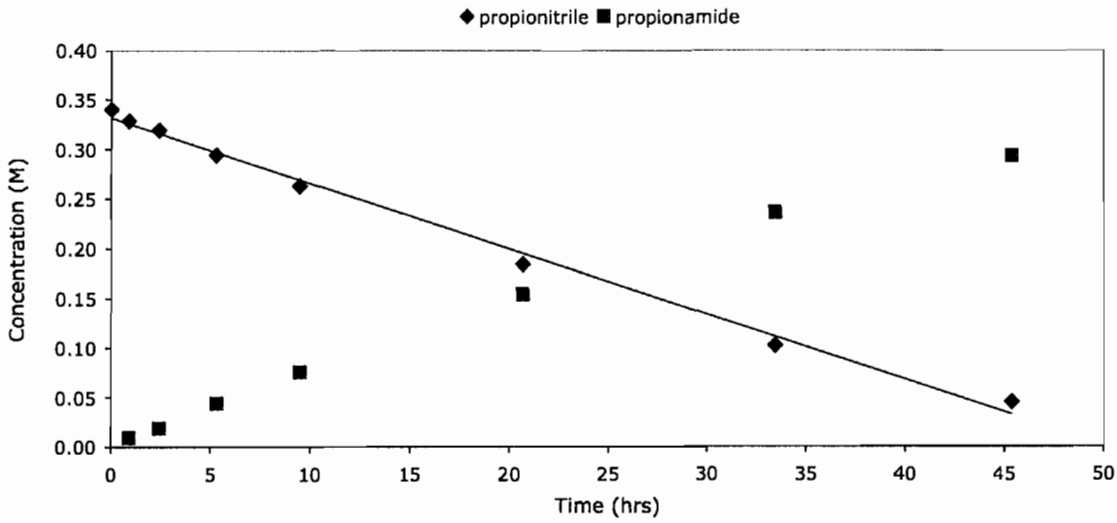

Figure 4. Plot of concentration versus time for the hydration of propionitrile catalyzed by $[PtCl(PMe_2OH)\{(PMe_2O)_2H\}]$ at 43 °C ($y = -0.0066x + 0.332$; $R^2 = 0.994$)

C.1 Crystallographic Data for $[PtCl(PMe_2OH)\{(PMe_2O)_2H\}]\cdot H_2O$

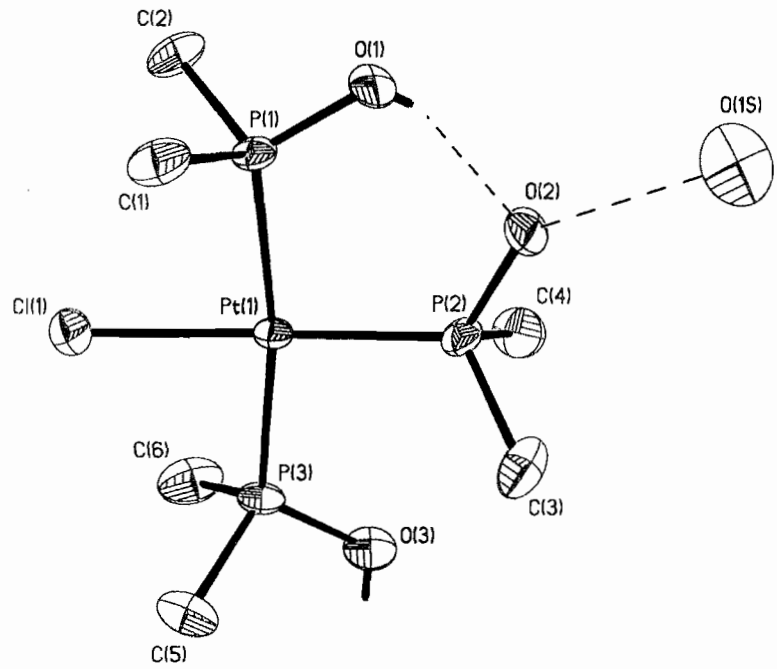

Figure 5. X-ray crystal structure of the $[PtCl(PMe_2OH)\{(PMe_2O)_2H\}]\cdot H_2O$ (tak5). The water protons were omitted. Thermal ellipsoids are drawn at the 50% probability level.

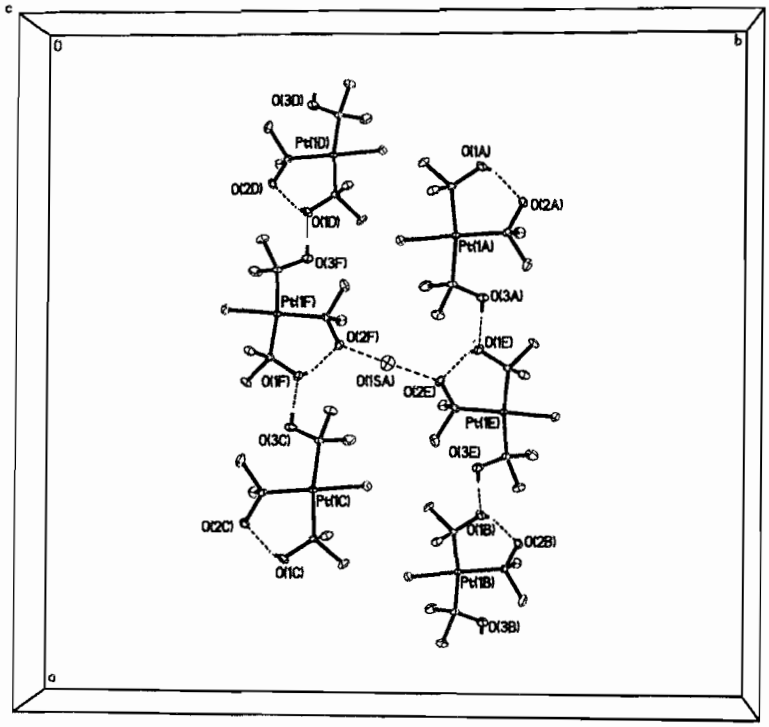

Figure 6. Hydrogen bonding network in crystalline $[PtCl(PMe_2OH)\{(PMe_2O)_2H\}]\cdot H_2O$ (tak5). The water protons were omitted. Thermal ellipsoids are drawn at the 50% probability level.

Table 1. Crystal data and structure refinement for $[PtCl(PMe_2OH)\{(PMe_2O)_2H\}]\cdot H_2O$

Identification code	tak5a
Empirical formula	C6 H21 Cl O3.50 P3 Pt
Formula weight	472.68
Temperature	173(2) K
Wavelength	0.71073 Å
Crystal system	Orthorhombic

Space group	Fdd2	
Unit cell dimensions	a = 30.422(2) Å	a= 90°.
	b = 32.575(2) Å	b= 90°.
	c = 5.9986(4) Å	g = 90°.
Volume	5944.6(7) $Å^3$	
Z	16	
Density (calculated)	2.113 Mg/m^3	
Absorption coefficient	9.933 mm^{-1}	
F(000)	3600	
Crystal size	0.12 x 0.08 x 0.04 mm^3	
Theta range for data collection	1.83 to 26.99°.	
Index ranges	-38<=h<=38, -41<=k<=41, -6<=l<=7	
Reflections collected	10025	
Independent reflections	2977 [R(int) = 0.0505]	
Completeness to theta = 26.99°	99.0 %	
Absorption correction	Semi-empirical from equivalents	
Max. and min. transmission	0.6921 and 0.3819	
Refinement method	Full-matrix least-squares on F^2	
Data / restraints / parameters	2977 / 1 / 141	
Goodness-of-fit on F^2	0.985	
Final R indices [I>2sigma(I)]	R1 = 0.0331, wR2 = 0.0551	
R indices (all data)	R1 = 0.0405, wR2 = 0.0577	
Absolute structure parameter	0.047(11)	
Largest diff. peak and hole	1.338 and -0.773 $e.Å^{-3}$	

Table 2. Atomic coordinates (x 10^4) and equivalent isotropic displacement parameters ($Å^2$x 10^3) for $[PtCl(PMe_2OH)\{(PMe_2O)_2H\}]\cdot H_2O$. U(eq) is defined as one third of the trace of the orthogonalized U^{ij} tensor.

	x	y	z	U(eq)
Pt(1)	3224(1)	926(1)	6971(1)	19(1)
Cl(1)	3287(1)	203(1)	7407(4)	33(1)
P(1)	2575(1)	867(1)	8969(3)	21(1)
P(2)	3172(1)	1603(1)	6608(4)	24(1)
P(3)	3891(1)	876(1)	5078(4)	26(1)
O(1)	2305(2)	1265(2)	9366(15)	35(2)
O(2)	2764(2)	1812(2)	7768(9)	34(2)
O(3)	4068(2)	1284(2)	4006(15)	50(2)
C(1)	2667(3)	654(3)	11702(15)	34(2)
C(2)	2205(3)	501(3)	7639(14)	36(3)
C(3)	3636(3)	1874(3)	7740(14)	40(3)
C(4)	3139(3)	1777(3)	3758(14)	44(3)
C(5)	4326(2)	702(3)	6878(17)	42(2)
C(6)	3886(3)	512(3)	2845(14)	49(3)
O(1S)	2500	2500	10471(16)	67(3)

Table 3. Bond lengths [Å] and angles [°] for $[PtCl(PMe_2OH)\{(PMe_2O)_2H\}]\cdot H_2O$

Pt(1)-P(2)	2.221(2)
Pt(1)-P(1)	2.317(2)
Pt(1)-P(3)	2.332(2)
Pt(1)-Cl(1)	2.379(2)
P(1)-O(1)	1.554(7)
P(1)-C(1)	1.802(9)
P(1)-C(2)	1.824(8)
P(2)-O(2)	1.579(6)
P(2)-C(3)	1.799(9)
P(2)-C(4)	1.804(9)
P(3)-O(3)	1.570(8)
P(3)-C(6)	1.788(9)
P(3)-C(5)	1.800(8)
P(2)-Pt(1)-P(1)	94.18(9)
P(2)-Pt(1)-P(3)	94.77(9)
P(1)-Pt(1)-P(3)	171.00(8)
P(2)-Pt(1)-Cl(1)	179.10(10)
P(1)-Pt(1)-Cl(1)	85.97(8)
P(3)-Pt(1)-Cl(1)	85.07(9)
O(1)-P(1)-C(1)	105.3(5)
O(1)-P(1)-C(2)	106.6(4)
C(1)-P(1)-C(2)	104.0(4)
O(1)-P(1)-Pt(1)	117.4(3)
C(1)-P(1)-Pt(1)	111.7(3)
C(2)-P(1)-Pt(1)	110.8(3)
O(2)-P(2)-C(3)	103.9(4)
O(2)-P(2)-C(4)	103.7(4)
C(3)-P(2)-C(4)	104.3(5)
O(2)-P(2)-Pt(1)	116.2(3)
C(3)-P(2)-Pt(1)	113.3(3)

C(4)-P(2)-Pt(1)	114.2(4)
O(3)-P(3)-C(6)	104.9(5)
O(3)-P(3)-C(5)	105.2(4)
C(6)-P(3)-C(5)	104.3(5)
O(3)-P(3)-Pt(1)	116.0(3)
C(6)-P(3)-Pt(1)	113.8(3)
C(5)-P(3)-Pt(1)	111.7(3)

Symmetry transformations used to generate equivalent atoms:

Table 4. Anisotropic displacement parameters ($Å^2 x\ 10^3$) for $[PtCl(PMe_2OH)\{(PMe_2O)_2H\}]\cdot H_2O$. The anisotropic displacement factor exponent takes the form: $-2p^2[\ h^2\ a^{*2}U^{11} + ...\ + 2\ h\ k\ a^*\ b^*\ U^{12}\ ]$

	U^{11}	U^{22}	U^{33}	U^{23}	U^{13}	U^{12}
Pt(1)	13(1)	24(1)	19(1)	0(1)	3(1)	0(1)
Cl(1)	31(1)	26(1)	41(2)	1(1)	4(1)	4(1)
P(1)	16(1)	29(1)	20(1)	3(1)	5(1)	-2(1)
P(2)	21(1)	24(1)	27(2)	2(1)	7(1)	-5(1)
P(3)	14(1)	37(2)	26(1)	-2(1)	7(1)	1(1)
O(1)	29(3)	32(4)	45(4)	9(4)	28(4)	9(3)
O(2)	31(3)	26(4)	43(4)	-3(3)	13(3)	6(3)
O(3)	22(3)	48(4)	81(6)	9(4)	33(4)	3(3)
C(1)	28(5)	47(6)	28(5)	4(5)	6(4)	-9(4)
C(2)	30(5)	40(6)	39(6)	-8(4)	-4(4)	-20(5)
C(3)	52(6)	31(6)	38(6)	-4(4)	13(5)	-13(5)
C(4)	40(6)	48(7)	43(6)	15(5)	2(5)	1(5)
C(5)	28(5)	58(7)	40(5)	1(6)	-6(5)	10(4)
C(6)	38(6)	68(8)	40(6)	-16(5)	13(5)	-9(6)
O(1S)	76(8)	65(8)	60(7)	0	0	10(7)

Table 5. Hydrogen coordinates (x 10^4) and isotropic displacement parameters ($Å^2$x 10^3) for $[PtCl(PMe_2OH)\{(PMe_2O)_2H\}]\cdot H_2O$

	x	y	z	U(eq)
H(1A)	2386	633	12497	52
H(1B)	2867	832	12538	52
H(1C)	2798	380	11559	52
H(2A)	1933	480	8508	55
H(2B)	2346	231	7568	55
H(2C)	2136	595	6127	55
H(3A)	3595	2170	7531	60
H(3B)	3905	1787	6970	60
H(3C)	3663	1813	9334	60
H(4A)	3117	2077	3731	66
H(4B)	2878	1658	3047	66
H(4C)	3403	1691	2948	66
H(5A)	4601	684	6030	64
H(5B)	4252	430	7472	64
H(5C)	4363	895	8114	64
H(6A)	4175	507	2125	73
H(6B)	3662	592	1751	73
H(6C)	3818	239	3434	73
H(1O)	2360(40)	1420(40)	8800(200)	100(60)
H(3O)	4320(30)	1270(40)	3520(170)	70(40)

Table 6. Torsion angles [°] for $[PtCl(PMe_2OH)\{(PMe_2O)_2H\}]\cdot H_2O$

P(2)-Pt(1)-P(1)-O(1)	2.4(4)
P(3)-Pt(1)-P(1)-O(1)	176.2(6)
Cl(1)-Pt(1)-P(1)-O(1)	-178.5(4)
P(2)-Pt(1)-P(1)-C(1)	-119.4(3)
P(3)-Pt(1)-P(1)-C(1)	54.3(7)
Cl(1)-Pt(1)-P(1)-C(1)	59.7(3)
P(2)-Pt(1)-P(1)-C(2)	125.1(3)
P(3)-Pt(1)-P(1)-C(2)	-61.1(7)
Cl(1)-Pt(1)-P(1)-C(2)	-55.8(3)
P(1)-Pt(1)-P(2)-O(2)	1.9(3)
P(3)-Pt(1)-P(2)-O(2)	-177.1(3)
Cl(1)-Pt(1)-P(2)-O(2)	-97(7)
P(1)-Pt(1)-P(2)-C(3)	122.0(3)
P(3)-Pt(1)-P(2)-C(3)	-57.0(3)
Cl(1)-Pt(1)-P(2)-C(3)	23(7)
P(1)-Pt(1)-P(2)-C(4)	-118.8(4)
P(3)-Pt(1)-P(2)-C(4)	62.2(4)
Cl(1)-Pt(1)-P(2)-C(4)	142(7)
P(2)-Pt(1)-P(3)-O(3)	-5.3(4)
P(1)-Pt(1)-P(3)-O(3)	-179(13)
Cl(1)-Pt(1)-P(3)-O(3)	175.6(4)
P(2)-Pt(1)-P(3)-C(6)	-127.1(4)
P(1)-Pt(1)-P(3)-C(6)	59.1(7)
Cl(1)-Pt(1)-P(3)-C(6)	53.8(4)
P(2)-Pt(1)-P(3)-C(5)	115.2(4)
P(1)-Pt(1)-P(3)-C(5)	-58.6(7)
Cl(1)-Pt(1)-P(3)-C(5)	-63.9(4)

Symmetry transformations used to generate equivalent atoms:

Table 7. Hydrogen bonds for $[PtCl(PMe_2OH)\{(PMe_2O)_2H\}]\cdot H_2O$ [Å and °].

D-H...A	d(D-H)	d(H...A)	d(D...A)	<(DHA)
O(1)-H(1O)...O(2)	0.63(12)	1.88(12)	2.459(9)	155(17)
O(3)-H(3O)...O(1)#1	0.82(9)	1.78(9)	2.588(8)	167(11)

Symmetry transformations used to generate equivalent atoms:

#1 x+1/4,-y+1/4,z-3/4

APPENDIX D

ADDITIONAL INFORMATION ON THE CONVERSION OF ACH AND THE SYNTHESIS AND REACTIVITY OF PT PHOSPHINITO CATALYSTS

D.1 Hydration of ACH using Potassium Borate

D.1.1 Results and Discussion

Schoenbeck et al.[1] demonstrated the hydrolysis of ketone-derived cyanohydrins under alkaline conditions (pH 7 – 11) using borate salts as catalysts. To test this synthetic method, boric acid (10 mol %) was added to a mixture of acetone, D_2O, and ACH and the mixture was subsequently adjusted to pH 10 using KOH. After 16.8 hours at 50 °C, the red reaction mixture showed 27 % conversion to hydroxyisobutyramide (HIBAM), and the ratio of acetone to ACH remained unchanged. No hydroxyisobutyric acid was observed.

Although the use of borate salts in the hydration of cyanohydrins has already been patented,[1] this synthetic procedure demonstrates that the reactivity of ACH is similar to that of most other nitriles. According to Commeyras and coworkers,[2,3] borate-catalyzed hydration of cyanohydrins proceeds in a manner similar to that proposed for other boric acid-catalyzed hydrolysis reactions. The first step of the cycle involves formation of a

borate ester catalyst-substrate complex though coordination to the α-hydroxy substituent of ACH. The activated ACH can then be hydrated by intramolecular nucleophilic attack of the boron-coordinated hydroxy group to form a five-membered intermediate or intramolecular transfer of a hydroxide group to give an acyclic intermediate. (See Scheme 5 in Chapter 1). No evidence was given to disprove either route. However, in either case, the proposed mechanistic pathways demonstrate that the nitrile carbon of ACH, like most other nitriles, is susceptible to attack by a nuclephile pending adequate activation by a Lewis acid. Furthermore, coordination of ACH to borate through the alcohol does not promote the release of CN. Instead, the borate actually acts as a Lewis acid protecting group that also activates the nitrile functionality.

An additional experiment was run to test the catalytic activity of $[PtCl(PMe_2OH)\{(PMe_2O)_2H\}]$ in the presence of borate ions. It was postulated that, in the presence of borate ions, $[PtCl(PMe_2OH)\{(PMe_2O)_2H\}]$ would bind through the nitrile functionality leading to enhanced activation and faster rates. Unfortunately, addition of complex $[PtCl(PMe_2OH)\{(PMe_2O)_2H\}]$ (5 mol %) to the reaction composition previously tested using borate did not give a faster rates compared with that previously observed for borate alone. The results are summarized in Table 2.

Table 1. Comparison of kinetic data for the hydration of ACH using selected Lewis acid catalysts

	$[B(OH)_4]^-$	**1***	[ACH]	TOF
$K[B(OH)_4]$	0.23	--	2.3	0.15
$K[B(OH)_4]$ AND **1**	0.23	6.2×10^{-3}	2.3	0.11

* **1** is used to denote $[PtCl(PMe_2OH)\{(PMe_2O)_2H\}]$

D.1.2 Experimental Procedures

ACH Hydration Catalyzed by Borate.

This procedure was taken from example 8 of the patented work.[1] H_3BO_3 (0.0125 g, 0.202 mmol), $(CH_3)_2CO$ (0.382 mL, 5.17 mmol), and D_2O (0.300 mL, 16.7 mmol) were added to a scintillation vial. The resulting solution was adjusted to pH 10 using KOH (0.0054 g, 0.096 mmol) and added to a 9 in NMR tube. ACH (0.180 mL, 1.97 mmol) was added to the reaction mixture, and the tube was subsequently flame sealed while frozen in liquid N_2. After thawing, the reaction mixture was heated to 50 °C in an oil bath. After 16.8 hours, 26.8 % conversion of ACH to α-hydroxyisobutramide was appearent in the ^1H NMR spectrum. Singlet ^1H resonances were observed for acetone (2.27 ppm, s, 6H, $(CH_3)_2CO$), acetone cyanohydrin (1.64 ppm, s, 6H, $HO(CH_3)_2CCN$), and α-hydroxyisobutramide (1.45 ppm, s, 6H, $(HO(CH_3)_2CC(O)ND_2)$. Note that the

ratio of acetone to ACH (57 %) was unchanged at 16.8 hours. The presence of α-hydroxyisobutramide was confirmed in the ^{13}C NMR spectrum at 181.5 ppm ($HO(CH_3)_2CC(O)ND_2$), 73.8 ppm ($HO(CH_3)_2CC(O)ND_2$), and 26.4 ppm ($HO(CH_3)_2CC(O)ND_2$).

ACH Hydration Catalyzed by Borate and [PtCl(PMe$_2$OH){(PMe$_2$O)$_2$H}].

The above procedure for the borate catalyzed reaction was followed exactly, except [PtCl(PMe$_2$OH){(PMe$_2$O)$_2$H}] (0.003 g, 0.005 mmol) and $TlPF_6$ (0.004 g, 0.013 mmol) were added to the scintillation vial prior to adjusting the pH with KOH. In this case, only 23 % conversion to hydroxyisobutyramide was observed in the ^1H NMR spectrum after 21 hours of reaction at 50 °C.

D.2 Attempt to Protect ACH using Trimethylsilane

D.2.1 Results and Discussion

The O-protected cyanohydrin TMS-ACH was prepared by reaction trimethylsilyl cyanide and acetone (eq 1).

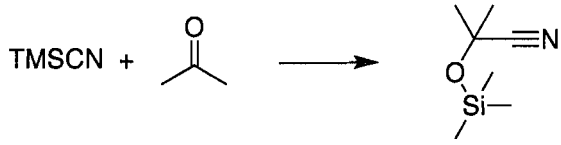

(1)

Unfortunately, hydration of the nitrile functionality of TMS-ACH was not competitive with hydrolysis of the silyl group in the presence of [PtCl(P(Me)$_2$OH)(P(Me)$_2$O)$_2$H]. Even at low heat (40 °C) and neutral pH, hydrolysis of the TMS group occurred readily to

give trimethylsilanol and acetone cyanohydrin (~65 % completion in 3 hours). No hydration was detectable by NMR spectroscopy.

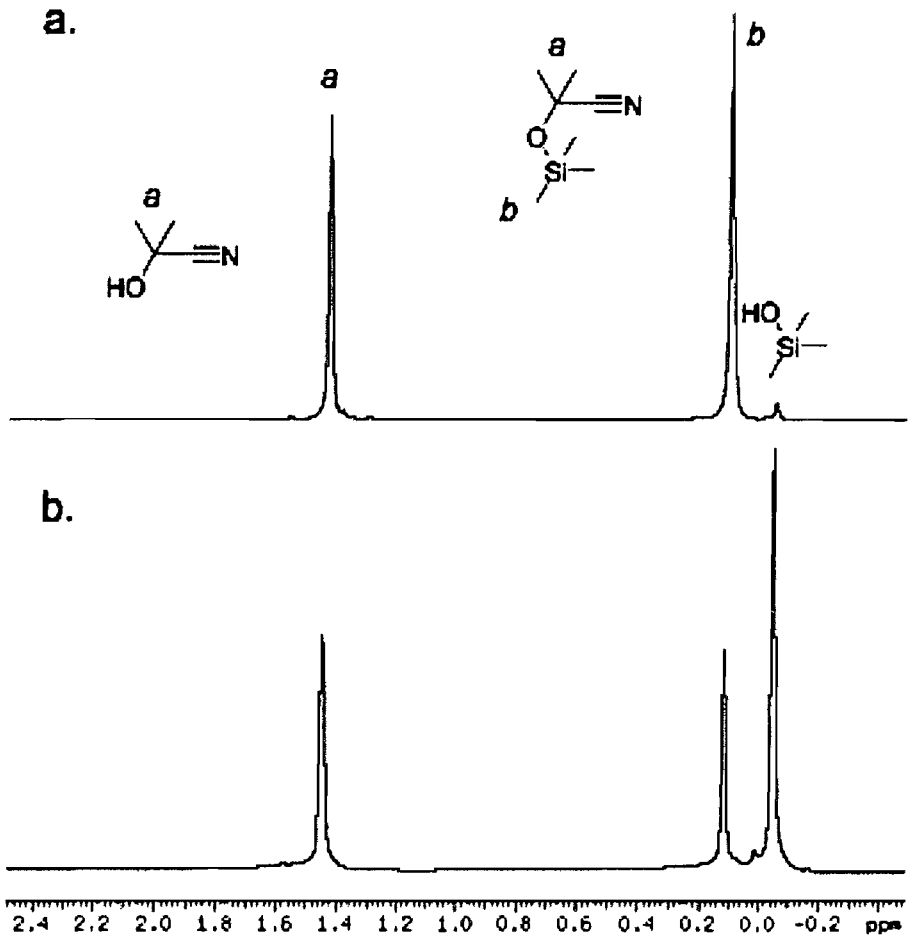

Figure 1. ^{1}H NMR spectra of TMS-ACH hydrolysis in the presence of $[PtCl(P(Me)_2OH)(P(Me)_2O)_2H]$ and TlOTf after (a) 0 hrs and (b) 3 hours of reaction.

D.2.2 Experimental Procedures

Synthesis of TMS-ACH.

A suspension of ZnI_2 (0.0065 g, 0.020 mmol) in TMSCN (2.98 g, 0.0300 mol) was added dropwise to acetone (1.78 g, 0.0306 mol) in a round bottom flask under N_2.

The reaction mixture was stirred for 1.5 hours after which time the product was distilled from the reaction vessel under reduced pressure (25 °C at ~1 torr). TMS-protected ACH was obtained (2.28 g, 43 % yield) as light golden oil. ^{1}H NMR ($CDCl_3$) δ 1.609 (s, 6H, $(CH_3)_3SiOC(CH_3)_2CN$) and 0.247 (s, 9H, $(CH_3)_3SiOC(CH_3)_2CN$). ^{13}C NMR (D_2O) δ 124.7 ($(CH_3)_3SiOC(CH_3)_2CN$), 68.7 ($(CH_3)_3SiOC(CH_3)_2CN$), 33.25 ($(CH_3)_3SiOC(CH_3)_2CN$), and 4.25 ($(CH_3)_3SiOC(CH_3)_2CN$).

Reaction of TMS-ACH with $[PtCl(P(Me)_2OH)(P(Me)_2O)_2H]$.

TMS-ACH (0.500 mL), D_2O (0.100 mL), $[PtCl(P(Me)_2OH)(P(Me)_2O)_2H]$ (0.0075 g, 0.016 mmol), and TlOTf (0.0076 g, 0.0215 mmol) were added to a 9 inch NMR tube, which was subsequently flame sealed while frozen. Hydrolysis of the TMS group was monitored by ^{1}H NMR (D_2O) spectroscopy at 40 °C by the disappearance of TMS-ACH resonance at 1.43 ppm (s, 6H, $(CH_3)_3SiOC(CH_3)_2CN$) and 0.097 (s, 9H, $(CH_3)_3SiOC(CH_3)_2CN$). Silanol and ACH products were observed at -0.056 ppm (s, 9H, $(CH_3)_3SiOH$) and 1.41 ppm (s, 6H, $HOC(CH_3)_2CN$), respectively. The presence of trimethylsilanol was also confirmed in the ^{13}C spectrum at 3.60 ppm ($(CH_3)_3SiOH$). ^{13}C resonances for ACH in the reaction mixture were observed at δ 125.0 ($HOC(CH_3)_2CN$), 67.2 ($HOC(CH_3)_2CN$), and 31.56 ($HOC(CH_3)_2CN$). No hydration was detected after 24 hours.

D.3 Synthesis and Characterization of $[PtCl\{(PEt_2O)_2H\}]_2$

D.3.1 Results and Discussion

The common Pt(II) precursor K_2PtCl_4 is known to react with diphenylphoshine

oxide and dimetyhlphosphine oxide to give tri-substituted monomeric species;[4,5] however, K_2PtCl_4 reacts with diethylphosphine oxide to yield a species with the empirical formula $PtClP_2C_4H_{11}O_2$ (Table 1), having only two phosphorus atoms and one chloride per Pt center. The ^{31}P spectrum of $PtClP_2C_4H_{11}O_2$ shows a singlet resonance with Pt satellites (δ 70.4 J^{P-Pt} = 4008 Hz), indicating only identical phosphorus environments for both phosphinito ligands (Figure 2b). The ^{195}Pt NMR spectrum shows coupling to the two P atoms (δ -4351, J^{Pt-P} = 4019 Hz, Figure 2a), which is consistent with a Cl bridging dimer containing two hydrogen bonded phosphinito ligands on each Pt center. On the basis of the empirical and NMR spectroscopic analyses, the dimeric structure **2** was proposed.

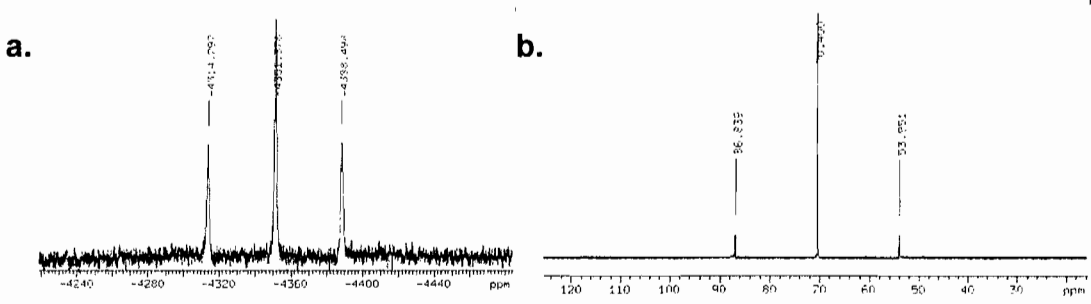

Figure 2. (a.) ^{195}Pt and (b.) ^{31}P NMR spectra of $[PtCl(P(Et)_2O)_2H)]_2$ **3** in $CDCl_3$ are indicative of two equivalent phosphinito ligands consistent with the proposed chloride bridging dimeric structure.

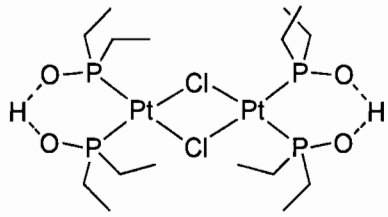

2

D.3.2 Synthesis of $PtClP_2C_4H_{11}O_2$

The synthesis of $[PtCl\{(PEt_2O)_2H\}]_2$ was adapted from the synthesis of $[PtCl(PMe_2OH)\{(PMe_2O)_2H\}]$.[5] Diethylphosphine oxide was prepared as described in the literature.[6] This procedure was performed under an atmosphere of dinitrogen using standard Schlenk line techniques.

A solution of diethylphosphine oxide (0.218 g, 2.05 mmol) in ethanol (5 mL) was added dropwise to K_2PtCl_4 (0.253 g , 0.610 mmol) in ethanol (20 mL) and DI water (10 mL). The pink solution turned light amber while stirring at room temperature for twelve hours. After this time, the reaction flask was warmed to 38 °C until the solution turned light yellow (~ six hours). The resulting solution was allowed to cool to room temperature, and activated charcoal was added to the flask. After stirring, the reaction mixture was filtered through celite. The yellow mother liquor was concentrated to 8 mL and 15 mL of DI water was added resulting in precipitation of the desired product as a white precipitate. The product was filtered using a fritted funnel, washed with water and diethyl ether, and dried in air (0.12 g, 43 % yield). ^{1}H NMR ($CDCl_3$) δ 1.85 (2H, m), 1.29 (3H, dt, J^{H-H} = 7.7 Hz). ^{31}P NMR (D_2O) δ 70.4 (J^{Pt-P} = 4008 Hz). ^{195}Pt NMR

($CDCl_3$) δ 4351 (J^{Pt-P} = 4019 Hz). Anal. Found: H, 4.58; C, 22.09; Cl, 7.69. Calculated for $PtClP_2C_4H_{11}O_2$: 4.80 % H, 21.77 % C, 7.93 % Cl.

D.5 Attempts to Synthesize [Pt*H*(PMe_2OH){($PMe_2O)_2H$}]

Several attempts were made to prepare the hydrido analog [PtH(PMe_2OH){($PMe_2O)_2H$}] by the published procedure, wherein tetrakistriphenyl phosphine Pt(0) s reacted with dimethylphosphine oxide (eq 2).[5]

$$Pt(PPh_3)_4 + 3\ P(O)Me_2H \xrightarrow[\text{Toluene}]{} [PtH(PMe_2OH)\{(PMe_2O)_2H\}] + 4\ PPh_3 \qquad (2)$$

However, the product obtained from eq 2 yields spectroscopic data that are inconsistent with the proposed empirical formula. Specifically, the ^{31}P NMR spectrum (solvent) of the Pt species resulting from eq 2 contains only a singlet resonance at 71.7 ppm (J^{Pt-P} = 2193 Hz), indicating only one distinct phosphorus environment. The IR spectrum of the product shows a small absorbance at 2005 cm^{-1}(nujol mull), instead of the Pt-H absorbance reported in the literature for the desired compound (1989 cm^{-1}, nujol mull). However, curiously, the elemental analysis of the Pt product is consistent with the molecular formula of [PtH(PMe_2OH){($PMe_2O)_2H$}] (Table 2). Unfortunately, only elemental analysis and IR data were reported for the hydride catalyst,[5] which restricted data comparison and interpretation. However, note that the product obtained from eq 2 was no more reactive than the chloro analog, [PtCl(PMe_2OH){($PMe_2O)_2H$}] toward ACH.

Table 2. Elemental analysis results for Product Generated in Eq 2

Element	Found	Calculated
H	4.46	4.93
C	16.64	16.79
P	23.19	21.65

REFERENCES

CHAPTER I

(1) Green, M. M.; Wittcoff, H. A. *Organic Chemistry Principles and Industrial Practice*, 2003.

(2) Nagasawa, T.; Yamada, H. *Trends Biotechnol.* **1989**, *7*, 153-8.

(3) Kobayashi, M.; Nagasawa, T.; Yamada, H. *Trends Biotechnol.* **1992**, *10*, 402-8.

(4) Matsuda, F. *CHEMTECH* **1977**, *7*, 306-8.

(5) Odian, G. *Principles of Polymerization* 4th ed.; John Wiley and Sons, Inc: Hoboken, NJ, 2004.

(6) Kukushkin, V. Y.; Pombeiro, A. J. L. *Inorg. Chim. Acta* **2005**, *358*, 1-21.

(7) Gruber, W.; Schroeder, G.; (Rohm G.m.b.H., Fed. Rep. Ger.), US Patent # 4,018,829, 1976, p 1-3.

(8) Harrop, T. C.; Mascharak, P. K. *Acc. Chem. Res.* **2004**, *37*, 253-260.

(9) Kovacs Julie, A. *Chem Rev* **2004**, *104*, 825-48.

(10) Mascharak, P. K. *Coord. Chem. Rev.* **2002**, *225*, 201-214.

(11) Tamura, K.; (Nitto Chemical Industry Co., Ltd., Japan). US Patent# 5,736,385, **1996**, p 1-7.

(12) Bousquet, A.; Musolino, A.; (SANOFI, Fr.). US Patent# 6,573,381, **1999**, p 1–8

(13) DeSantis, G.; Zhu, Z.; Greenberg, W. A.; Wong, K.; Chaplin, J.; Hanson, S. R.; Farwell, B.; Nicholson, L. W.; Rand, C. L.; Weiner, D. P.; Robertson, D. E.; Burk, M. J. *J. Am. Chem. Soc.* **2002**, *124*, 9024-9025.

(14) Layh, N.; Parratt, J.; Willetts, A. *J. Mol. Catal. B: Enzym.* **1998**, *5*, 467-474.

(15) Osprian, I.; Fechter, M. H.; Griengl, H. *J. Mol. Catal. B: Enzym.* **2003**, *24-25*, 89-98.

(16) Reisinger, C.; Osprian, I.; Glieder, A.; Schoemaker, H. E.; Griengl, H.; Schwab, H. *Biotechnol. Lett.* **2004**, *26*, 1675-1680.

(17) Ress-loeschke, M.; Friedrich, T.; Hauer, B.; Mattes, R.; Engels, D.; (BASF A.-G., Germany). US Patent # 6,869,783, **2000**, p 1-21.

(18) Yamamoto, K.; Oishi, K.; Fujimatsu, I.; Komatsu, K. *Appl. Environ. Microbiol.* **1991**, *57*, 3028-32.

(19) Wechsberg, M.; Schoenbeck, R.; (Chemie Linz A.-G., Austria). US Patent #4,222,960, **1980**, p. 1-4.

(20) Jammot, J.; Pascal, R.; Commeyras, A. *Tetrahedron Lett.* **1989**, *30*, 563-4.

(21) Jammot, J.; Pascal, R.; Commeyras, A. *J. Chem. Soc., Perkin Trans. 2* **1990**, 157-62.

(22) Parkins, A. W.; Ghaffar, T.; (UK). US Patent# 5.932,756, **1999**, p 1-6.

(23) Ghaffar, T.; Parkins, A. W. *J. Mol. Catal. A: Chem.* **2000**, *160*, 249-261.

(24) Breno, K. L.; Pluth, M. D.; Tyler, D. R. *Organometallics* **2003**, *22*, 1203-1211.

(25) Kuo, L. Y.; Perera, N. M. *Inorg. Chem.* **2000**, *39*, 2103-2106.

(26) Kuo, L. Y.; Kuhn, S.; Ly, D. *Inorg. Chem.* **1995**, *34*, 5341-5.

(27) Kuo, L. Y.; Barnes, L. A. *Inorg. Chem.* **1999**, *38*, 814-817.

(28) Kuo, L. Y.; Blum, A. P.; Sabat, M. *Inorg. Chem.* **2005**, *44*, 5537-5541.

(29) Kuo, L. Y.; Adint, T. T.; Akagi, A. E.; Zakharov, L. *Organometallics* **2008**, *27*, 2560-2564.

(30) Kuo Louis, Y.; Blum Angela, P.; Sabat, M. *Inorg. Chem.* **2005**, *44*, 5537-41.

(31) Breno, K. L.; Pluth, M. D.; Landorf, C. W.; Tyler, D. R. *Organometallics* **2004**, *23*, 1738-1746.

(32) Breno, K. L.; Ahmed, T. J.; Pluth, M. D.; Balzarek, C.; Tyler, D. R. *Coord. Chem. Rev.* **2006**, *250*, 1141-1151.

(33) Zachmanoglou, C. E.; Docrat, A.; Bridgewater, B. M.; Parkin, G.; Brandow, C. G.; Bercaw, J. E.; Jardine, C. N.; Lyall, M.; Green, J. C.; Keister, J. B. *J. Am. Chem. Soc.* **2002**, *124*, 9525-9546.

(34) Jourdain, I. V.; Fourmigue, M.; Guyon, F.; Amaudrut, J. *Organometallics* **1999**, *18*, 1834-1839.

(35) Churchill, D. G.; Janak, K. E.; Wittenberg, J. S.; Parkin, G. *J. Am. Chem. Soc.* **2003**, *125*, 1403-1420.

(36) Churchill, D. G.; Bridgewater, B. M.; Parkin, G. *J. Am. Chem. Soc.* **2000**, *122*, 178-179.

(37) Conway, S. L. J.; Dijkstra, T.; Doerrer, L. H.; Green, J. C.; Green, M. L. H.; Stephens, A. H. H. *J. Chem. Soc., Dalton Trans.* **1998**, 2689-2696.

(38) Green, J. C.; Harvey, J. N.; Poli, R. *J. Chem. Soc., Dalton Trans.* **2002**, 1861-1866.

(39) Pons, V.; Conway, S. L. J.; Green, M. L. H.; Green, J. C.; Herbert, B. J.; Heinekey, D. M. *Inorg. Chem.* **2004**, *43*, 3475-3483.

(40) Labella, L.; Chernega, A.; Green, M. L. H. *J. Chem. Soc., Dalton Trans.* **1995**, 395-402.

(41) Labella, L.; Chernega, A.; Green, M. L. H. *J. Organomet. Chem.* **1995**, *485*, C18-C21.

(42) Janak, K. E.; Shin, J. H.; Parkin, G. *J. Am. Chem. Soc.* **2004**, *126*, 13054-13070.

(43) Chernega, A.; Cook, J.; Green, M. L. H.; Labella, L.; Simpson, S. J.; Souter, J.; Stephens, A. H. H. *J. Chem. Soc., Dalton Trans.* **1997**, 3225-3243.

(44) Churchill, D. G.; Bridgewater, B. M.; Zhu, G.; Pang, K.; Parkin, G. *Polyhedron* **2006**, *25*, 499-512.

(45) Churchill, D.; Shin, J. H.; Hascall, T.; Hahn, J. M.; Bridgewater, B. M.; Parkin, G. *Organometallics* **1999**, *18*, 2403-2406.

(46) Prout, K.; Cameron, T. S.; Forder, R. A.; Critchley, S. R.; Denton, B.; Rees, G. V. *Acta Crystallogr., Sect. B* **1974**, *30B*, 2290-304.

(47) Schultz, A. J.; Stearley, K. L.; Williams, J. M.; Mink, R.; Stucky, G. D. *Inorg. Chem.* **1977**, *16*, 3303-6.

(48) Unpublished work.

(49) Cloke, F. G. N.; Day, J. P.; Green, J. C.; Morley, C. P.; Swain, A. C. *J. Chem. Soc., Dalton Trans.* **1991**, 789-96.

(50) Berry, M.; Cooper, N. J.; Green, M. L. H.; Simpson, S. J. *J. Chem. Soc., Dalton Trans.* **1980**, 29-40.

(51) Green, J. C. *Chem. Soc. Rev.* **1998**, *27*, 263-272.

(52) Balzarek, C.; Weakley, T. J. R.; Kuo, L. Y.; Tyler, D. R. *Organometallics* **2000**, *19*, 2927-2931.

(53) Kuo, L. Y.; Kanatzidis, M. G.; Sabat, M.; Tipton, A. L.; Marks, T. J. *J. Am. Chem. Soc.* **1991**, *113*, 9027-45.

(54) Ghaffar, T.; Parkins, A. W. *Tetrahedron Lett.* **1995**, *36*, 8657-60.

(55) Cobley, C. J.; Van den Heuvel, M.; Abbadi, A.; De Vries, J. G. *Tetrahedron Lett.* **2000**, *41*, 2467-2470.

(56) Jiang, X.-b.; Minnaard, A. J.; Feringa, B. L.; De Vries, J. G. *J. Org. Chem.* **2004**, *69*, 2327-2331.

CHAPTER II

(1) Breno, K. L.; Ahmed, T. J.; Pluth, M. D.; Balzarek, C.; Tyler, D. R. *Coord. Chem. Rev.* **2006**, *250*, 1141-1151.

(2) Breno, K. L.; Pluth, M. D.; Landorf, C. W.; Tyler, D. R. *Organometallics* **2004**, *23*, 1738-1746.

(3) Breno, K. L.; Pluth, M. D.; Tyler, D. R. *Organometallics* **2003**, *22*, 1203-1211.

(4) Breno, K. L.; Tyler, D. R. *Organometallics* **2001**, *20*, 3864-3868.

(5) Balzarek, C.; Tyler, D. R. *Angew. Chem., Int. Ed. Engl.* **1999**, *38*, 2406-2408.

(6) Balzarek, C.; Weakley, T. J. R.; Tyler, D. R. *J. Am. Chem. Soc.* **2000**, *122*, 9427-9434.

(7) Kuo, L. Y.; Barnes, L. A. *Inorg. Chem.* **1999**, *38*, 814-817.

(8) Kuo, L. Y.; Blum, A. P.; Sabat, M. *Inorg. Chem.* **2005**, *44*, 5537-5541.

(9) Kuo, L. Y.; Finigan, D. M.; Tadros, N. N. *Organometallics* **2003**, *22*, 2422-2425.

(10) Kuo, L. Y.; Kuhn, S.; Ly, D. *Inorg. Chem.* **1995**, *34*, 5341-5.

(11) Kuo, L. Y.; Perera, N. M. *Inorg. Chem.* **2000**, *39*, 2103-2106.

(12) Kuo, L. Y.; Weakley, T. J. R.; Awana, K.; Hsia, C. *Organometallics* **2001**, *20*, 4969-4972.

(13) Chin, J. *Acc. Chem. Res.* **1991**, *24*, 145-52.

(14) Churchill, D.; Shin, J. H.; Hascall, T.; Hahn, J. M.; Bridgewater, B. M.; Parkin, G. *Organometallics* **1999**, *18*, 2403-2406.

(15) Chernega, A.; Cook, J.; Green, M. L. H.; Labella, L.; Simpson, S. J.; Souter, J.; Stephens, A. H. H. *J. Chem. Soc., Dalton Trans.* **1997**, 3225-3243.

(16) Churchill, D. G.; Bridgewater, B. M.; Zhu, G.; Pang, K.; Parkin, G. *Polyhedron* **2006**, *25*, 499-512.

(17) Janak, K. E.; Shin, J. H.; Parkin, G. *J. Am. Chem. Soc.* **2004**, *126*, 13054-13070.

(18) Labella, L.; Chernega, A.; Green, M. L. H. *J. Chem. Soc., Dalton Trans.* **1995**, 395-402.

(19) Labella, L.; Chernega, A.; Green, M. L. H. *J. Organomet. Chem.* **1995**, *485*, C18-C21.

(20) Pons, V.; Conway, S. L. J.; Green, M. L. H.; Green, J. C.; Herbert, B. J.; Heinekey, D. M. *Inorg. Chem.* **2004**, *43*, 3475-3483. .

(21) Green, J. C.; Harvey, J. N.; Poli, R. *J. Chem. Soc., Dalton Trans.* **2002**, 1861-1866.

(22) Comte, V.; Blacque, O.; Kubicki, M. M.; Moiese, C. *Organometallics* **1997**, *16*, 5763-5769.

(23) Conway, S. L. J.; Dijkstra, T.; Doerrer, L. H.; Green, J. C.; Green, M. L. H.; Stephens, A. H. H. *J. Chem. Soc., Dalton Trans.* **1998**, 2689-2696.

(24) Jourdain, I. V.; Fourmigue, M.; Guyon, F.; Amaudrut, J. *Organometallics* **1999**, *18*, 1834-1839.

(25) Churchill, D. G.; Bridgewater, B. M.; Parkin, G. *J. Am. Chem. Soc.* **2000**, *122*, 178-179.

(26) Churchill, D. G.; Janak, K. E.; Wittenberg, J. S.; Parkin, G. *J. Am. Chem. Soc.* **2003**, *125*, 1403-1420.

(27) Zachmanoglou, C. E.; Docrat, A.; Bridgewater, B. M.; Parkin, G.; Brandow, C. G.; Bercaw, J. E.; Jardine, C. N.; Lyall, M.; Green, J. C.; Keister, J. B. *J. Am. Chem. Soc.* **2002**, *124*, 9525-9546.

(28) Chin, J.; Banaszczyk, M.; Jubian, V.; Zou, X. *J. Am. Chem. Soc.* **1989**, *111*, 186-90.

(29) Chin, J.; Zou, X. *J. Am. Chem. Soc.* **1988**, *110*, 223-5.

(30) Hendry, P.; Sargeson, A. M. *J. Am. Chem. Soc.* **1989**, *111*, 2521-7.

(31) Kou, X.; Cheng, S.; Du, J.; Yu, X.; Zeng, X. *J. Mol. Catal. A: Chem.* **2004**, *210*, 23-29.

(32) Hegg, E. L.; Mortimore, S. H.; Cheung, C. L.; Huyett, J. E.; Powell, D. R.; Burstyn, J. N. *Inorg. Chem.* **1999**, *38*, 2961-2968.

(33) Deal, K. A.; Burstyn, J. N. *Inorg. Chem.* **1996**, *35*, 2792-8.

(34) Deal, K. A.; Hengge, A. C.; Burstyn, J. N. *J. Am. Chem. Soc.* **1996**, *118*, 1713-18.

(35) Itoh, T.; Hisada, H.; Usui, Y.; Fujii, Y. *Inorg. Chim. Acta* **1998**, *283*, 51-60.

(36) Fujii, Y.; Itoh, T.; Onodera, K.; Tada, T. *Chem. Lett.* **1995**, 305-6.

(37) Bazzicalupi, C.; Bencini, A.; Berni, E.; Bianchi, A.; Fedi, V.; Fusi, V.; Giorgi, C.; Paoletti, P.; Valtancoli, B. *Inorg. Chem.* **1999**, *38*, 4115-4122.

(38) Bonfa, L.; Gatos, M.; Mancin, F.; Tecilla, P.; Tonellato, U. *Inorg. Chem.* **2003**, *42*, 3943-3949.

(39) Itoh, T.; Fujii, Y.; Tada, T.; Yoshikawa, Y.; Hisada, H. *Bull. Chem. Soc. Jpn.* **1996**, *69*, 1265-1274.

(40) Koike, T.; Kimura, E. *J. Am. Chem. Soc.* **1991**, *113*, 8935-41.

(41) Schwemlein, H.; Brintzinger, H. H. *J. Organomet. Chem.* **1983**, *254*, 69-73.

(42) Persson, C.; Andersson, C. *Inorg. Chim. Acta* **1993**, *203*, 235-8.

(43) Ren, J. G.; Tomita, H.; Minato, M.; Osakada, K.; Ito, T. *Chem. Lett.* **1994**, 637-40.

(44) Balzarek, C.; Weakley, T. J. R.; Kuo, L. Y.; Tyler, D. R. *Organometallics* **2000**, *19*, 2927-2931.

(45) Kuo, L. Y.; Kanatzidis, M. G.; Sabat, M.; Tipton, A. L.; Marks, T. J. *J. Am. Chem. Soc.* **1991**, *113*, 9027-45.

(46) Schultz, A. J.; Stearley, K. L.; Williams, J. M.; Mink, R.; Stucky, G. D. *Inorg. Chem.* **1977**, *16*, 3303-6.

(47) Ren, J.-G.; Tomita, H.; Minato, M.; Ito, T.; Osakada, K.; Yamasaki, M. *Organometallics* **1996**, *15*, 852-9.

(48) Adams, M. A.; Folting, K.; Huffman, J. C.; Caulton, K. G. *Inorg. Chem.* **1979**, *18*, 3020-3.

CHAPTER III

(1) Ahmed, T. J.; Zakharov, L. N.; Tyler, D. R. *Organometallics* **2007**, *26*, 5179-5187.

(2) Breno, K. L.; Ahmed, T. J.; Pluth, M. D.; Balzarek, C.; Tyler, D. R. *Coord. Chem. Rev.* **2006**, *250*, 1141-1151.

(3) Breno, K. L.; Pluth, M. D.; Landorf, C. W.; Tyler, D. R. *Organometallics* **2004**, *23*, 1738-1746.

(4) Breno, K. L.; Pluth, M. D.; Tyler, D. R. *Organometallics* **2003**, *22*, 1203-1211.

(5) Kuo, L. Y.; Barnes, L. A. *Inorg. Chem.* **1999**, *38*, 814-817.

(6) Kuo, L. Y.; Blum, A. P.; Sabat, M. *Inorg. Chem.* **2005**, *44*, 5537-5541.

(7) Kuo, L. Y.; Perera, N. M. *Inorg. Chem.* **2000**, *39*, 2103-2106.

(8) Zachmanoglou, C. E.; Docrat, A.; Bridgewater, B. M.; Parkin, G.; Brandow, C. G.; Bercaw, J. E.; Jardine, C. N.; Lyall, M.; Green, J. C.; Keister, J. B. *J. Am. Chem. Soc.* **2002**, *124*, 9525-9546.

(9) Pons, V.; Conway, S. L. J.; Green, M. L. H.; Green, J. C.; Herbert, B. J.; Heinekey, D. M. *Inorg. Chem.* **2004**, *43*, 3475-3483.

(10) Janak, K. E.; Shin, J. H.; Parkin, G. *J. Am. Chem. Soc.* **2004**, *126*, 13054-13070.

(11) Balzarek, C.; Weakley, T. J. R.; Kuo, L. Y.; Tyler, D. R. *Organometallics* **2000**, *19*, 2927-2931.

(12) Hegg, E. L.; Mortimore, S. H.; Cheung, C. L.; Huyett, J. E.; Powell, D. R.; Burstyn, J. N. *Inorg. Chem.* **1999**, *38*, 2961-2968.

(13) Deal, K. A.; Burstyn, J. N. *Inorg. Chem.* **1996**, *35*, 2792-8.

(14) Balzarek, C.; Tyler, D. R. *Angew. Chem., Int. Ed.* **1999**, *38*, 2406-2408.

(15) Ren, J. G.; Tomita, H.; Minato, M.; Osakada, K.; Ito, T. *Chem. Lett.* **1994**, 637-40.

(16) Stabler, R. N.; Chesick, J. P. *Int. J. Chem. Kinet.* **1978**, *10*, 461-9.

(17) Weigert, F. J. *Comput. Chem.* **1987**, *11*, 273-80.

CHAPTER IV

(1) Baxley, G., A Dissertation. Department of Chemistry. University of Oregon, 1997.

(2) Ren, J.G.; Tomita H.; Minato M.; Osakada, K.; Ito, T. *Chem. Lett.* **1994**, 637-640.

(3) Balzarek, C.; Tyler, D. R. *Angew. Chem., Int. Ed.* **1999**, *38*, 2406-2408.

(4) Ahmed, T.J.; Zakharov, L. N.; Tyler, D. R. *Organometallics* **2007**, *26*, 5179-5187.

(5) Kuo, L.Y.; Kanatzidis, M. G.; Sabat, M.; Tipton, A. L.; Marks, T. J. *J. Am. Chem. Soc.* **1991**, *113*, 9027-9045.

(6) Breno, K.L.; Ahmed, T. J.; Pluth, M. D.; Balzarek, C.; Tyler, D. R. *Coord. Chem. Rev.* **2006**, *250*, 1141-1151.

(7) Balzarek, C.; Weakley, T. J. R.; Kuo, L. Y.; Tyler, D. R. *Organometallics* **2000**, *19*, 2927-2931.

(8) Zachmanoglou, C. E.; Docrat, A.; Bridgewater, B. M.; Parkin, G.; Brandow, C. G.; Bercaw, J. E.; Jardine, C. N.; Lyall, M.; Green, J. C.; Keister, J. B. *J. Am. Chem. Soc.* **2002**, *124*, 9525-9546.

(9) Janak, K. E.; Shin, J. H.; Parkin, G. *J. Am. Chem. Soc.* **2004**, *126*, 13054-13070.

(10) Ahmed, T.J.; Tyler, D. R. *Organometallics* **2008**, *27*, 2608-2613.

CHAPTER V

(1) Green, M. M.; Wittcoff, H. A. *Organic Chemistry Principles and Industrial Practice*, 2003.

(2) Kukushkin, V. Y.; Pombeiro, A. J. L. *Inorg. Chim. Acta* **2005**, *358*, 1-21.

(3) Ghaffar, T.; Parkins, A. W. *Tetrahedron Lett.* **1995**, *36*, 8657-60.

(4) Ghaffar, T.; Parkins, A. W. *J. Mol. Catal. A: Chem.* **2000**, *160*, 249-261.

(5) Parkins, A. W.; Ghaffar, T.; (UK). US Patent # 5,932,756 , 1996, p 1–6.

(6) Cobley, C. J.; Van den Heuvel, M.; Abbadi, A.; De Vries, J. G. *Tetrahedron Lett.* **2000**, *41*, 2467-2470.

(7) Jiang, X.-b.; Minnaard, A. J.; Feringa, B. L.; De Vries, J. G. *J. Org. Chem.* **2004**, *69*, 2327-2331.

(8) Ren, J. G.; Tomita, H.; Minato, M.; Osakada, K.; Ito, T. *Chem. Lett.* **1994**, 637-40.

(9) Kirchmeyer, S.; Mertens, A.; Arvanaghi, M.; Olah, G. A. *Synthesis* **1983**, 498-500.

(10) Stewart, T. D.; Fontana, B. J. *J. Am. Chem. Soc.* **1940**, *62*, 3281-5.

(11) Breno, K. L.; Pluth, M. D.; Tyler, D. R. *Organometallics* **2003**, *22*, 1203-1211.

(12) Ahmed, T. J.; Zakharov, L. N.; Tyler, D. R. *Organometallics* **2007**, *26*, 5179-5187.

(13) Balzarek, C.; Weakley, T. J. R.; Tyler, D. R. *J. Am. Chem. Soc.* **2000**, *122*, 9427-9434.

(14) Breno, K. L.; Tyler, D. R. *Organometallics* **2001**, *20*, 3864-3868.

(15) Schlesinger, G.; Miller, S. L. *J. Amer. Chem. Soc.* **1973**, *95*, 3729-35.

APPENDIX D

(1) Wechsberg, M.; Schoenbeck, R.; (Chemie Linz A.-G., Austria). Application: AT AT, 1980, p 4.

(2) Jammot, J.; Pascal, R.; Commeyras, A. *Tetrahedron Lett.* **1989**, *30*, 563-4.

(3) Jammot, J.; Pascal, R.; Commeyras, A. *J. Chem. Soc., Perkin Trans. 2* **1990**, 157-62.

(4) Jiang, X.-b.; Minnaard, A. J.; Feringa, B. L.; De Vries, J. G. *J. Org. Chem.* **2004**, *69*, 2327-2331.

(5) Ghaffar, T.; Parkins, A. W. *J. Mol. Catal. A: Chem.* **2000**, *160*, 249-261.

(6) Hays, H. R. *J. Org. Chem.* **1968**, *33*, 3690-4.